EVALUATION OF THE SENSITIVITY OF RADAR CROSS SECTION PREDICTIONS TO UNCERTAINTIES IN MATERIAL CHARACTERISTICS

THESIS

Greg A. Barnhart, Captain, USAF

AFIT/GE/ENG/95D-02

DEPARTMENT OF THE AIR FORCE
AIR UNIVERSITY
AIR FORCE INSTITUTE OF TECHNOLOGY

Wright-Patterson Air Force Base, Ohio

DISCLAIMER NOTICE

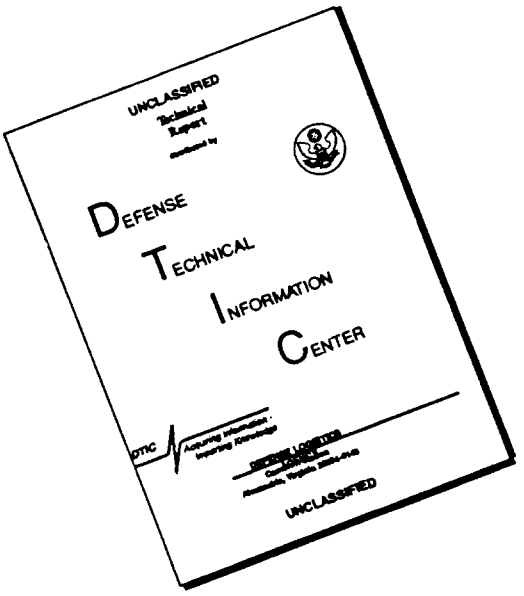

THIS DOCUMENT IS BEST QUALITY AVAILABLE. THE COPY FURNISHED TO DTIC CONTAINED A SIGNIFICANT NUMBER OF PAGES WHICH DO NOT REPRODUCE LEGIBLY.

AFIT/GE/ENG/95D-02

EVALUATION OF THE SENSITIVITY OF RADAR CROSS SECTION PREDICTIONS TO UNCERTAINTIES IN MATERIAL CHARACTERISTICS

THESIS

Greg A. Barnhart, Captain, USAF

AFIT/GE/ENG/95D-02

Approved for public release; distribution unlimited

The views expressed in this thesis are those of the author an do not reflect the official policy or position of the Department of Defense or the U. S. Government

AFIT/GE/ENG/95D-02

EVALUATION OF THE SENSITIVITY OF RADAR CROSS SECTION PREDICTIONS TO UNCERTAINTIES IN MATERIAL CHARACTERISTICS

THESIS

Presented to the Faculty of the School of Engineering

of the Air Force Institute of Technology

Air University

In Partial Fulfillment of the

Requirements for the Degree of

Master of Science in Electrical Engineering

Greg A. Barnhart, B.S.E.E.

Captain, USAF

December 1995

Acknowledgments

I wish to express my sincere appreciation to the people who have contributed to this thesis. My special thanks to my thesis advisor Dr. Andrew Terzuoli, my sponsor Major Dennis Andersh of Wright Lab, and my thesis committee Major Paul Skinner, Major Gerald Gerace, and Captain Joe Sacchini who provided valuable feedback throughout this effort. I would like to thank Captain Mike Proudfoot, Stan Bayshore, and Fred Jones for their support in performing the material and RCS measurements. I would also like to thank Rob Layden, Andy MacFarland, and Bill Kent of Mission Research Corporation for their advice and assistance with Xpatch. I thank my cat Bugs for her entertaining distractions. Finally, I am eternally grateful to my wife Leslie for her understanding, motivation, and moral support from 1,500 miles away throughout the entire AFIT master's degree program.

Greg A. Barnhart

Table of Contents

Page

List of Figures

Page

List of Tables

Abstract

The purpose of this study was to evaluate the effects of material characteristics uncertainties on Radar Cross Section (RCS) predictions. Many methods have been developed to predict the RCS of metal objects, but for material coated objects, these methods depend on the accuracy of measured material characteristics.

Material characteristics of three dielectrics were measured by two separate X-band waveguide set-ups. RCS measurements were then made to evaluate the accuracy of RCS predictions using these measured material characteristics. A six inch square slab of each material was measured with and without a metal plate backing. A six inch square flat metal plate was also measured to qualify the accuracy of the range.

RCS predictions were made using two methods. The first method calculated the reflection coefficients of the materials using transmission line theory and then applied physical optics theory to predict the RCS. The second method utilized Xpatch, a high frequency RCS prediction code.

The comparison of RCS measurements to RCS predictions indicated that the X-band waveguide set-ups used were only able to accurately determine the effective material characteristics of thin homogeneous materials. The results of the correlation of material characteristic variations with corresponding RCS prediction variations were positive. In general, the variations in RCS predictions were correlated with the variations of the imaginary part of the dielectrics' permittivities. Qualitatively, the relative magnitude of these variations in the RCS predictions were highly correlated with the relative magnitude of the reflection coefficient.

EVALUATION OF THE SENSITIVITY OF RADAR CROSS SECTION PREDICTIONS TO UNCERTAINTIES IN MATERIAL CHARACTERISTICS

1. Introduction

1.1 Background

Radar operates by radiating electromagnetic waves and detecting echoes from an object. There are two purposes of radar, one is to determine the location of an object, the second is to identify the object. Such identification is possible because every object has a unique radar return called the Radar Cross Section (RCS). The RCS is defined as the equivalent area of the object as if it were an isotropically scattering metal sphere. The RCS is primarily a function of the object's size, shape, composition, and orientation with respect to the radar. Since it can give insight into an object's identity, much research has been devoted to RCS characterization.

There are many methods that can predict an object's RCS. An important factor in evaluating the accuracy of a RCS prediction is understanding the accuracy of the object model. If the object's size or shape is erroneous, the resulting RCS prediction is faulty, but these can typically be measured quite accurately. This is not true, however, when evaluating the accuracy of the object's material composition.

The determination of material characteristics is not an exact science. Both measurement uncertainties and manufacturing tolerances play a large role in not being able to identify their exact values. At best, a material's specifications may provide an estimate of these characteristics under certain frequency and temperature conditions. The actual

values, however, may vary by five to twenty percent or more. These uncertainties reduce the confidence that can be put into identifying a Radar Absorbing Material (RAM) coated object from a RCS prediction.

1.2 Problem Definition

The Air Force Wright Laboratory Target Recognition Branch, WL/AARA, is investigating ways to accurately simulate the RCS of objects. Many computer models have been developed to do this, but WL/AARA has concentrated on developing and maturing the code called Xpatch. WL/AARA has sponsored three recent theses at the Air Force Institute of Technology (AFIT) to validate Xpatch as an RCS prediction tool [6], [13], [14]. All of these theses analyzed Perfect Electric Conducting (PEC) objects, which are made of metal. To avoid radar detection, an object may be coated with a layer of RAM that will reduce its RCS and make it appear smaller. The accurate RCS prediction of an object coated with RAM is therefore critical both to locate enemy stealthy objects and to hide friendly ones. Xpatch has the capability to analyze the RCS of PEC, non-PEC, and PEC objects coated with RAM. A study performed by the Mission Research Corporation (MRC) for WL/AARA, however, indicated that the Xpatch RCS prediction of a RAM coated object was inaccurate. This study concluded that although the Xpatch code performed properly, the provided material characteristics were inaccurate [9].

The primary objective of this thesis was to evaluate the sensitivity of RCS predictions to uncertainties in material characteristics. In conjunction with this objective and as a part of a continuing effort to validate and improve Xpatch as an RCS prediction tool, this research evaluated its RAM coated object RCS prediction capabilities through comparisons to RCS measurements and theoretical RCS predictions. The following four efforts were required to accomplish these objectives:

1. Statistically analyzing material characteristics measurements.

2. Statistically analyzing RCS measurements of air backed and PEC backed materials at normal incidence.

3. Using transmission line theory and physical optics to predict the RCS of air backed and PEC backed materials at normal incidence using measured material characteristics.

4. Using Xpatch simulations to predict the RCS of air backed and PEC backed materials at normal incidence using measured material characteristics.

Although some research has been performed in the area of RCS prediction accuracy of RAM coated objects, it was conducted as part of classified projects and remains inaccessible. The research for this thesis is limited to properties of commercially available dielectric materials. It provides the fundamentals of RCS materials error analysis which can be applied to specific situations, either classified or unclassified.

2. Background

This chapter provides an overview of the knowledge required to understand the basics of this research. It is divided into four sections. First is a review of the concepts of material characteristics and their measurements. Second is the application of these concepts to the analysis of material layers. Third is a brief introduction of radar cross section theory and measurement techniques. Fourth is a presentation of the Xpatch RCS prediction software along with prior evaluations of its accuracy. In depth coverage of the actual application of these concepts to this thesis research will be provided in the next chapter.

2.1 Material Characteristics

The first step to investigating the RCS of a RAM coated object is to examine the electromagnetic characteristics of the material itself. Although the basics of these characteristics as they apply to various technologies has been well known for years, attempts to use these characteristics in RCS prediction models require a more precise understanding of their behavior when subjected to radar. The fundamentals of these characteristics can be found in many good electromagnetic texts.

There are two properties that identify a material's electromagnetic behavior: 1) permittivity, designated by ε, which characterizes the material's ability to store electrical energy; and 2) permeability, designated by μ, which characterizes the material's ability to store magnetic energy. All materials have these characteristics referenced to their relative value compared to free space. These material values are defined by $\varepsilon = \varepsilon_r \varepsilon_o$ and $\mu = \mu_r \mu_o$ where ε_o and μ_o are the values for free space and ε_r and μ_r are the complex relative permittivity and permeability respectively. These parameters determine the intrinsic characteristic impedance and the refractive index of a material.

A material has distinctive properties when exposed to electromagnetic fields. It may be linear or nonlinear, homogeneous or inhomogeneous, isotropic or anisotropic, lossless or lossy. For the lossy case, the permittivity and permeability are complex quantities in the frequency domain in which the imaginary parts represent the material's ability to dissipate energy [2]. Throughout this paper, the notation used is: $\varepsilon_r = \varepsilon_r' - j\,\varepsilon_r''$ and $\mu_r = \mu_r' - j\,\mu_r''$. In addition, virtually all material properties are dependent on the electromagnetic frequency and are called dispersive. All of these material properties can tremendously complicate the prediction of how electromagnetic waves behave in the material and can therefore make the RCS prediction of a material coated object difficult.

2.2 Material Characteristics Measurements

The characteristics of a material can be measured using many methods [1]. Knott provides specific advantages and disadvantages for the most common technique using transmission lines [8]. Transmission lines are well suited for material measurements for several reasons. Foremost, transmission line theory is well understood and documented. In addition, the transmission lines are an enclosed environment so that energy losses are minimized. This allows for any measured losses to be attributed to the material and not to the measurement equipment. Lastly, transmission lines are common and convenient to use and operate.

Transmission line measurements require small samples to be fitted into short transmission line holders. The accuracy of the sample's physical characteristics used in the transmission line measurements is critical. Also, the sample needs to be an accurate representation of the material being characterized, otherwise the measured characteristics may not be valid for the material on the object. Any inhomogenaities in the sample must be much smaller than the measurement wavelength. In addition, the sample must fit snugly

within the sample holder. Adherence to these requirements will reduce material measurement errors.

The two transmission lines used for material measurements are coaxial lines and rectangular waveguides. The primary benefit of using the coaxial line is that it supports TEM modes so it is able to test the material sample over a very wide frequency range. Its main disadvantage is that the required washer-shaped samples are difficult to fabricate and complicated to handle. The primary advantage of the rectangular waveguide is that the samples only need to be simple rectangular slabs. The major disadvantage is that rectangular waveguides cannot support TEM modes. This creates both frequency cutoff conditions and a risk of supporting multiple modes of propagation. Thus, rectangular waveguide material measurements are limited to the waveguide supported frequency bands.

2.3 Layered Materials

The analysis of electromagnetic waves incident to and propagating through layered materials is typically reduced to an equivalent transmission line model. This model can determine the reflection, transmission, and attenuation of the electromagnetic fields through the layers. Only the basic formulation of this model is discussed here. Many electromagnetics texts can provide the details to the derivations using Maxwell's equations to satisfy boundary conditions.

In its simplest form, a complex layered material at normal incidence can be converted to an equivalent transmission line model as shown in Figure 1. In Figure 1(a), Z_i is the intrinsic impedance of the ith material, d_i is the material thickness, and R_i represents an infinitely thin resistive sheet which may be placed between absorbers. The value of Z_N can be either zero for a PEC backed material or Z_o for an air backed material, such as a radome. The reflection coefficient can then be easily calculated from the equivalent model in Figure 1(b) using:

$$\Gamma = \frac{Z_{eq} - Z_o}{Z_{eq} + Z_o} \tag{1}$$

The key to the translation of a layered material to a transmission line model is determining the equivalent input impedance, Z_{eq} .

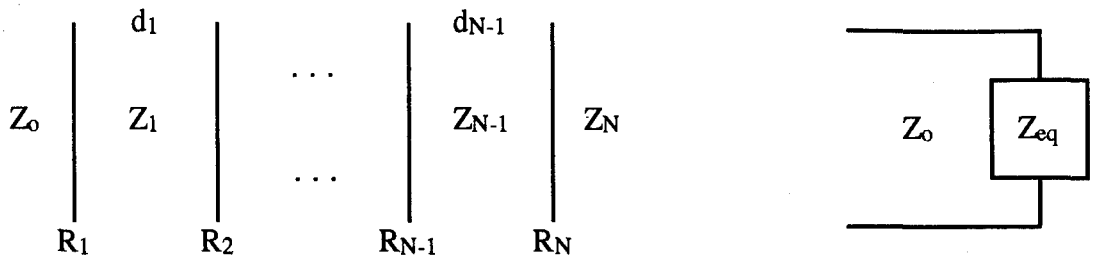

(a) Layered Material (b) Equivalent Model

Figure 1. Transmission Line Conversion of Layered Materials

The following analysis can be performed on a layered material to determine Z_{eq}. From Figure 2, the effective input impedance, Zin_n , as seen prior to the resistive sheet R_n is:

$$Zin_n = \frac{R_n Z_n}{R_n + Z_n} \tag{2}$$

If there is no resistive sheet, this reduces to $Zin_n = Z_n$. The effective input impedance, Zin'_{n-1} , as seen from the front of the n-1 layer, is:

$$Zin'_{n-1} = Z_{n-1} \frac{Zin_n + j\, Z_{n-1} \tan (k_{n-1}\, d_{n-1})}{Z_{n-1} + j\, Zin_n \tan (k_{n-1}\, d_{n-1})} \tag{3}$$

where $k=2\pi/\lambda$ is the wave number and λ is the wavelength within the material layer. These steps can be performed iteratively until the equivalent input impedance, Z_{eq} , is determined so that the reflectivity of the layered material can be calculated from Equation (1).

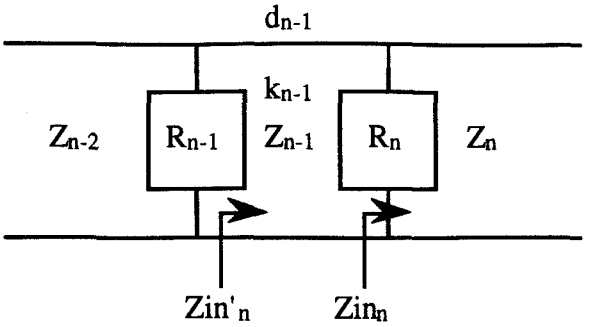

Figure 2. Model for Equivalent Input Impedance

There are two common types of layered absorbers. The simplest is the Dallenbach layer which has only one material layer and no resistive sheets over a PEC object. The second is the Salisbury Screen which has one resistive sheet placed over a free space equivalent layer over a PEC object. The usage of these absorber types depends on the desired absorption properties over a specified frequency range.

Another approach to analyze material layers is described by Knott. In this method, the field coefficients can be calculated by relating the fields on either side of a boundary [8]. From Figures 3 and 4, the electric and magnetic fields are defined by:

$$E = Ae^{-jkx} + Be^{+jkx} \tag{4}$$

$$H = Y(Ae^{-jkx} - Be^{+jkx}) \tag{5}$$

where A and B are the forward and backward field amplitudes in each layer, Y is the intrinsic admittance of the layers, k is the wave number, and x is the position within the layered material. By satisfying boundary conditions, Knott shows:

$$A_m = \frac{e^{+jk_m x_n}}{2Y_m}\left[A_n(Y_m + Y_n + G)e^{-jk_n x_n} + B_n(Y_m - Y_n + G)e^{+jk_n x_n}\right] \tag{6}$$

$$B_m = \frac{e^{-jk_m x_n}}{2Y_m}\left[A_n(Y_m - Y_n - G)e^{-jk_n x_n} + B_n(Y_m + Y_n - G)e^{+jk_n x_n}\right] \tag{7}$$

where G is the conductance of an infinitely thin sheet between the layers, and m and n are layer indices defined by Figure 4. Starting with $A_1 = 1$ and $B_1 = -1$ for PEC backed targets or $A_1 = 1$ and $B_1 = 0$ for air backed targets and iteratively applying these equations, the reflection coefficient can be determined from:

$$\Gamma = \frac{B_{N+1}}{A_{N+1}} \tag{8}$$

Knott goes further by modifying the equations for bistatic situations at oblique incidence for either vertical or horizontal polarizations. These robust equations are used to calculate the reflection coefficients in this thesis even though only normal incidence is investigated.

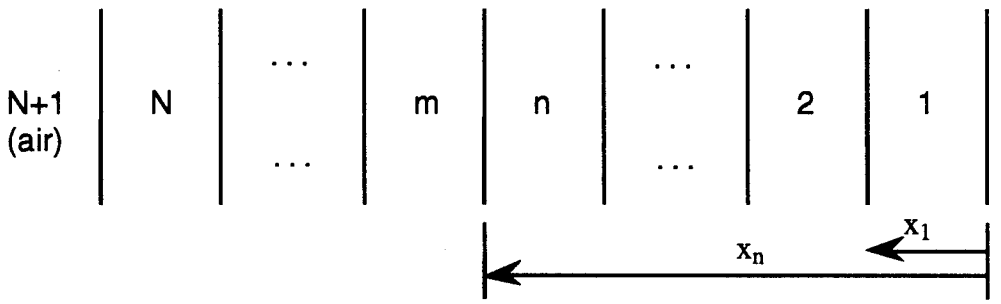

Figure 3. Sequence of N Material Layers

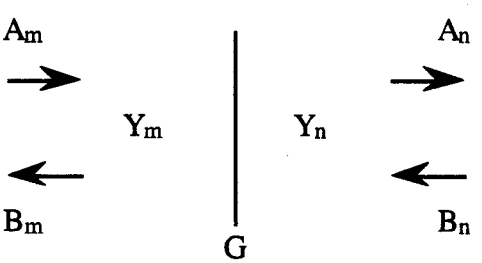

Figure 4. Propagating Waves at Layer Boundary with Resistive sheet

2.4 Radar Cross Section

The radar cross section of an object is its equivalent area as if it were an isotropically scattering metal sphere. Its mathematical definition is:

$$\sigma = \lim_{R\to\infty} 4\pi R^2 \frac{|E_s|^2}{|E_i|^2} \tag{9}$$

where R is the distance from the radar to the object and E_i and E_S are the incident and scattered electric fields in the frequency domain.

An RCS indoor range is a facility where accurate RCS measurements are made to characterize radar signatures of objects. To properly model a true radar situation in an indoor range, two primary conditions must be met. One is that the object must be in the far field to eliminate any distance dependencies, which requires that the incident fields must be nearly planar. The second is that the scattering phenomena measured must come solely from the object. This stringent requirement is met by the combination of five methods: 1) the indoor facility is typically an anechoic chamber where all the surfaces are covered with pyramid and wedge shaped absorbers to minimize clutter; 2) hardware gating is used to isolate deterministic signals from non-object scatterers such as from the back wall; 3) software gating is used to process out multi-bounce returns caused by interactions between the object and range; 4) vector background subtraction is used to reduce clutter at the same range as the object; 5) pulse integration is used to reduce noise [7].

Several range measurements are required to determine an object's RCS. Since an electric field cannot be measured directly, a comparison method is used. This method compares the measured field magnitude and phase of the unknown object against the field magnitude and phase of a known object while compensating for measured background noise. The result is:

$$\sigma = \frac{E_{Object} - E_{ObjectBackground}}{E_{Known} - E_{KnownBackground}} * \sigma_{Known} \quad (10)$$

Typically, the known object is a sphere where σ_{Known} is the exact Mie series solution for the RCS of a sphere [16].

Measuring the RCS of a material coated object is a free space method of evaluating the properties of the material. Typically, the RCS method is used to determine the power absorbed by the material compared to an equivalent PEC object. The equation

$$\Gamma = 20 \log \left(\sqrt{\frac{\sigma_{Object}}{\sigma_{Ref}}}\right) \quad (11)$$

converts reflection coefficients at normal incidence to RCS values and vice-versa where Γ is the reflection coefficient in dB, σ_{Object} is the RCS of the material coated object in square meters, and σ_{Ref} is the RCS of the reference equivalent PEC object in square meters. This relationship allows the comparison of theoretical RCS data to measured RCS data given the material characteristics which determine the reflection coefficient.

2.5 Xpatch

Xpatch is a high frequency RCS prediction code based on the Shooting and Bouncing Ray (SBR) technique. In SBR, a dense grid of rays is shot from the radar source toward the object. The rays are traced according to geometrical optics theory, including the effects of polarizations, ray divergence factors, and layered material transmissions and reflections. At the ray exit point, Xpatch performs a physical optics integration to calculate the scattered fields. Since physical optics theory does not predict edge diffraction, Xpatch compensates for this by calculating Incremental Length Diffraction Coefficients (ILDC) [10].

The Xpatch code has gained popularity primarily due to its flexibility. It is capable of performing both frequency domain RCS analysis for both monostatic and bistatic situations and time domain analysis for Synthetic Aperature Radar (SAR) images. From this data, Xpatch can construct frequency sweeps, azimuth and elevation scans, and range profiles. In addition, Xpatch operates on models created by several Computer Aided Design (CAD) formats. Finally, Xpatch can incorporate given materials which compose an object. It requires the characteristics of the materials being used including thickness and permittivity and permeability characteristics, or reflectivity and transmission coefficients.

There are limitations to Xpatch which must be kept in mind for any analysis. Xpatch can only compensate for first order edge diffractions, not for higher orders or for tip diffractions. It is also unable to predict surface traveling waves. When analyzing non-PEC models, Xpatch only uses physical optics theory to determine their effect on the RCS. It calculates the reflection and transmission coefficients from the material characteristics and performs a PO integration to determine the scattered fields. In addition, Xpatch cannot model inhomogeneous, non-linear, or anisotropic materials. At present, material scattering phenomena is not well understood and no high frequency RCS prediction theory can overcome all these material limitations.

Three recent theses have been written at the Air Force Institute of Technology (AFIT) to validate Xpatch as an RCS prediction tool. The first of these three validated Xpatch version 4.0 and researched its sensitivity to object modeling parameters [14]. Miller concluded that although cruder facetization resulted in faster computation time, it generated more inaccurate RCS predictions. The second thesis sponsored by WL/AARA validated Xpatch version 6.1 and researched radar imaging [6]. Jernejcic performed several experiments in the AFIT indoor RCS test range to qualitatively confirm the Xpatch SAR image predictions. The most recent thesis validated Xpatch version 7.4 and researched quantitative error analysis of Xpatch predictions [13].

The most recent Xpatch validation effort was performed by the Mission Research Corporation for WL/AARA. The goal of the study was to compare data from two RCS prediction codes, Xpatch and NoseScat [9]. The object analyzed was a nose radome test body with an absorber in front of the bulkhead as shown in Figure 5. Two materials were included in the test body. The first was a wet glass epoxy lay-up used for the fiberglass radome. The second was a Rantec FL 0750 STD three layer foam absorber used over the bulkhead.

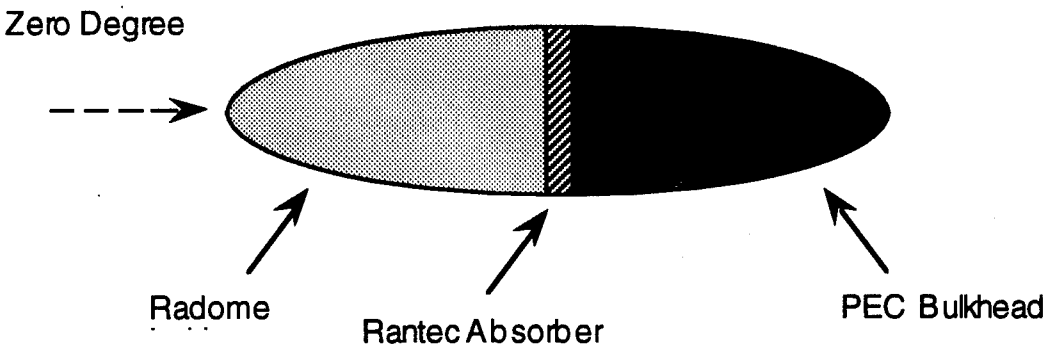

Figure 5. MRC Nose Radome Test Body

A major conclusion of the MRC study was that "relatively moderate uncertainties in material electrical properties can have significant effects in the scattering spectrum" [9]. The radome dielectric material was specified as having a constant permittivity which may vary according to the manufacturing tolerances of the resin content. The Rantec absorber, on the other hand, had no specified material characteristics. Thus, MRC measured its transmission coefficients in a transmission tunnel from 2-18 GHz. With this data, MRC backed out the best estimate of equivalent permittivity and permeability values to obtain the same coefficients. In both material cases, MRC concluded that the material uncertainties substantially limited the accuracy of the Xpatch RCS predictions.

3. Methodology

An analysis of the accuracy of RCS predictions requires a comparison of the predicted data to the measured data. The issue that arises with material coated objects is that the predicted RCS data, which ideally is exact, depends on measured material characteristics. As previously mentioned, these characteristics may vary according to manufacturing tolerances and measurement errors. The performance of this research involved four primary tasks:

1. Waveguide measurements of three materials.
2. RCS measurements of air backed and PEC backed materials.
3. RCS predictions using transmission line theory and physical optics.
4. RCS predictions using Xpatch.

A final evaluation of Xpatch used the measured material data to compare simulations of the MRC test body with prior MRC measured and predicted RCS data.

3.1 Material Characteristics Measurements

For this research, three commercially available materials were evaluated. The first was ECCOSORB VF-60 by Emerson & Cuming Incorporated. The VF-60 material is a dispersive, homogeneous, conductive plastic film dielectric, which has $\mu_r = 1.0$ for all microwave frequencies. It is a 0.15 cm thick absorber and can be used to make a Salisbury Screen type absorber [3]. This material was chosen to evaluate a thin radar absorbing material. Since styrofoam was used for a spacer behind the VF-60 for the Salisbury Screen, a sample of it was also measured to determine its characteristics.

The second material is ECCOSORB AN-73 by Emerson & Cuming Incorporated. The AN-73 material is a dispersive, inhomogeneous foam material dielectric, which has $\mu_r = 1.0$ for all microwave frequencies. It is 1.0 cm thick and is comprised of three thin

foam layers glued together [4]. Each thin foam layer has different, but unknown material characteristics. Only the effective characteristics of the whole material were evaluated. Because the three thin layers' contribution to different reflection and transmission properties depend on which side of the AN-73 is facing towards the radar, it is important to identify its orientation. For this research, the bronze colored side was directed toward the radar and the white side away from it. It should be noted that this is exactly opposite the intended facing [4]. Although this error wasn't realized until the measurements were complete, it has no impact on evaluating the sensitivity of the RCS predictions to the material uncertainties. This material was chosen to evaluate a thick radar absorbing material.

The third material is a Rantec FL 0750 STD foam. The Rantec absorber is a 2.0 cm thick dispersive, inhomogeneous foam material dielectric, which has $\mu_r = 1.0$ for all microwave frequencies. Although this foam is also comprised of three thin layers glued together, only the effective characteristics of the whole material were evaluated. Because the three layers' contribution to different reflection and transmission properties depend on which side of the Rantec is facing toward the radar, it is important to identify its orientation. For this research, the blue colored side was directed towards the radar and the white side away from it. This material was chosen since it was used on the nose radome test body in the MRC study. Xpatch simulations were repeated on this object to evaluate the change in the predicted RCS with different material characteristic inputs.

The characteristics of these materials were measured using rectangular waveguides. The waveguide method simplified the fabrication of material test samples. Since rectangular waveguides are more common and easier to use than other material measurement techniques, two different waveguide set-ups were available. Performing measurements on the same material samples using two separate set-ups was beneficial in evaluating material measurement uncertainties. Both set-ups used were X-band

waveguides. This necessarily limited measurements to the 8-12 GHz frequency range. Data was taken in this range every 0.25 GHz.

The primary pieces of equipment for these set-ups were network analyzers which measure the parameters of a network consisting of a length of waveguide containing the material sample by comparing the incident signal with the reflected signal [5]. The network analyzer displays the measured data in the form of the complex scattering matrix parameters S_{11} and S_{21} which are defined in Figure 6 for a two-port device.

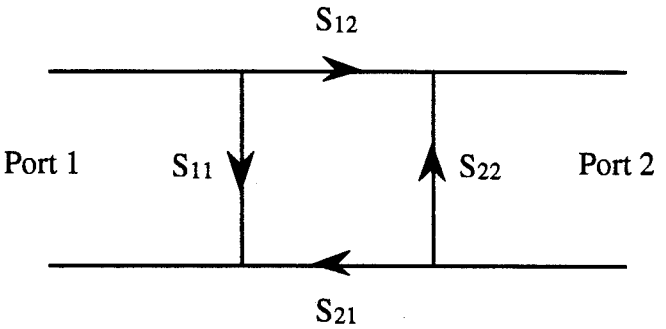

Figure 6. S-Parameter Definition for Two-Port Network

From the S-parameter data, the material complex permittivity and permeability can be calculated using the equations documented by Weir [18].

The first rectangular waveguide set-up was available from WL/XPN, Wright Laboratories, Signature Technology Directorate, Wright-Patterson AFB, OH. Data from this set-up will heretofore be labeled XPN data to identify its origin. The XPN set-up, as shown in Figure 7, was a reflectometer in which port #2 is a short. The reflectometer can only analyze dielectrics because it can only measure S_{11}. Since all the materials measured for this research were dielectrics, which have a permeability equal to that of free space, $\mu_r = 1.0$, this restriction was not an issue. The HP 8510 network analyzer was controlled by an external computer running SCAL-ALL, a menu-driven program which collects and stores the raw S-parameter data and automatically computes the material permittivity [15]. A constraint of the reflectometer set-up is that it requires an estimate of the permittivity

value so that it can converge on a solution. In addition, the material sample must be flush against the short, which may be difficult to achieve for thin, non-rigid samples. An advantage of using the HP 8510 is that it uses software time domain gating to reduce transmission line mismatch errors [5].

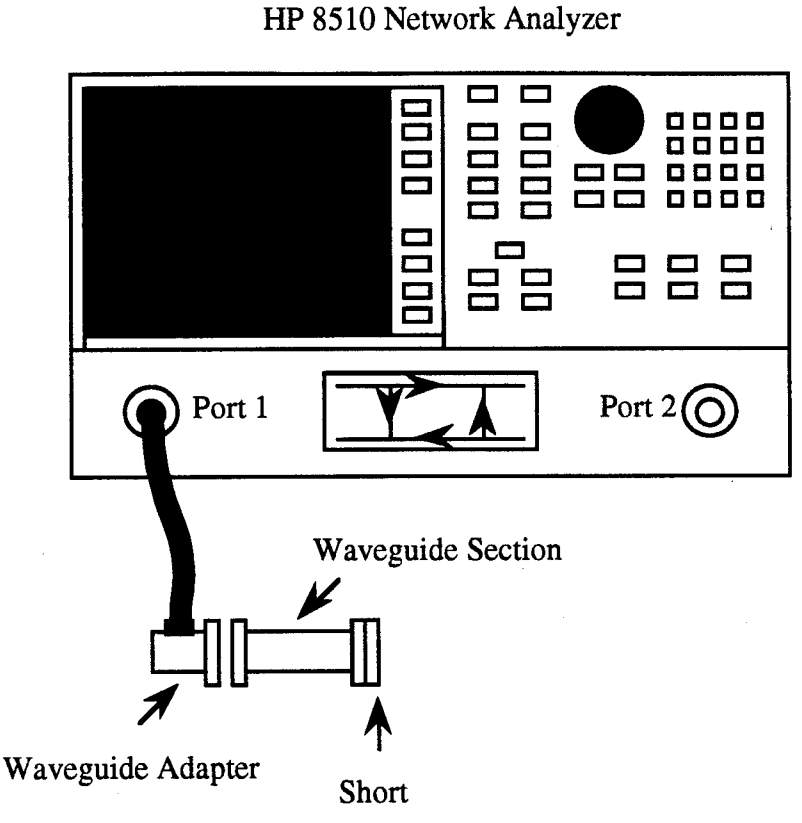

Figure 7. WL/XPN Waveguide Material Measurement Set-Up

The second rectangular waveguide set-up was available from the AFIT Engineering Labs, Wright-Patterson AFB, OH. Data from this set-up will heretofore be labeled AFIT data to identify its origin. The AFIT set-up, as shown in Figure 8, was a full two-port configuration. Because of this, it has the capability to measure both S_{11} and S_{21} to compute both the material permittivity and permeability. In this set-up, data had to be transferred from the HP 8720C to an external computer to calculate these characteristics.

The material sample must be placed in a sample holder which is a section of waveguide of the same thickness as the sample.

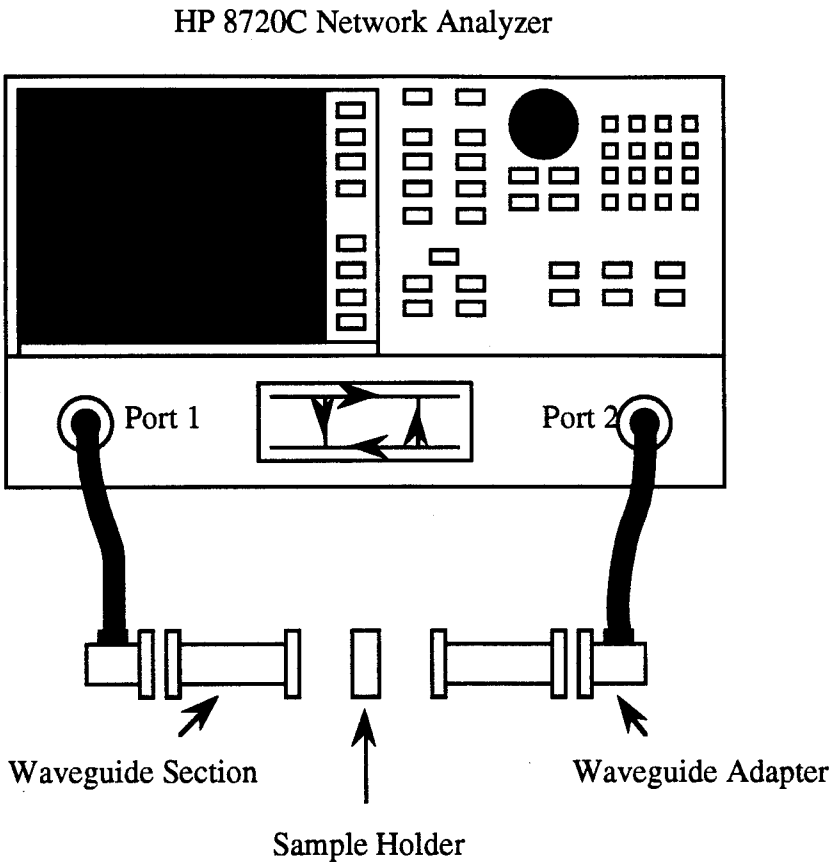

Figure 8. AFIT Waveguide Material Measurement Set-Up

Several procedures were followed to obtain accurate, representative data for the materials. To prevent a few bad measurements from unduly biasing the data, each material was measured twenty times in each set-up. To insure that the samples were representative of the material sheets they were cut from, two samples of each were included in these repetitive measurements. The measurements were performed over several days to minimize the effect of bad calibrations affecting large portions of the sample data. In addition, prior to each measurement, the sample was physically removed from the waveguide and holder to allow a certain measurement randomness that would expect to occur from slight

misalignment errors. No attempt was made to measure the same sample several times consecutively to obtain precise data -- this would have defeated the purpose of examining material characteristics measurement uncertainties.

Many measurement errors can occur that may invalidate data. The samples must be properly placed in the waveguide. The sample faces must be positioned perpendicular to the waveguide walls to insure normal incidence measurements. For the AFIT set-up, the sample holder should be the exact thickness of the sample to minimize phase shifts [5]. Lastly, the thickness of the material plays a role in acquiring accurate data. If the sample is more than $\lambda/2$ thick, where λ is the wavelength as measured in the material, then the solutions to the characteristic equations are not unique [8]. As mentioned, this requires either prior knowledge of the characteristics or else multiple sample measurements to isolate the correct solution. In addition, if sample losses are small, it may be difficult to isolate material losses for a thin sample. Thus, the sample should be between $\lambda/8$ and $\lambda/4$ in thickness [8]. The HP 8510 product note also indicates that large instrumentation errors may occur for thin or very low loss materials. Furthermore, it suggests a sample thickness of $\lambda/4$ and a loss tangent, which is the ratio $\varepsilon_r'' / \varepsilon_r'$, greater than 0.1 to minimize these errors [5]. All of these situations can contribute to erroneous waveguide material measurements.

3.2 Range RCS Measurements

To evaluate the accuracy of RCS predictions, it is usually helpful to know the exact theoretical value. When predicting the RCS of material coated objects, this is complicated by the uncertainty of the exact material characteristics. RCS measurements provide the best estimate of the exact RCS for material coated objects. Unfortunately, the RCS measurement accuracy must be qualified by the range equipment sensitivity, the range clutter, and the object placement precision.

The AFIT Engineering Laboratories RCS measurement range at Wright-Patterson AFB, OH, was used for RCS measurements because of its availability. It is a far field range in an anechoic chamber which can operate over the 6-18 GHz frequency range in a pulsed mode. The objects were mounted on a tapered metal ogive pylon placed 8.5 meters from the dual transmitting and receiving antenna. Far field constraints over the frequency range limit the object size to about 0.3 meters. The AFIT hardware is controlled by an external computer using Lintek's 4000 Series software [11]. Post processing of the measured data was performed on a VaxStation using WS post-processing software developed at Ohio State University [16].

Due to the scope of this research, measurements were only performed in the frequency domain over the 8-12 GHz band in 0.25 GHz increments. This allowed direct comparisons with RCS predictions which were limited by the X-band waveguide material measurements. To minimize unnecessary complications, measurements were only performed on flat square objects at normal incidence. This object shape was chosen for its simplified fabrication and RCS prediction and analysis requirements, raising the valid concern about making sure the flat object is perfectly perpendicular to the antenna. Any misalignments could cause sharp drops in the measured RCS since a flat object's RCS is dominated by the specular scattering pattern. To minimize these tilt errors, Knott suggests making the plate's dimensions less than 25λ [8]. For this reason, a six inch square was chosen as the plate's dimensions, which are well below 25λ in the 8-12 GHz range.

As with the material measurements, several procedures were followed to obtain accurate, representative data for the RCS measurements. To minimize isolated bad measurements from biasing all the data, each object was measured twenty times. The measurements were performed over several days to minimize the impact of bad system calibrations. In addition, prior to each measurement, the object was physically removed from the object support to allow a certain measurement randomness that would expect to

occur from slight misalignment errors. No attempt was made to measure the object's RCS several times consecutively to obtain precise data -- this would have defeated the purpose of examining measurement uncertainties. This doesn't mean that the object wasn't aligned properly each time. Each object was aligned with a plumb bob to minimize vertical tilt. In addition, its azimuth was positioned on the object's peak to minimize horizontal tilt. The purpose of these consistent alignment procedures was to reduce large RCS errors due to misalignment.

The first object measured was a six inch square PEC plate. Two reasons required these measurements. A square PEC plate has a theoretical RCS that can be calculated by various methods. Thus, the PEC plate measurements allow a quantitative analysis of the accuracy of the AFIT range and equipment. These measurements also permit a qualitative analysis of the object alignment procedure. Inconsistent alignments would be indicated by large variances in the RCS due to non-specular scattering patterns. The actual tilt that exists between the antenna and the object aligned with the plumb bob can be calculated using the physical optics equation for off normal incidence of a square PEC plate:

$$\sigma_{PEC} = \frac{4\pi A^2}{\lambda^2} \cos^2\theta \frac{\sin^2(kd \sin\theta \cos\phi)}{(kd \sin\theta \cos\phi)^2} \frac{\sin^2(kd \sin\theta \sin\phi)}{(kd \sin\theta \sin\phi)^2} \qquad (12)$$

where A is the area of the plate, λ is the wavelength, k is the wave number, d is the square's dimensions, θ is the vertical tilt, and ϕ is the horizontal tilt. Knowing the measured RCS at a certain frequency and knowing $\phi = 0$ from precise azimuth alignment on the RCS peak, the vertical tilt can be calculated.

A six inch square slab was cut from each of the three materials examined. Each of these square slabs was measured by itself (i.e. air backed) and as a coating to the square PEC plate (i.e. PEC backed). Thus, the effects of material characteristic uncertainties on RCS predictions could be evaluated for both cases. The VF-60 material required special

attention to its mounting. Since it was thin and flimsy, it was attached to a 1.5 cm thick styrofoam square slab. This styrofoam layer was maintained in the PEC backed measurements to create a Salisbury Screen type absorber. As identified in the material characteristics measurements, the AN-73 bronze side and the Rantec blue side were oriented to face the antenna.

Measured range data on the MRC nose radome test body shown in Figure 5 was provided by MRC. Although this data covered the 2-18 GHz frequency range, only the 8-12 GHz range was used due to the X-band waveguide restrictions on the material measurements. MRC measured three different test body configurations. Only the configuration which had Rantec absorber over the bulkhead was used because the other two configurations contained no materials evaluated for this research.

3.3 RCS Theoretical Predictions

As discussed in the last chapter, the equivalent reflection coefficient may be determined for a layered material from the material characteristics. The issue is how to apply this information to predict the RCS of a material coated object. To accomplish this, the theoretical RCS must be calculated as if the object were completely PEC. Although there are many methods capable of doing this accurately, this research used physical optics (PO) for its simplicity. The largest restriction on PO theory is that it is only accurate for electrically large objects. Since all measurements were done in X-band on six inch square objects, PO theory was a valid method.

At high frequencies, the RCS of a RAM coated object is:

$$\sigma = |\Gamma|^2 \sigma_{PEC} \tag{13}$$

where Γ is the field reflection coefficient and σ_{PEC} is the RCS of a PEC equivalent object in square meters [17]. Although not necessary for this research, Γ can be modified for

oblique incidence and vertical or horizontal polarizations [8]. Since only flat square plates are evaluated,

$$\sigma_{PEC} = \frac{4\pi A^2}{\lambda^2} \tag{14}$$

as defined by PO theory at normal incidence from Equation (12) in the last section.

The theoretical RCS was predicted for all materials and objects evaluated. The first object was a simple six inch square PEC plate over the X-band frequency range using Equation (14). Then for every material waveguide measurement made, the reflection coefficient was calculated using the method detailed in Chapter 2. Since three materials were measured twenty times with two different waveguide methods, a reflection coefficient was computed for each situation over the 8-12 GHz range in 0.25 GHz steps. Equation (13) was then applied to obtain the theoretical RCS for each of the objects evaluated. These included the VF-60/styrofoam, AN-73, and Rantec materials backed with and without the PEC square plate. As mentioned in the previous section, a styrofoam slab was kept behind the VF-60 material to give it structural rigidity and to simulate a Salisbury Screen absorber.

3.4 Xpatch Simulations

The final tasks performed involved Xpatch simulations of all the objects at normal incidence. These were done to evaluate Xpatch's ability to predict the RCS of RAM objects, given the material's characteristics and thickness, compared to RCS measurements and theoretical RCS predictions. Xpatch has several methods of modeling materials in its RCS prediction code. The method used in this research made use of material characteristics tables. The permittivity and permeability values of all these materials from 8-12 GHz in 0.25 steps were entered into the ramlib.d file in Xpatch.

Since only the frequency domain is evaluated, the program Xpatchf version 2.1 was run using the following steps: 1) a CAD model was created of a six inch square plate;

2) this plate was identified as being PEC only, layered materials with air backing, or layered materials with PEC backing; 3) if the plate consisted of materials, the number of layers was identified along with each layer's thickness and the material characteristics in the ramlib.d file; and 4) the program then evaluated the object at normal incidence [10]. This procedure was performed for a PEC plate, and each of the VF-60/styrofoam, AN-73, and Rantec materials backed both with and without the PEC plate.

The last Xpatch simulations were performed on the MRC test body. Although MRC performed simulations on three object configurations, only the Rantec absorber over bulkhead was repeated in this research. The other two configurations contained no materials evaluated as part of this research. Since the material data was limited to X-band, the simulations were only run from 8-12 GHz. Other than this restriction, the identical simulations were run on the MRC test body for the following cases: 30° incidence for vertical polarization (V-pol), 30° incidence for horizontal polarization (H-pol), 75° incidence for V-pol, and 75° incidence for H-pol. Qualitative comparisons of these simulations with measured material characteristics evaluated Xpatch's ability to accurately predict a complicated material coated object.

3.5 Data Analysis Techniques

Ideally, an evaluation of the accuracy and precision of RCS measurements and predictions would compare the data to exact analytical solutions. Unfortunately, the only applicable exact solution in this research was for the RCS of a square PEC plate. All other exact solutions would require exact, true values of the material characteristics. Since there was no identifiable true value associated with the material characteristics, the mean of the measured material data was adopted as the best estimate of the true value. This mean was called the sample mean since it depended on a sample set of measurements [12].

The measured material characteristics were susceptible to measurement errors. The part of the random error which occurred during repeated measurements in immediate succession and under constant conditions is called the replication error. Given the sample mean of the repeated measurements, the sample standard deviation of the replication error defined the root mean square (RMS) deviation from the sample mean and was defined as:

$$\sigma_s = \sqrt{\frac{\sum_{i=1}^{N} (x_i - \overline{x})^2}{N - 1}} \tag{15}$$

where σ_s was the sample standard deviation, x_i was a data point, $\overline{x}$ was the sample mean, and N was the total number of data points [12]. These two statistical values described the best estimate of the true value for accuracy and the deviation of the trials for precision of the measured material data. These values were also used in describing the RCS measurements, theoretical predictions, and Xpatch simulations.

To quantitatively compare the RCS measurements, predictions, and Xpatch simulations, the RMS error was used to evaluate the average error. RMS error was defined by:

$$\text{RMSE} = \sqrt{\frac{\sum_{i=1}^{N} (x_i - y_i)^2}{N}} \tag{16}$$

where x_i and y_i were the compared data points. To clarify the main difference between the sample standard deviation and the RMSE, the sample standard deviation applied to the analysis of data to its own mean. RMSE, on the other hand, applied to the comparison of data to another measured or calculated value.

The RMS error was used in two different ways in this research. The first was an overall agreement of two data sets across the X-band frequency range. In this case, x_i and

y_i were the data points for a frequency at increment i, and N was the total number of frequency increments. This type of error analysis provided a single numerical value to describe the total average error for the data sets. For this reason, this error was labeled as Total RMSE to identify how the analysis was done.

The second method of RMS error analysis compared data points from one data set to the sample mean of the other data set at a specified frequency. In this case, x_i was the set of data points in the first data set, y_i was the sample mean of the second data set, and N was the number of trials performed at the specified frequency. This type of error analysis provided an indication of how the two data sets varied across the frequency range. For this reason, this error analysis was labeled as Freq RMSE to identify how the analysis was done.

The primary focus of this research was to evaluate how uncertainties or variations in material characteristics measurements influenced the RCS of a material coated object. Ideally, this would have involved identifying an average material permittivity and permeability and statistically varying each of them to evaluate the RCS prediction fluctuations. This procedure was complicated by several factors.

One factor was that RCS variations may be dependent on the magnitude of both the material characteristics and the RCS value. Another factor was that the RCS prediction process was non-linear. Thus, a larger material variation may or may not have lead to a larger RCS variation. Lastly, related to this non-linear situation, was the fact that the permittivity and permeability were complex numbers in which the real parts were not independent of the imaginary parts. The combination of these factors caused a pure statistical approach to an RCS variations analysis to be unfeasible.

Instead of statistically varying the material characteristics, this research evaluated the variations of actual material characteristics measurements, applied the inseparable real

and imaginary parts to RCS prediction equations, and evaluated the total RCS prediction variations. The Xpatch simulations were done in the same manner.

4. Results and Analysis

This chapter presents the measurement, prediction, and simulation data collected in this research. It is comprised of five sections. The first section presents the material characteristic measurement's results. The second section reports on the measured RCS data and qualifies the accuracy of the range from the PEC plate measurements. The third section presents and analyzes the accuracy of the RCS predictions and Xpatch simulations using the measured material data compared to the RCS measurements. The fourth section presents and analyzes the precision of the RCS predictions and Xpatch simulations using the measured material data compared to the sample means. The fifth section compares Xpatch simulations of the MRC test body using MRC and XPN measured material data. Due to the large volume of data acquired, only the most representative examples were chosen for presentation. The complete set of results is compiled in the appendices.

4.1 Material Characteristics Measurements

This section presents the results obtained from measuring the characteristics of the material samples using the X-band waveguide transmission line set-ups. Possible indications of measurement errors are provided for each material. Since there was no true value of the characteristics, the measurement accuracy cannot be directly deduced. The accuracy of the measurements plays a role in the RCS predictions so it is discussed in the section on RCS predictions accuracy. The impact of variations in the measurements is discussed in the section on RCS prediction variations.

The characteristics of the VF-60 material were measured twenty times with both the XPN and AFIT X-band waveguide set-ups. The sample means over 8-12 GHz are shown in Figure 9. To evaluate the measurement accuracies, the VF-60 specification provided an approximate relative dielectric constant of 37.0 at 8.6 GHz [3]. The XPN measurements

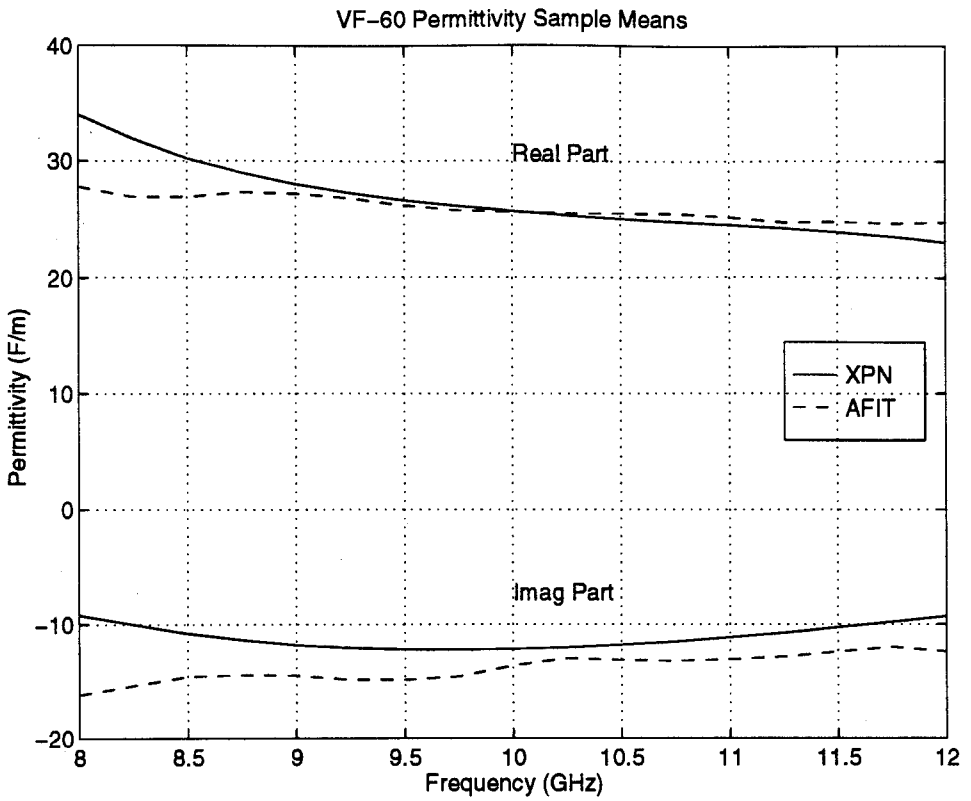

Figure 9. Relative VF-60 Permittivity Sample Means for XPN and AFIT Waveguide Measurements

averaged about 30 and the AFIT measurements averaged about 27 at this frequency. There were fairly large discrepancies between the XPN and AFIT material measurements as seen in Figure 9 as well as between them and the specification at 8.6 GHz. The AFIT set-up measured the permeability as well as the permittivity. The relative permeability was measured to be about 1.0 which was consistent with the expected value for a dielectric.

As discussed in the last chapter, waveguide measurements were less prone to errors if the material samples were between one-eighth and one-fourth wavelengths thick and if the loss tangent was less than 0.1. The material wavelength was calculated from the VF-60 material characteristics sample means. It was determined that the sample thickness of 0.15 cm was greater than one-fourth wavelength at frequencies above 9.0 GHz for both set-ups,

so less confidence could be placed in the accuracy of this data. The loss tangent, however, never dropped below the 0.1 threshold so errors from this restriction were not an issue.

The characteristics of the AN-73 material were measured twenty times with both the XPN and AFIT X-band waveguide set-ups. The sample means over 8-12 GHz from the two techniques are shown in Figure 10. Since the AN-73 material was measured with the wrong side up, its specification can't be used to evaluate the accuracy. Readily seen from the graph are the discrepancies in the results from the two measurement set-ups. In addition, large errors were associated with the permeability measured by the AFIT set-up. Figure 11 shows the real part was measured well below 1.0 and the imaginary part varied significantly from zero. Since both of these cases are not possible for a dielectric, no confidence can be put into the accuracy of the AFIT measured data for the AN-73 material.

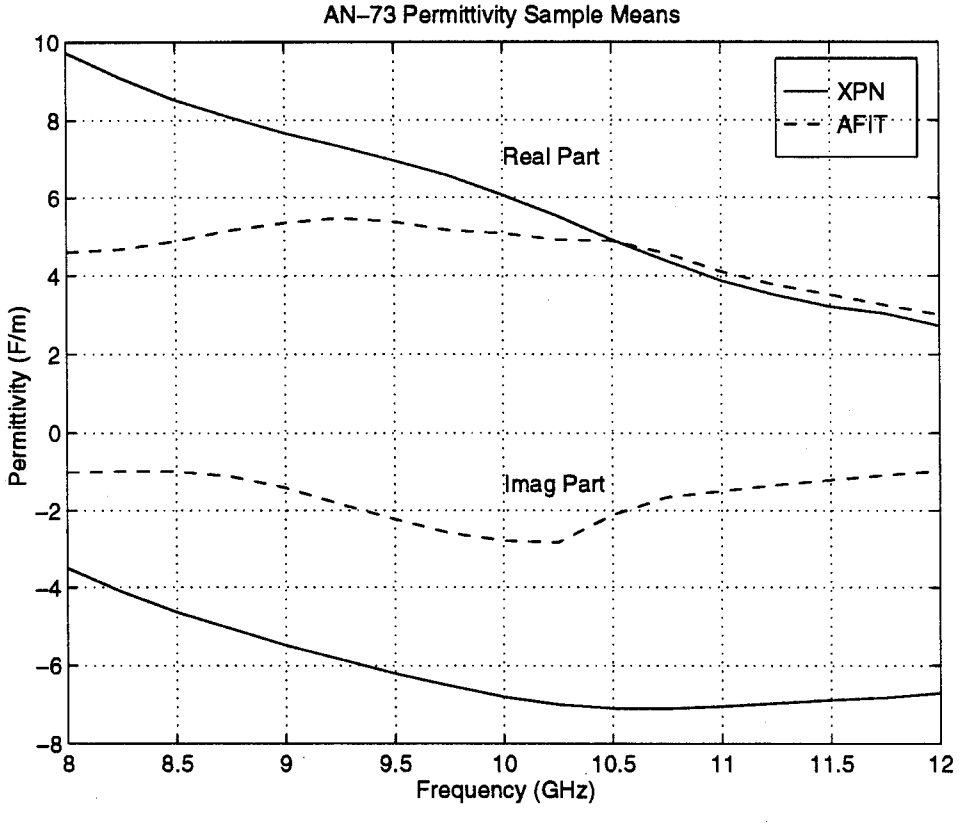

Figure 10. Relative AN-73 Permittivity Sample Means for XPN and AFIT Waveguide Measurements

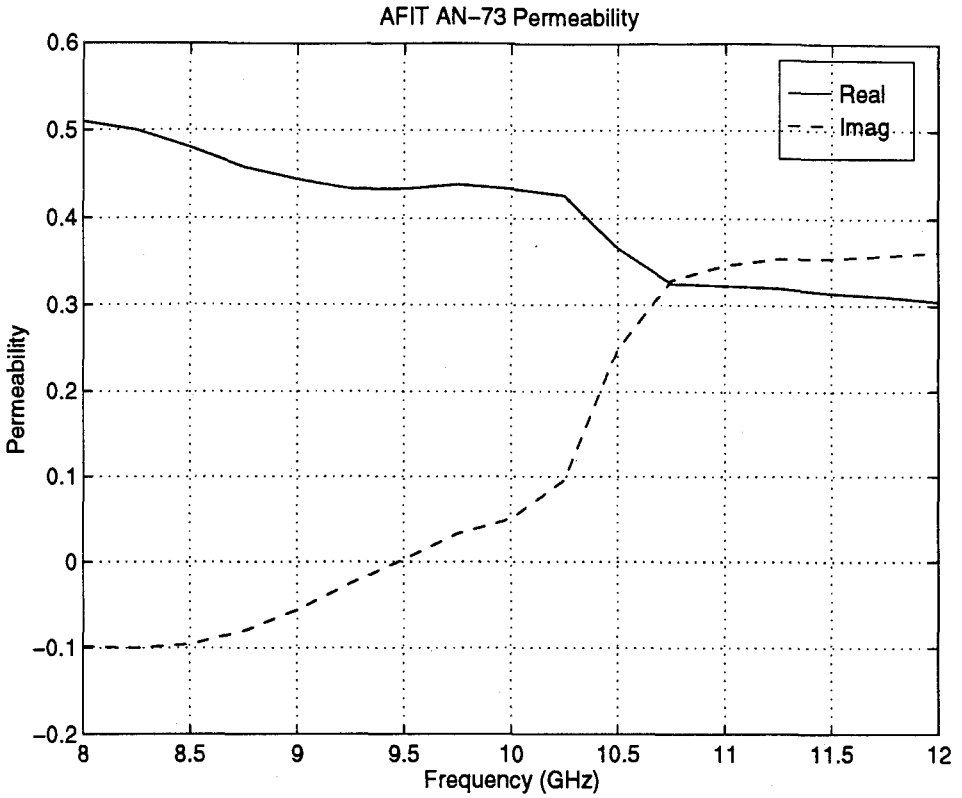

Figure 11. Relative AN-73 Permeability Sample Mean for AFIT Waveguide Measurements

The material wavelength was calculated from the AN-73 material characteristics sample means. It was determined that the sample thickness of 1.0 cm was between one-half and one wavelength for both set-ups. Thus, the measured characteristics may be in error due to multiple modes existing in the sample. The loss tangent, however, never dropped below the 0.1 threshold so errors from this restriction were not an issue.

The characteristics of the Rantec material were measured twenty times with both the XPN and AFIT X-band waveguide set-ups. The sample means over 8-12 GHz from the two techniques are shown in Figure 12. No material specification was available on the Rantec material to directly evaluate the accuracy of the measurements. Troubling results were obtained from the AFIT measurements. Between 8.0 and 9.5 GHz, the relative permittivity real part was measured to be below 1.0; and, between 9.25 and 10.25 GHz,

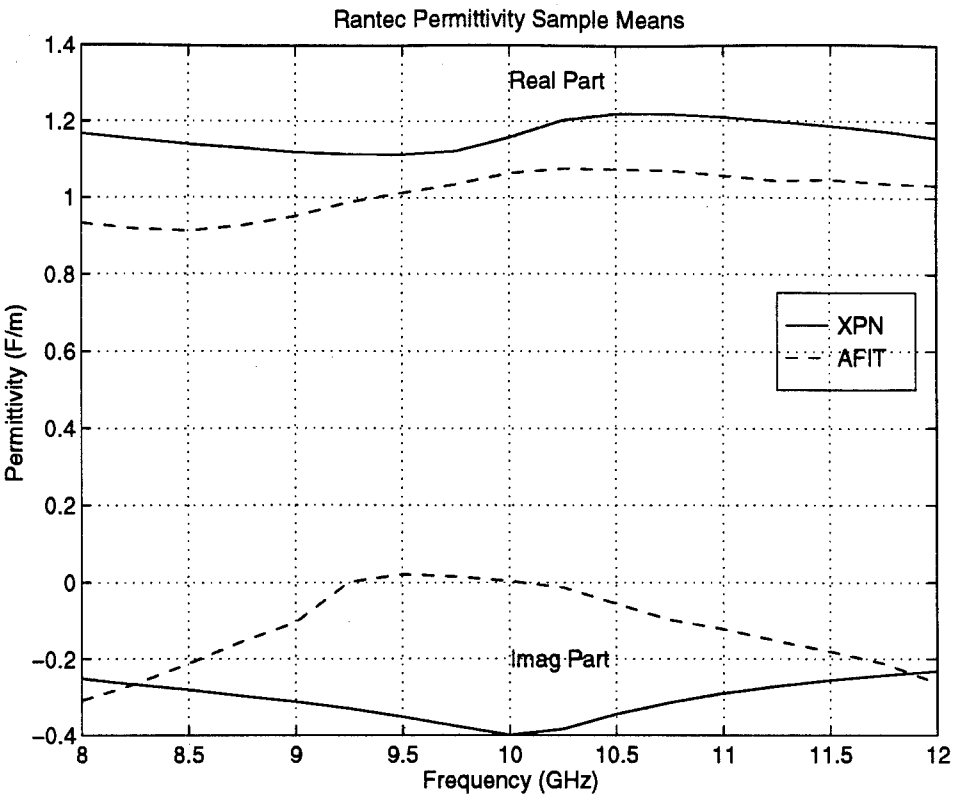

Figure 12. Relative RANTEC Permittivity Sample Means for XPN and AFIT Waveguide Measurements

the imaginary part was measured to be positive. In addition, as seen in Figure 13, the permeability real part was measured below 1.0 and the imaginary part was measured to be positive above 9.0 GHz. Since these situations are not physically possible, no confidence can be put into the accuracy of the AFIT measured data for the Rantec material.

The Rantec material wavelength was calculated from the material characteristics sample means. As with the AN-73 material, the sample thickness of 2.0 cm was between one-half and one wavelength for both set-ups. Thus, the measured characteristics may be in error due to multiple modes existing in the sample. With the XPN set-up, the loss tangent never dropped below 0.1 so errors from this restriction were not an issue. Due to the erroneous AFIT permittivity values, however, the AFIT Rantec loss tangent did drop below the 0.1 threshold between 9.0 and 10.75 GHz.

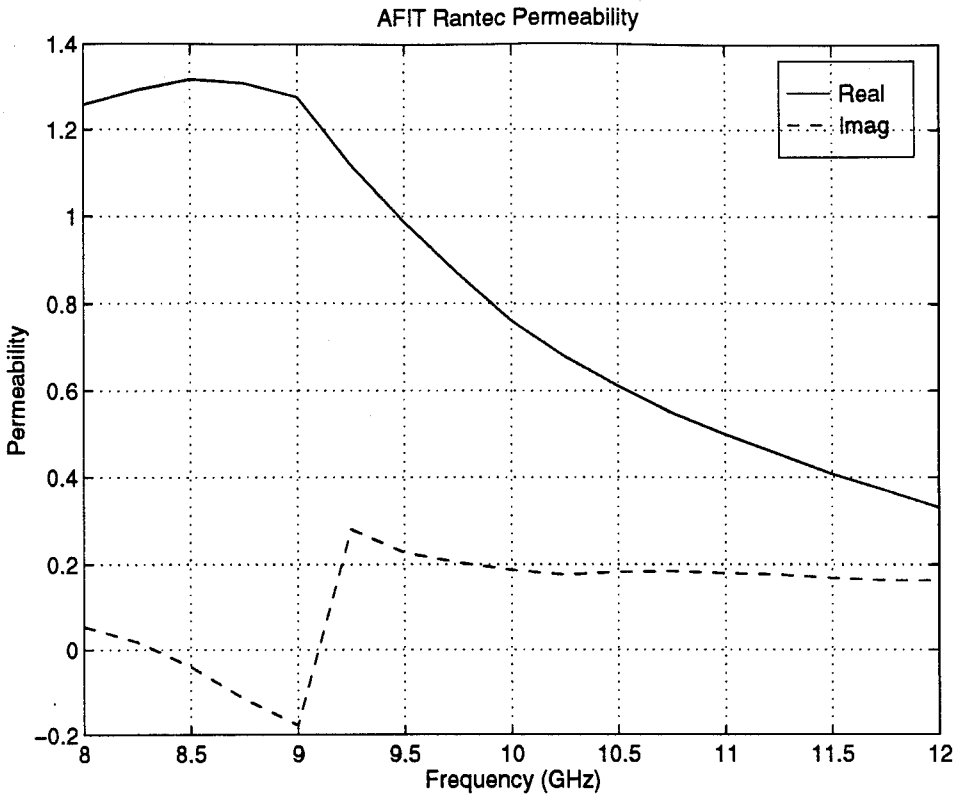

Figure 13. Relative RANTEC Permeability Sample Mean for AFIT Waveguide Measurements

Several conclusions can be made about the material characteristics measurements. Since the AFIT set-up was for a full two port network measurement, it was susceptible to errors in both its S_{11} and S_{21} measurements which were used to calculate the material's permittivity and permeability. In this research, only dielectrics were measured so the permeability was ideally that of free space with $\mu_r = 1.0$. For the homogeneous, thin VF-60 material, the permeability real part was measured to be about 1.0 and the imaginary part was about zero across the frequency range. For the inhomogeneous, three layer AN-73 and Rantec foams, however, the permeability real part was measured to be less than 1.0 and the imaginary part was non-zero and even positive which is not physically possible. It therefore appears that very little confidence can be placed in the AFIT set-up measurements of these two materials. Although the XPN set-up should have been be susceptible as well,

these errors may have been less of an impact on S_{11} only measurements. Its ability to time gate the data to reduce transmission line mismatch errors may also have contributed to more accurate results from the XPN set-up. The best way to minimize multiple mode errors is to use thinner samples. Since the foam materials were comprised of three separate layers, each layer needed to be measured individually and then the effective material characteristics determined from the resulting data. This was not done as a part of this research.

Table 1 shows an overall analysis of the measurements. It shows the average Total RMSE and the average correlation of the individual permittivity measurements compared to the sample mean. The largest RMS errors occurred for the VF-60 material which had the largest permittivity values. In general, the RMS errors equated to about ten to twenty percent of the materials' permittivities, both real and imaginary parts. The measured Rantec permittivities were very correlated with their sample means. The VF-60 and AN-73 materials had a higher correlation among their real parts than among their imaginary parts.

Table 1

Summary of Measured Relative Permittivity RMS Errors and Correlations

	Permittivity Real Part		Permittivity Imaginary Part	
	RMSE	Corr Coef (%)	RMSE	Corr Coef (%)
XPN Set-Up				
VF-60	2.895	99.6	1.762	91.6
AN-73	0.722	99.5	0.377	96.6
Rantec	0.012	99.1	0.025	99.1
AFIT Set-Up				
VF-60	1.514	97.4	3.022	90.2
AN-73	0.271	97.1	0.263	91.3
Rantec	0.019	99.6	0.024	99.7

4.2 Range RCS Measurements

This section presents the results obtained from measuring the RCS of each material backed both with and without the square PEC plate. The accuracy of the range was determined from the RCS measurements of the square PEC plate. These results play an important role in evaluating the accuracy of the RCS predictions.

The RCS of a six inch square PEC plate was measured twenty times in the AFIT RCS range. The sample mean of these measurements in comparison to the physical optics theoretical value using Equation (14) is shown in Figure 14. This plot shows a discrepancy of about 0.5 dB between the measured and ideal value. It was assumed that this error was primarily due to plate tilt. Using Equation (12) and assuming that the horizontal tilt was zeroed from azimuth alignment, this 0.5 dB error equated to a 1.05° vertical tilt. Considering that the plate was aligned with a plumb bob to be precisely perpendicular to the ground, the best explanation of this tilt was that the range antenna was not precisely parallel to the ground, but had a slight vertical tilt in its beam pattern.

Table 2 summarizes all the range measurements using Total RMSE and correlation with the sample mean. The above tilt description explains why the sample mean may be offset from the ideal, but it does not explain the large average sample standard deviations of all the RCS measurements shown in Table 2. Through observation, it was found that the largest factor in RCS measurement precision was system calibration error. In this research, the system was calibrated for every ten measurements, about once each hour. It was noticed that during this time, the RCS measurements tended to drift lower in magnitude by as much as 0.5 dB. Due to the number of measurements made in this research, it was deemed impractical to perform a system calibration prior to each measurement to reduce this drift. In addition, each object was measured five times on four separate days and system calibrations across this time period predictably had some associated precision error.

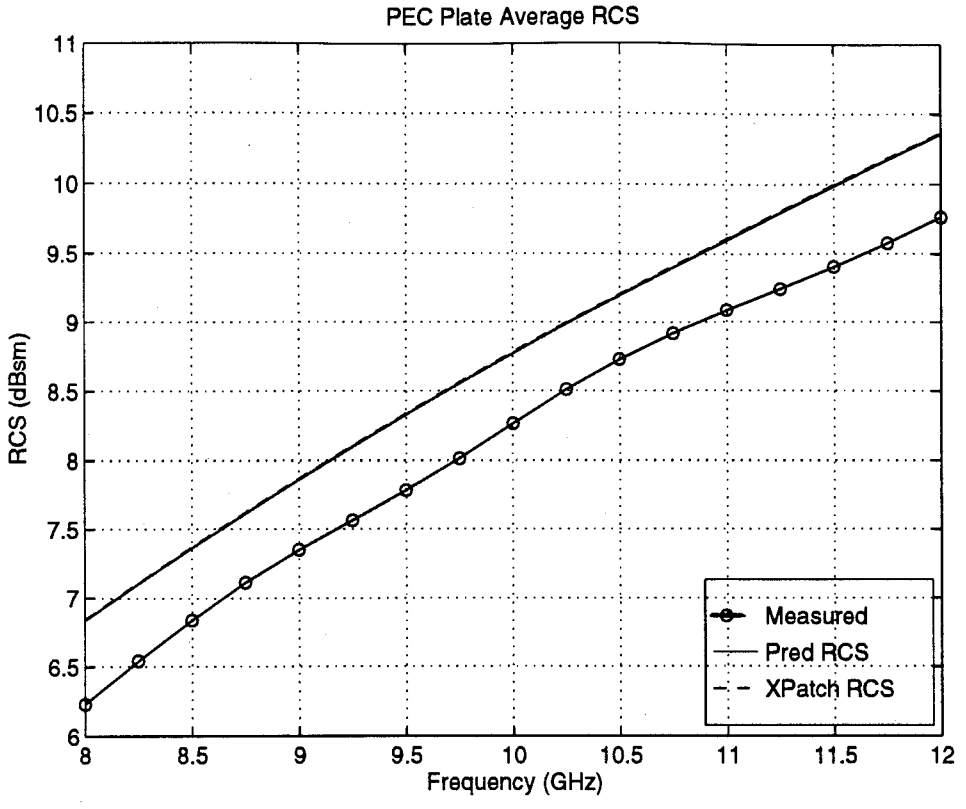

Figure 14. RCS Prediction and Measured Sample Means for Six Inch Square PEC Plate

Table 2 shows exceptional correlations of the individual measurements with their sample means. There were two exceptions. The VF-60 material over the PEC plate was a semi-Salisbury screen configuration which had a RCS half-wavelength null at about 9.5 GHz. The null's bandwidth and magnitude tended to be slightly inconsistent from measurement to measurement. The second exception was the Rantec material over the PEC plate. The largest contribution to the correlation errors was from a varying plate tilt or from improper placement of the material over the PEC plate. The first error was reduced by the plumb bob alignment. The second error was reduced by examining the target prior to each measurement. Thus, the results in Table 2 confirm that the RCS measurements were precise except for a drifting bias from the tilt and calibration errors.

Table 2

Summary of Measured RCS RMS Errors and Correlations

	RCS Measurements	
	RMSE (dB)	Corr Coef (%)
PEC Plate	0.155	99.9
Air Backed Material		
VF-60	0.101	99.9
AN-73	0.272	99.9
Rantec	0.428	99.9
PEC Backed Material		
VF-60	0.167	99.0
AN-73	0.411	99.9
Rantec	0.417	96.1

The RCS measurements provided the best estimate of the true RCS value of the objects. The range accuracy was evaluated to be good, having only a 0.5 dB discrepancy for a six inch square PEC plate. The largest error source was the varying calibration bias. Other alignment errors were not deemed significant as supported by the high correlation of the data to the sample means. The confidence in the measured RCS plays an important role in evaluating the accuracy of RCS predictions for objects which have no theoretical RCS values.

4.3 RCS Prediction Accuracy

As previously mentioned, RCS measurements are the best estimates of the true RCS of material coated objects. Thus, the accuracy of the RCS predictions and Xpatch simulations using measured material characteristics were compared to the RCS

measurements performed in the AFIT range. Since the AFIT range was found to have about a 0.5 dB tilt loss in the PEC square plate measurements, this bias-like error was taken into account in the accuracy evaluations. Tables 3(a) and 3(b) summarize all the data acquired by presenting the Total RMS error and correlation between the RCS predictions, Xpatch simulations, and RCS measurements using the XPN and AFIT measured material characteristics. Since the Xpatch simulations were very similar to the RCS predictions, only large discrepancies are pointed out in this discussion.

Table 3(a)

Summary of Predicted and Xpatch RCS RMS Errors and Correlations Compared to RCS Measurements Using XPN Material Characteristics

	Predicted RCS		Xpatch RCS	
	RMSE (dB)	Corr Coef (%)	RMSE (dB)	Corr Coef (%)
Air Backed Material				
VF-60	0.723	99.0	0.730	99.0
AN-73	0.533	97.6	0.544	98.0
Rantec	1.746	99.1	1.790	99.1
PEC Backed Material				
VF-60	1.025	89.2	1.105	90.1
AN-73	1.484	99.3	1.426	99.0
Rantec	1.880	17.8	1.747	23.4

Table 3(b)

Summary of Predicted and Xpatch RCS RMS Errors and Correlations Compared to RCS Measurements Using AFIT Material Characteristics

	Predicted RCS		Xpatch RCS	
	RMSE (dB)	Corr Coef (%)	RMSE (dB)	Corr Coef (%)
Air Backed Material				
VF-60	0.838	99.8	0.844	99.8
AN-73	2.527	70.2	2.408	68.8
Rantec	6.467	7.0	7.408	6.8
PEC Backed Material				
VF-60	1.386	91.5	1.458	92.4
AN-73	5.890	75.1	6.251	71.2
Rantec	7.284	31.4	6.307	26.7

The first object analyzed was the VF-60 material backed by a 1.5 cm styrofoam spacer. Figure 15 shows the predicted RCS sample mean using the XPN measured material characteristics to be between 0.75 and 1.3 dB above the measured sample mean. This discrepancy was primarily due to the range plate tilt. Very similar results were obtained using the AFIT measured material characteristics. Tables 3(a) and 3(b) show the average magnitude of this error across the frequency band using both XPN and AFIT material data, which approximates a bias as confirmed by the high correlation.

The second object analyzed was the VF-60 material backed by the styrofoam slab and the PEC plate. Figure 16 shows the predicted RCS sample mean using the XPN measured material data to be consistent with the measured RCS sample mean. The larger RMS errors and lower correlations seen in Table 3(a) are associated with the RCS

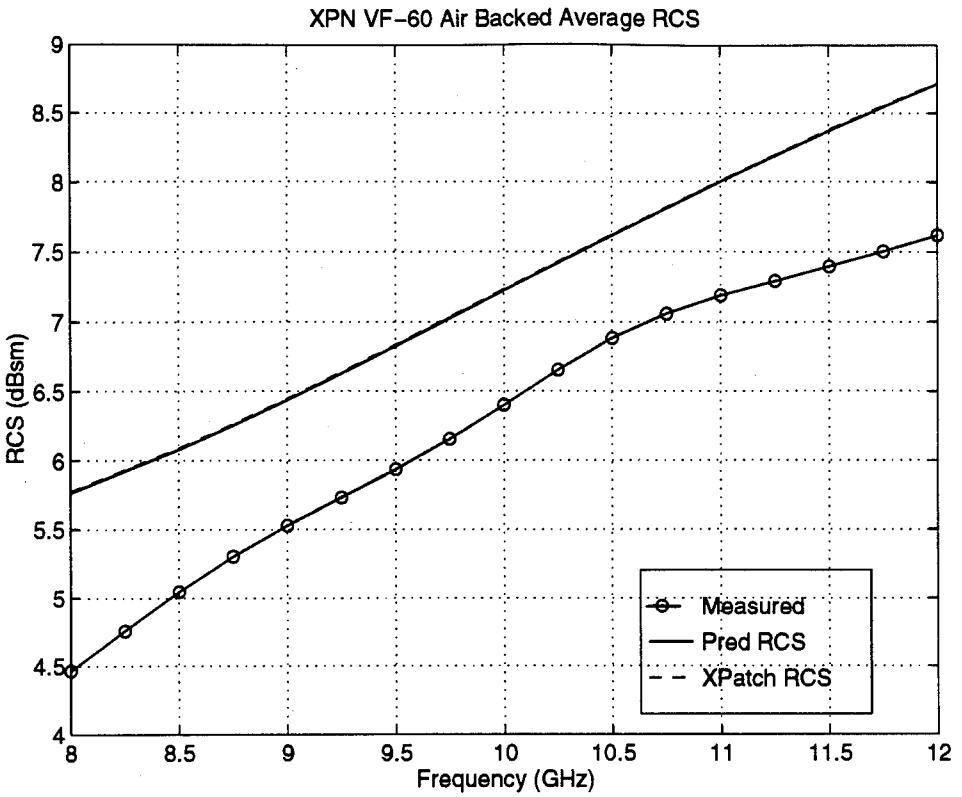

Figure 15. RCS Prediction and Measured Sample Means for Air Backed VF-60 Material Using XPN Measured Material Characteristics

measurements unable to pick up the sharpness of the predicted null. Very similar results were obtained using the AFIT measured material characteristics.

Referring to Figure 9, the permittivity sample means measured by these two set-ups were not equivalent. The fact that the XPN and AFIT RCS predictions were similar for both the air backed and PEC backed VF-60 materials is an interesting phenomenon.

The third object analyzed was the AN-73 material backed by air. Figure 17 shows comparable results of the measured and predicted RCS sample means using XPN material data. Table 3(a) shows a low Total RMS error and a high correlation. Unfortunately, these results are compromised by the fact that the RCS prediction is below the RCS measurements at frequencies up to 9.75 GHz. Due to the range plate tilt, the measured

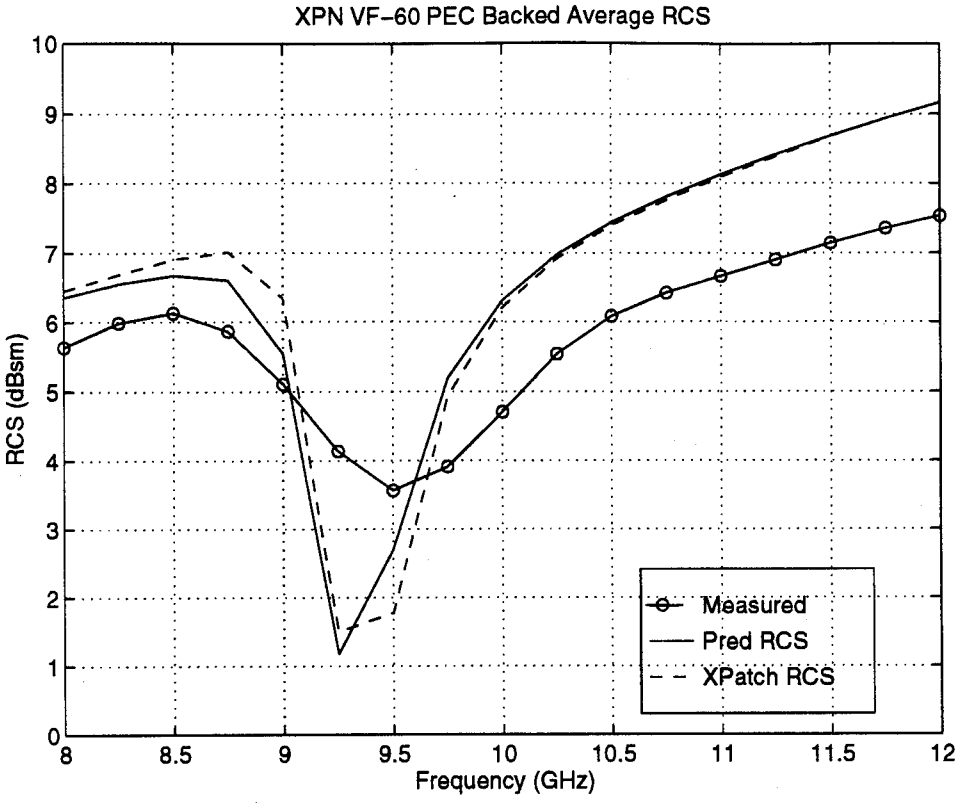

Figure 16. RCS Prediction and Measured Sample Means for PEC Backed VF-60 Material Using XPN Measured Material Characteristics

RCS should be at least 0.5 dB below the predicted RCS as was seen in the VF-60 results. The results obtained using the AFIT material data were even worse as seen in Table 3(b).

The fourth object analyzed was the AN-73 material backed by the PEC plate. As with the air backed AN-73 material, the RCS predictions using the XPN material data were between 0.75 and 1.75 dB below the RCS measurements. This again, invalidates the data in Table 3(a), which appears good, because the inherent tilt in the RCS range should have resulted in a lower RCS measurement compared to the prediction. Using the AFIT material data, the same situation arose in addition to the data being poorly correlated.

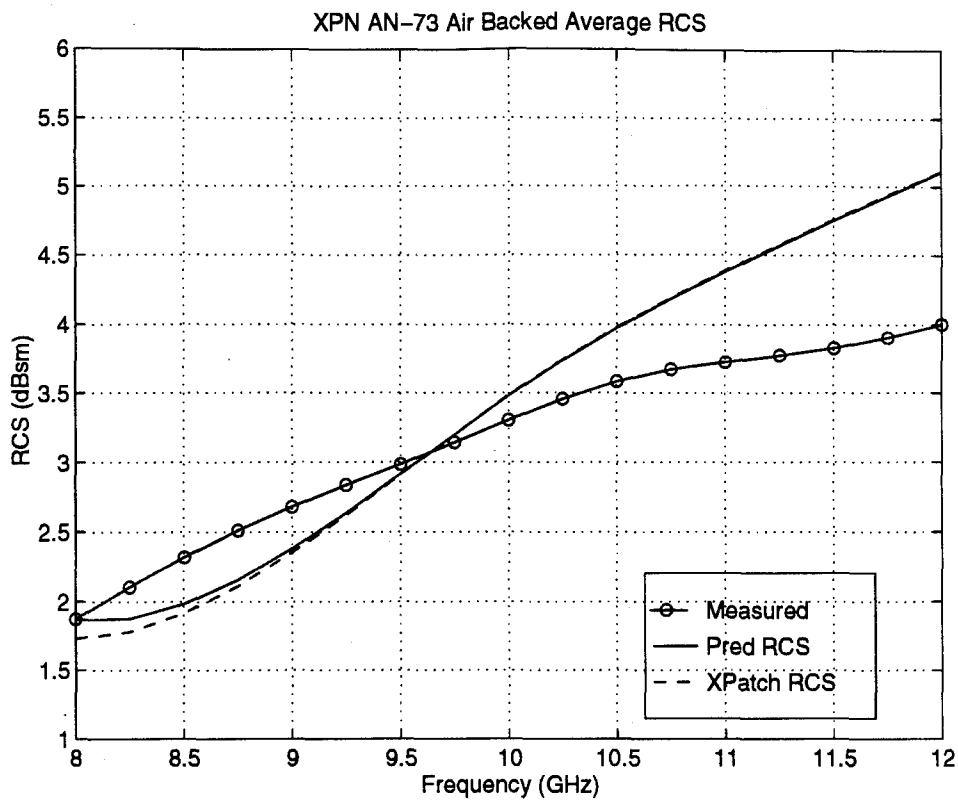

Figure 17. RCS Prediction and Measured Sample Means for Air Backed AN-73 Material Using XPN Measured Material Characteristics

The fact that the XPN predictions were inconsistent with the known RCS range measurement errors placed suspicion on the accuracy of the XPN material characteristics measurements. The AFIT material data, already suspect due to invalid permeability measurements, also produced inaccurate RCS predictions.

The fifth object analyzed was the Rantec material backed by air. Figure 18 shows the measured RCS sample mean compared to the predicted RCS sample mean using the XPN material data. As Table 3(a) indicates, there was very good correlation of the data, but the Total RMS error was high. In addition, although the measured RCS data was below the predicted RCS as it should have been, the magnitude of this error was not consistent across the frequency range. The results obtained using the AFIT material data were poor.

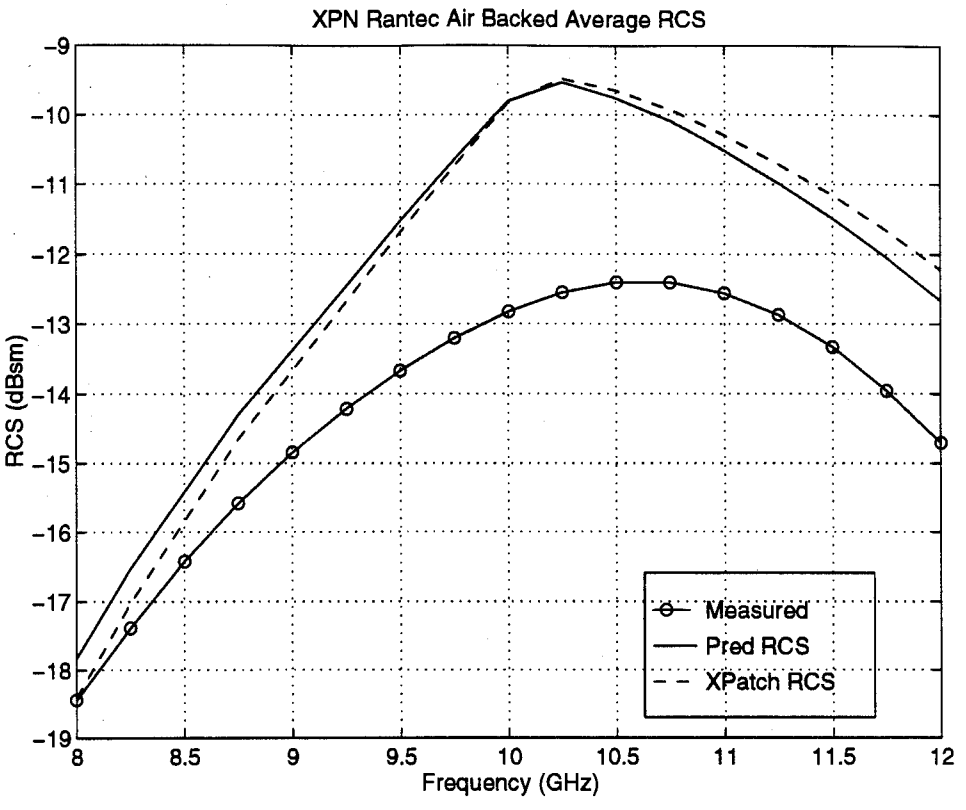

Figure 18. RCS Prediction and Measured Sample Means for Air Backed RANTEC Material Using XPN Measured Material Characteristics

The sixth object analyzed was the Rantec material backed by the PEC plate. In the case of using XPN material data, the Total RMS error was high and the correlation was low. In fact, the predicted RCS data showed a null at about 10.25 GHz which was nonexistent in the measured RCS data. Again, the results obtained using the AFIT material data were poor.

Although the air backed RCS predictions using XPN data looked good, the inconsistent results for the PEC backed RCS indicated that the XPN Rantec material characteristics measurements were inaccurate. The AFIT material data, already suspect due to invalid permeability measurements, produced very poor RCS predictions. A large

discrepancy between the RCS predictions and the Xpatch simulations occurred for the AFIT material data backed by the PEC plate between 9.25 and 10.25 GHz. The AFIT waveguide set-up measured positive permittivity imaginary parts in this frequency range. Xpatch automatically set the material signs to positive for the real part and negative for the imaginary part. It was unable to predict the RCS properly using the invalid data.

It appeared that the XPN and AFIT waveguide set-ups were able to accurately measure the material characteristics of the thin VF-60 material. Though the measured permittivities were different from each set-up, the RCS predictions were quite similar. Neither set-up was able to accurately measure the thick AN-73 and Rantec three layer foam materials. Poor correlations of RCS predictions with RCS measurements were the greatest indication of this. Inconsistencies with known AFIT range errors also placed suspicion on the material data accuracy.

4.4 RCS Prediction Variations

Although the accuracy of some material characteristics measurements were in question, the evaluation of how the material characteristics variations affected the RCS predictions was still valid. This evaluation was independent of the comparisons to RCS measurements. The material characteristics measurements, RCS predictions, and Xpatch simulations were statistically evaluated using Freq RMS error and correlation indicators. The results were then evaluated to identify trends. It was determined that variations in the imaginary part of the permittivity and the magnitude of the reflection coefficient had the largest influences on the RCS variations. To demonstrate these relationships, the correlation of RCS prediction variations with the imaginary part of the permittivity variations and the reflection coefficient magnitude are presented in Tables 4(a) and 4(b) for XPN and AFIT measured material characteristics respectively.

Table 4(a)

Summary of Correlations of Predicted and Xpatch RCS Variations to Permittivity Imaginary Part Variations and Reflection Coefficient Magnitude Using XPN Measured Material Characteristics

	Predicted RCS Variations		Xpatch RCS Variations	
	Corr to ε_r'' Var (%)	Corr to Refl Coeff (%)	Corr to ε_r''	Corr to Refl Coeff (%)
Air Backed Material				
VF-60	55.5	-97.3	55.8	-97.2
AN-73	77.9	-59.6	85.2	-75.0
Rantec	88.1	61.9	88.3	61.7
PEC Backed Material				
VF-60	-33.9	-95.0	-33.2	-94.7
AN-73	22.2	-97.8	17.4	-97.1
Rantec	78.6	-88.2	75.4	-89.6

The first object analyzed was the VF-60 material backed by the styrofoam layer. Large relative permittivity variations of up to 4.0 from both the XPN and AFIT waveguide set-ups resulted in small RCS variations of less than 0.2 dB. From Table 4(a) for the XPN set-up, there was a high negative correlation of RCS variations with the reflection coefficient. For the AFIT data, however, there was a high positive correlation of RCS variations with the variations of the imaginary part of the relative permittivity.

Table 4(b)

Summary of Correlations of Predicted and Xpatch RCS Variations to Permittivity Imaginary Part Variations and Reflection Coefficient Magnitude Using AFIT Measured Material Characteristics

	Predicted RCS Variati		Xpatch RCS Variations	
	Corr to ε_r'' Var (%)	Corr to Refl Coeff (%)	Corr to ε_r'' Var (%)	Corr to Refl Coeff (%)
Air Backed Material				
VF-60	96.4	-79.8	96.4	-79.8
	-61.5	-76.5	-56.5	-65.8
Rantec	83.9	-84.8	84.7	-84.7
PEC Backed Material				
VF-60	22.8	-89.9	18.3	-82.1
AN-73	-14.9	-60.7	-11.4	-51.0
Rantec	78.6	84.8	75.4	11.5

The second object analyzed was the VF-60 material backed by the styrofoam layer and the PEC plate. Larger RCS variations of up to 1.0 dB occurred at the null in the RCS predictions for both the XPN and AFIT set-ups. It appeared that slight material variations at this frequency were magnified by the changing reflection coefficient. Tables 4(a) and 4(b) confirm this with high negative correlations of the RCS variations with the reflection coefficient magnitude. For the XPN data, this relationship is shown in Figure 19 of the variations and in Figure 20 of the reflection coefficient.

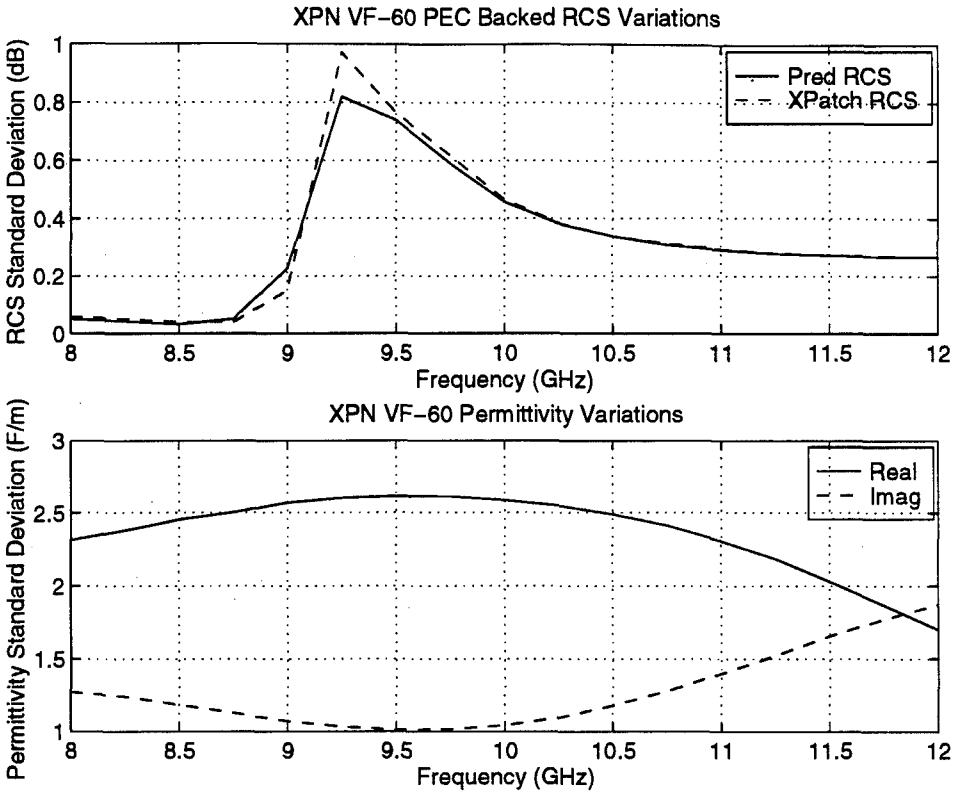

Figure 19. XPN VF-60 Permittivity Measurement Variations and RCS Prediction Variations for PEC Backed VF-60 Material

The third object analyzed was the AN-73 material backed by air. For the XPN data, permittivity variations of up to 1.0 caused relatively small RCS variations of less than 0.15 dB. In addition, as shown in Table 4(a), there were correlations of RCS variations with the permittivity variations, shown in Figure 21, and slightly with the reflection coefficient, shown in Figure 22. For the AFIT data, the RCS variations had similar correlation with the reflection coefficient, but poor correlation with the permittivity variations.

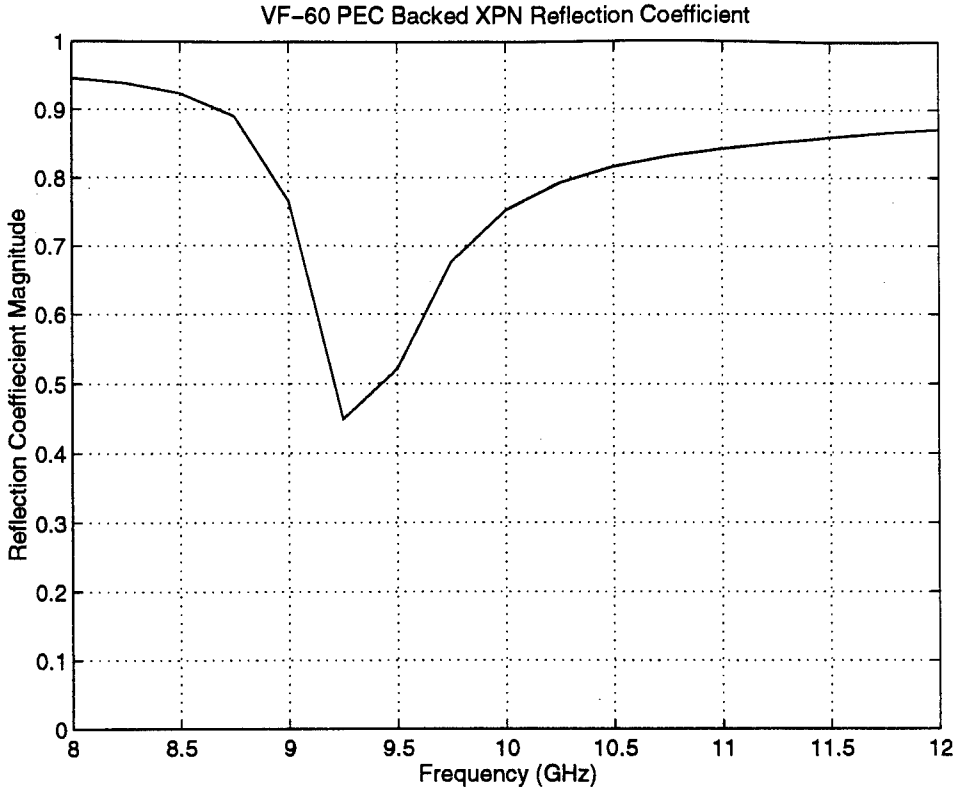

Figure 20. Average Reflection Coefficient for PEC Backed VF-60 Material Using XPN Measured Material Characteristics

The fourth object analyzed was the AN-73 material backed by the PEC plate. For the XPN data, a high negative correlation was achieved between the RCS variations and the reflection coefficient. For the AFIT data, however, only marginal correlation existed between the two. Neither set-up provided results that showed a correlation of RCS variations to permittivity variations.

The fifth object analyzed was the Rantec material backed by air. For the XPN data, the RCS variations were well correlated with the very small permittivity variations. The correlation with the reflection coefficient was good, but in a positive way. The AFIT data had very small permittivity variations of less than 0.03 which caused large RCS variations of up to 3.0 dB. These RCS variations were well correlated with both the material variations and the reflection coefficient.

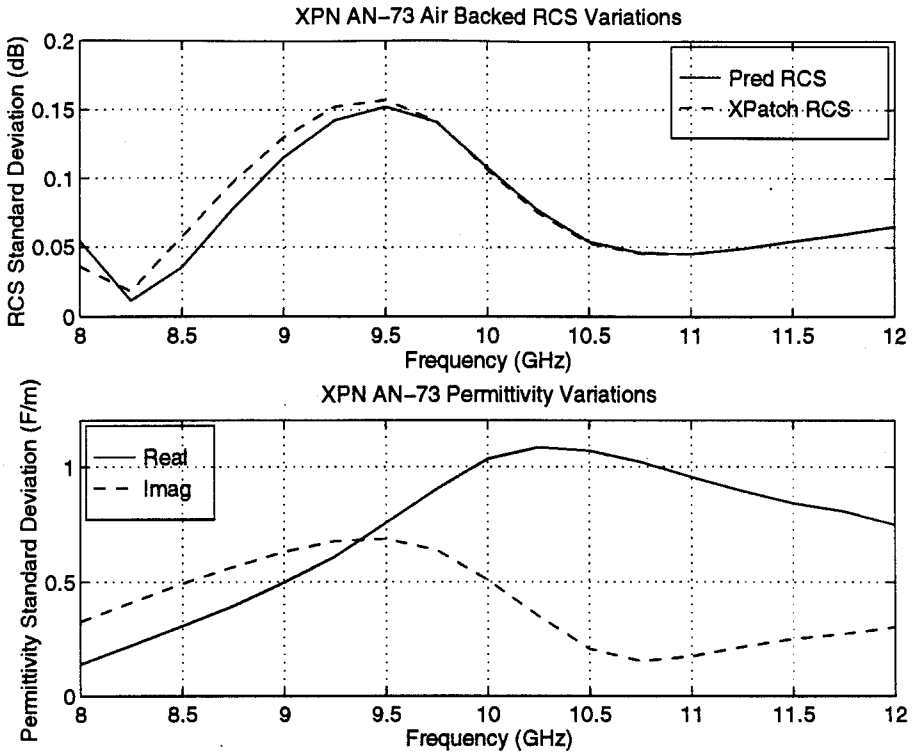

Figure 21. XPN AN-73 Permittivity Measurement Variations and RCS Prediction Variations for Air Backed AN-73 Material

The sixth object analyzed was the Rantec material backed by the PEC plate. In the case of XPN data, the RCS variations of up to 1.2 dB were correlated with both the small permittivity variations and the reflection coefficient. For the AFIT data, however, good correlation existed between the RCS and permittivity variations, but a very small positive correlation existed with the reflection coefficient.

Examination of all the acquired data indicated two general trends in the RCS variations. First and foremost, the RCS variations were highly influenced by the relative magnitude of the reflection coefficient. Except for a couple of exceptions, these quantities were negatively correlated. In other words, as the reflection coefficient increased, the RCS was less influenced by material variations and vice versa. The primary reason for this relationship was that higher reflection coefficients were the result of lower electromagnetic

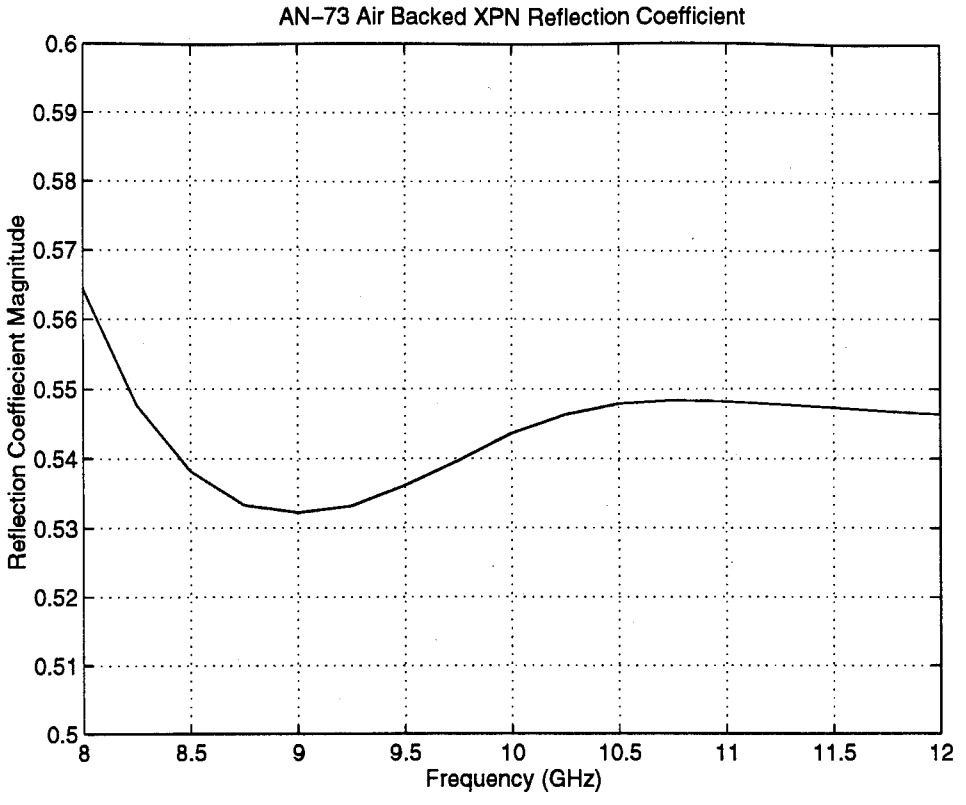

Figure 22. Average Reflection Coefficient for Air Backed AN-73 Material Using XPN Measured Material Characteristics

absorption of the material. Since the material had a lower effect on the total RCS, slight uncertainties in its characteristics caused only slight variations. On the other hand, for a highly absorbing material in which the reflection coefficient was low, the material properties dominated the electromagnetic scattering mechanisms. In this situation, slight material characteristic variations were magnified in the variations of the RCS.

The other trend in the data was more subtle. The RCS variations appeared to be directly dependent on the material characteristic variations. Unfortunately, this trend was typically overwhelmed by the reflection coefficient effects. This trend can be seen, however, at frequencies where the reflection coefficient is not rapidly changing. In this situation, the material variations are magnified equally across the frequency range. The best example of this occurred for the air backed VF-60 material using AFIT measured

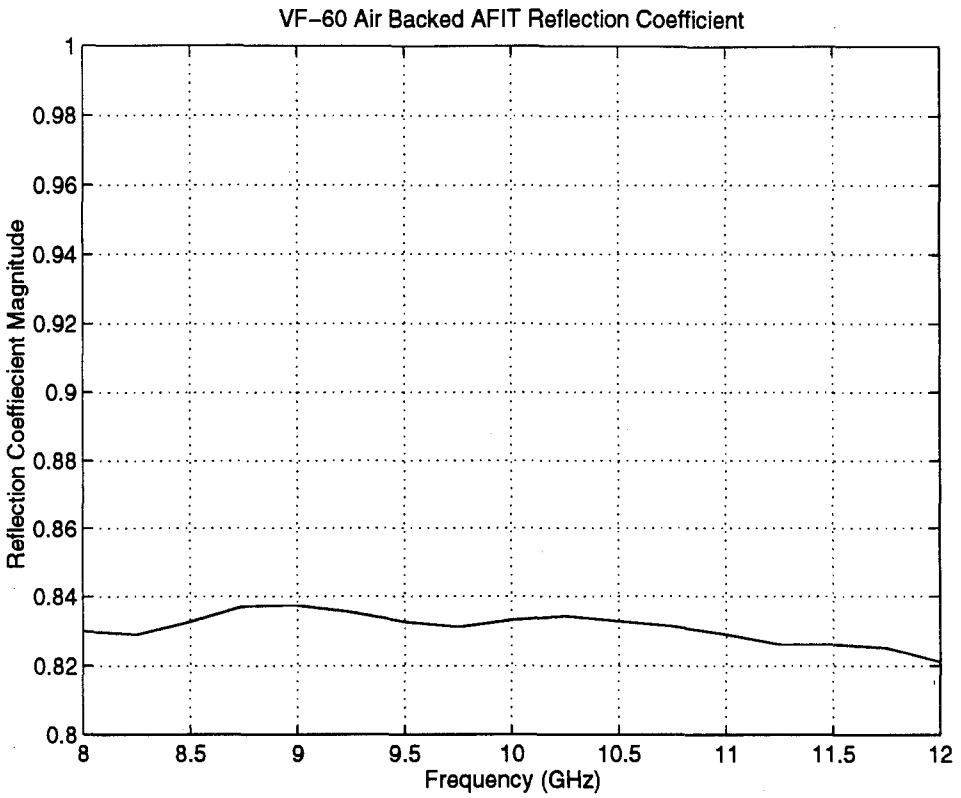

Figure 23. Average Reflection Coefficient for Air Backed VF-60 Material Using AFIT Measured Material Characteristics

material data. This case had a high correlation of RCS variations with the imaginary part permittivity variations and was an exception to the first trend. As seen in Figure 23, the reflection coefficient was relatively constant between 0.82 and 0.84. Since the material variations were magnified about equally across the frequency band, Figure 24 shows the very high direct correlation between the RCS variations and variations in the permittivity imaginary part.

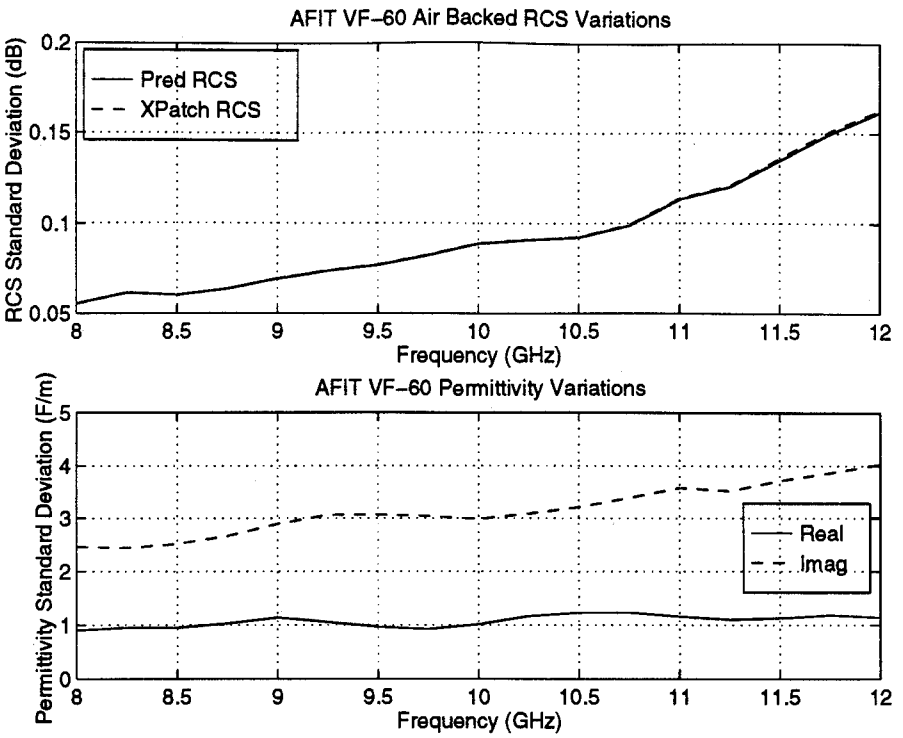

Figure 24. AFIT VF-60 Permittivity Measurement Variations and RCS Prediction Variations for Air Backed VF-60 Material

4.5 Xpatch Performance

The MRC study report concluded that Xpatch appeared to predict the RCS of coated targets properly if it was provided accurate material characteristics. The results obtained for the material coated plates at normal incidence supports this argument. In all the situations, Xpatch simulations provided equivalent results to the theoretical RCS predictions. The one exception occurred for the air backed Rantec material using AFIT material data. Even though the imaginary part of the permittivity was measured to be positive, Xpatch converted it to negative. This was not an Xpatch limitation since the material data was invalid.

Although Xpatch simulations and RCS predictions were equivalent, they were not identical. The RCS predictions were simplified by taking the theoretical PO RCS for a square plate and adjusting it by the reflected power determined by the reflection coefficient.

Xpatch, on the other hand, performed a PO integration of the electromagnetic fields at the object's surface after accounting for the reflection coefficient effects. Thus, the Xpatch method was more accurate even though both methods worked well for these simple objects.

Xpatch simulations were performed on the MRC test body, a complex material coated object, using XPN measured material characteristics. The RCS predictions were compared to RCS measurements made by MRC. The Total RMS error and correlation of the data is presented in Table 5. For comparison, Table 5 also shows the same information for the Xpatch simulations using MRC measured material characteristics. The results were inconclusive. None of the Xpatch simulations using either the XPN or MRC measured permittivities compared well with the measured data. The RCS predictions using the XPN material characteristics weren't expected to produce accurate results since the XPN data had already been identified as having errors. Table 5 shows that the calculated errors were more pronounced at the 30 degree incidence situations. Figure 25 shows the data for the

Table 5

Summary of Xpatch RCS RMS Errors and Correlations Compared to RCS Measurements of MRC Nose Radome Test Body Using MRC and XPN Measured Material Characteristics

	MRC Material Data		XPN Material Data	
	RMSE (dB)	Corr (%)	RMSE (dB)	Corr (%)
Test Body Config				
30 Degree H-Pol	5.864	64.0	7.195	58.9
30 Degree V-Pol	5.107	33.6	11.351	-57.5
75 Degree H-Pol	2.398	33.1	2.559	31.8
75 Degree V-Pol	3.307	-27.1	3.124	-37.3

H-pole 30 degree incidence case. At this incidence, more of the Rantec material was exposed so material inaccuracies were more noticeable. It was determined that the Rantec material coated surface of the MRC test body played a minor role in the RCS simulations. The radome surface, however, was larger and was the outermost surface. Thus, the characterization of the radome material data was more critical to accurately predicting the RCS of the MRC test body. The radome material was a formed fiberglass material and was not deemed a feasible material to measure in the waveguides used for this research.

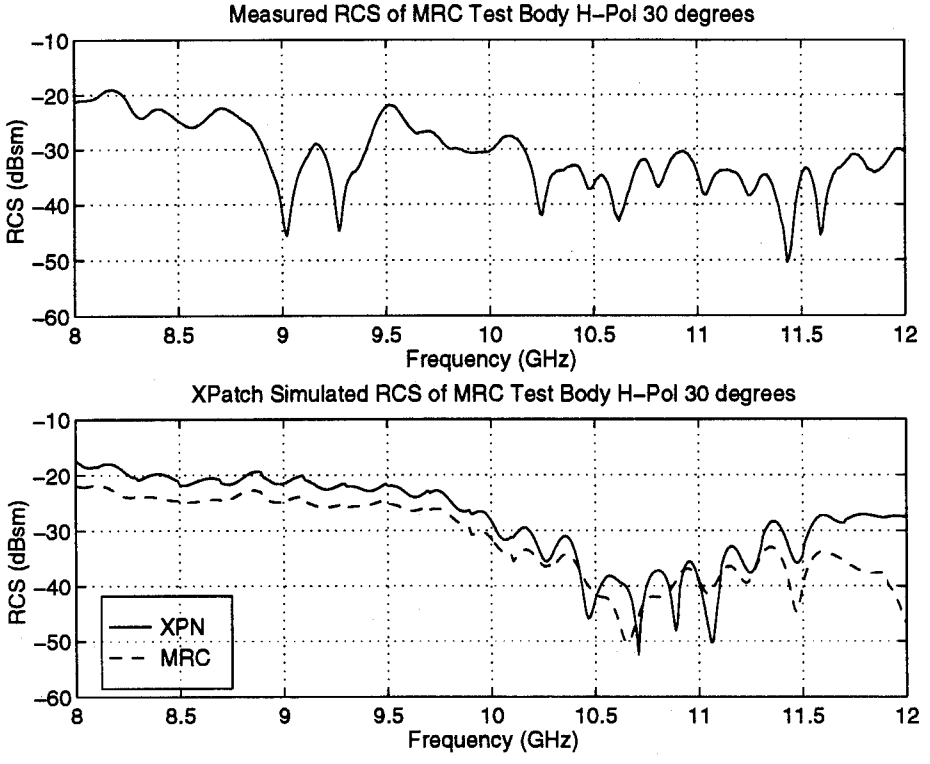

Figure 25. RCS of MRC Test Body at 30 Degree Incidence at H-pol Measured vs Xpatch Predictions Using MRC and XPN Measured Material Characteristics

There was one Xpatch process which may have affected the discrepancy between the simulations using the MRC and XPN material data. The MRC material characteristics were measured at every 1.0 GHz while the XPN characteristics were measured at every

0.25 GHz. Xpatch took this material data and linearly interpolated their values for the frequencies between the data entries. Thus, any material data fluctuations would have been smoothed out which would result in inaccurate RCS predictions between the frequency entries. Since the Rantec material characteristics did not fluctuate significantly, this was not deemed important for the MRC test body simulations.

5. Conclusions and Recommendations

This chapter summarizes the main points of this thesis research, emphasizes the main conclusions, and suggests further areas of promising research.

5.1 Conclusions

The material characteristics of three dielectrics were measured using two different X-band waveguide transmission lines. The VF-60 material was a thin homogenous plastic film while the AN-73 and Rantec materials were thick three layer foams. Although manufacturing tolerances could have affected the results, only replication errors from repeated measurements were considered. It was immediately determined that the AFIT waveguide set-up produced inaccurate results for the thick materials due to invalid measured permeability values.

The RCS of a six inch square PEC plate was measured in the AFIT indoor range. It was determined that a 1.05° tilt from the range antenna caused a bias from the theoretical RCS value. In addition, calibration error was deemed the largest source of error in RCS measurement precision. RCS measurements were then made of each material backed both with and without the square PEC plate. Using the measured material characteristics, RCS predictions were then made using two methods: 1) calculating the reflection coefficient and applying physical optics theory; and 2) utilizing Xpatch, a high frequency RCS prediction code.

Through comparisons of the RCS measurements and RCS predictions using both methods, it was deterimined that the measured material characteristics of the two thick materials were inaccurate from both of the waveguide measurement set-ups. Only the thin material measurements equated to accurate RCS predictions.

The primary objective of this thesis research was to evaluate the sensitivity of RCS predictions to uncertainties in measured material characteristics. In general, it was found that the RCS variations were most influenced by the relative magnitude of the reflection coefficient. Qualitatively, a lower reflection coefficient resulted in a larger RCS variation. It was also deterimined that for a relatively constant reflection coefficient across the frequency band, the RMS error of the RCS predictions was directly proportional to the replication error in the imaginary part of the dielectric permittivity.

The secondary objective of this research was to validate the capability of Xpatch to accurately predict the RCS of RAM coated objects. Although only normal incidence predictions were performed on the material coated plates, it was shown that Xpatch properly characterized the materials and correctly predicted the RCS of the objects. As with the theoretical predictions, the accuracy of Xpatch depended on the accuracy of the provided material characteristics. The only limitation of Xpatch was that it linearly interpolated the material characteristics between the entries of its material input file. This could have significant effects for materials whose characteristics fluctuate between the frequency entries.

5.2 Recommendations

Based upon the results of this thesis research, it is recommended that future research concentrate on quantifying the relationship between RCS prediction variations and the reflection coefficient magnitude and the material characteristics uncertainties. A better understanding of this relationship would be required for accurate object identification of a RAM coated object.

Continued research is necessary to accurately characterize materials for use in prediction models. Better methods of measuring the characteristics of thick materials needs to be evaluated. This may involve measuring the individual layers of multi-layered

materials such as were used in this research. In addition, materials with a permeability component could also be included to analyze how its imaginary part also affects the RCS variations. Lastly, this research concentrated only on replication error of material measurements. The magnitude of manufacturing tolerances within a material sheet and from sheet to sheet could also be analyzed.

Finally, although this thesis research evaluated normal incidence situations, both off normal and bistatic situations situations are recommended for study. In all of these future efforts, it is recommended that the flexible and accurate Xpatch code be utilized to compare its RCS predictions with measurements and calculations.

Appendix A: Material Measurements and Properties

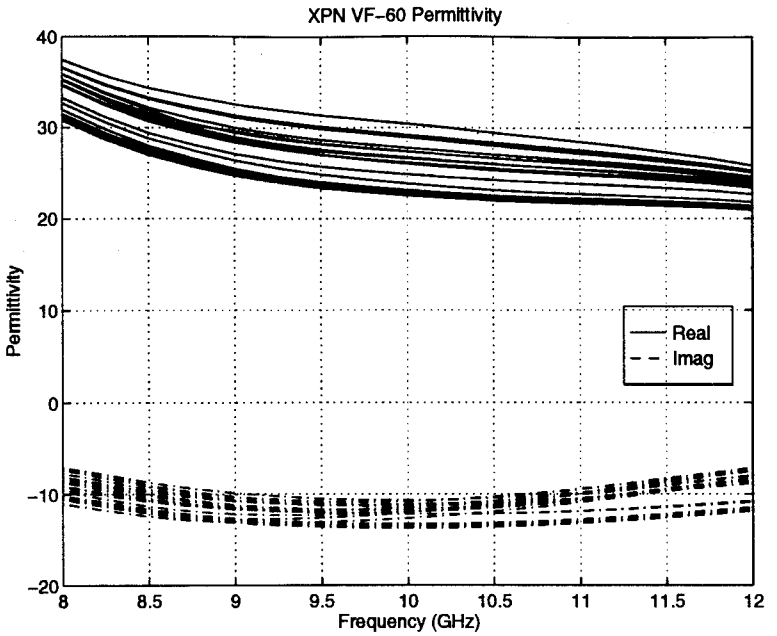

Figure A-1. XPN Waveguide Measurements of Relative VF-60 Permittivity

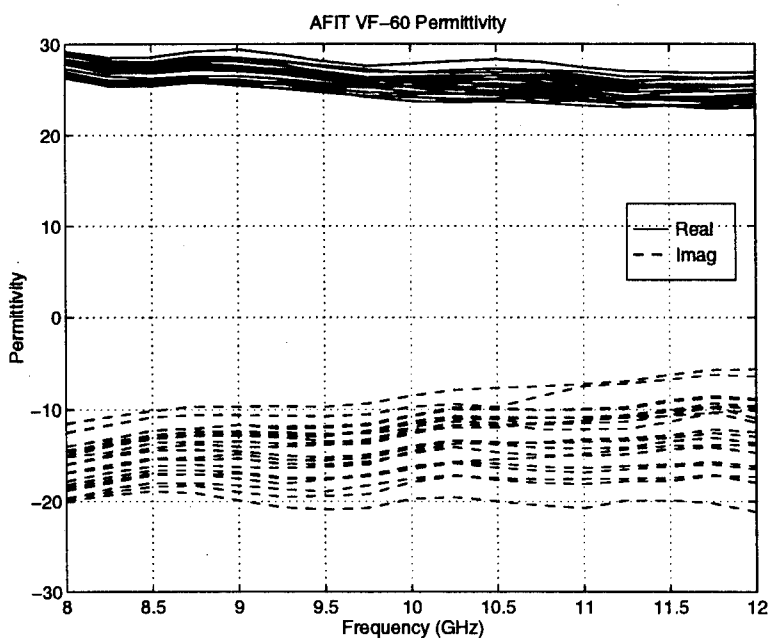

Figure A-2. AFIT Waveguide Measurements of Relative VF-60 Permittivity

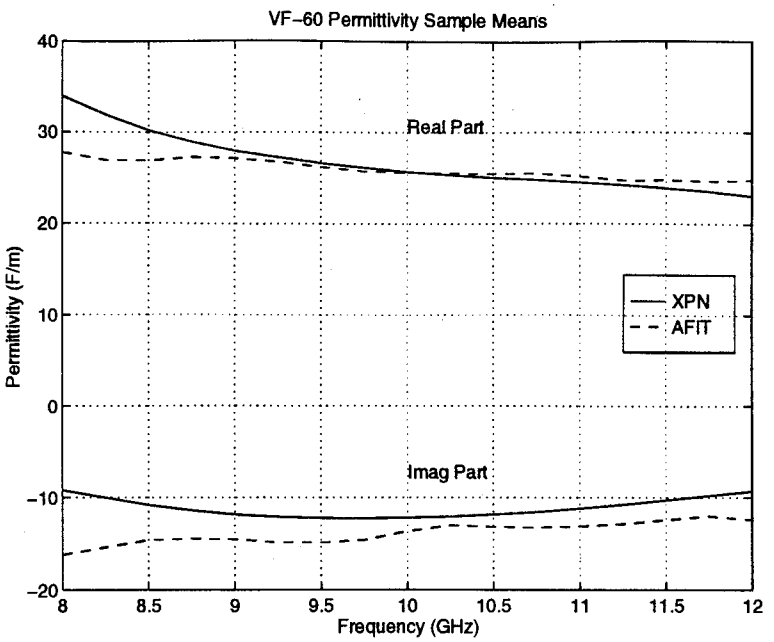

Figure A-3. Relative VF-60 Permittivity Sample Means for XPN and AFIT Waveguide Measurements

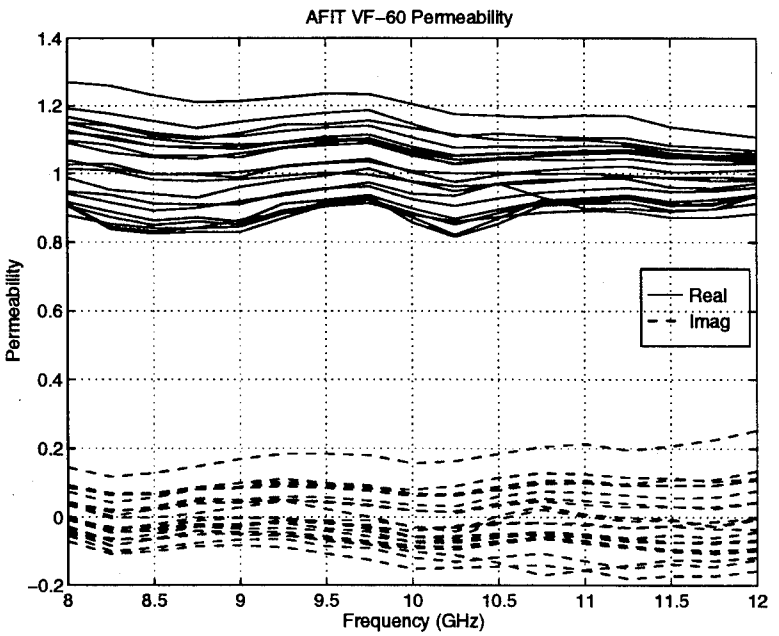

Figure A-4. AFIT Waveguide Measurements of Relative VF-60 Permeability

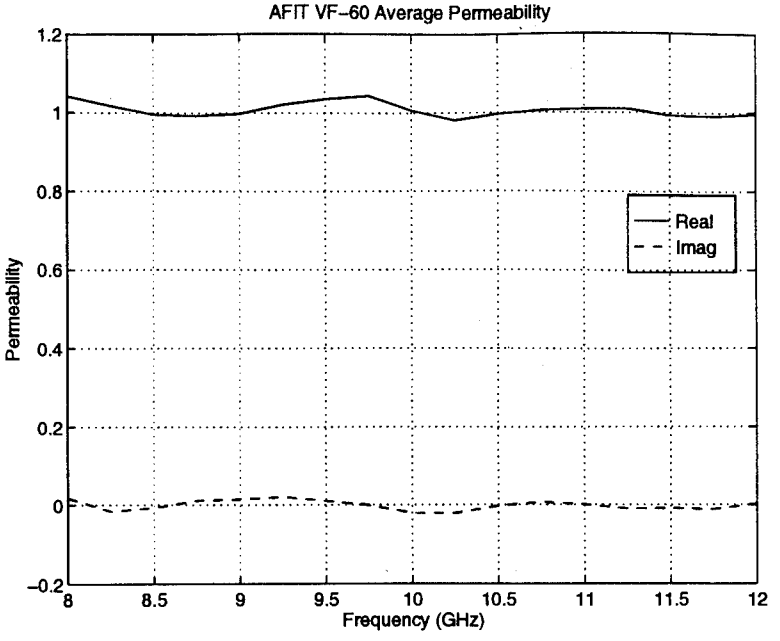

Figure A-5. Relative VF-60 Permeability Sample Mean for AFIT Waveguide Measurements

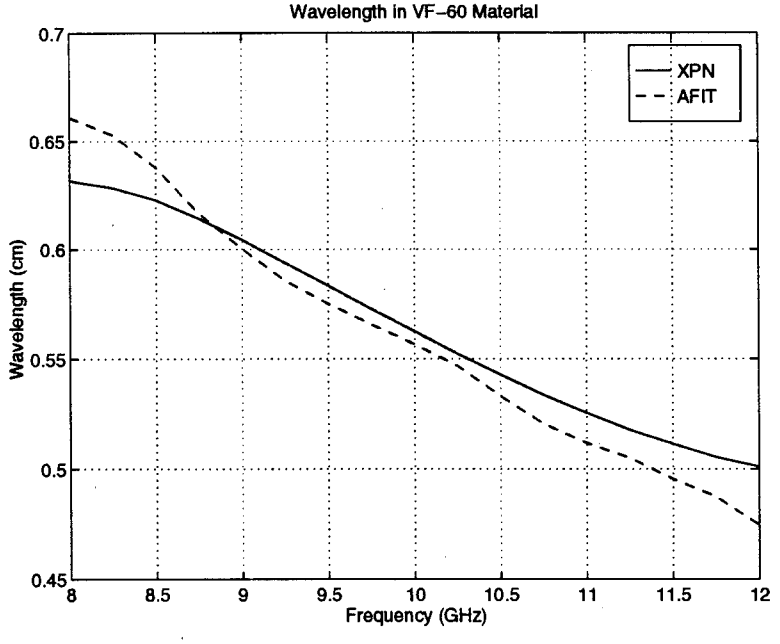

Figure A-6. Average Measured VF-60 Material Wavelength

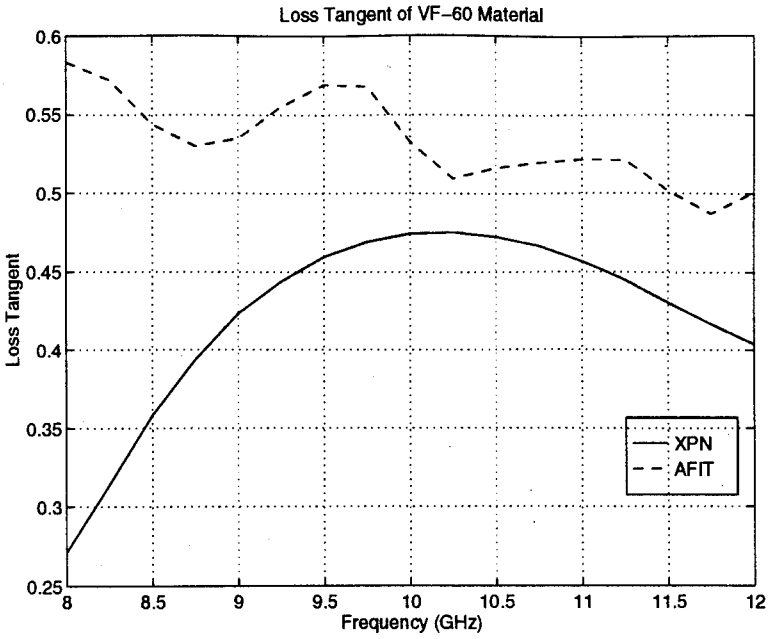

Figure A-7. Average Measured VF-60 Loss Tangent

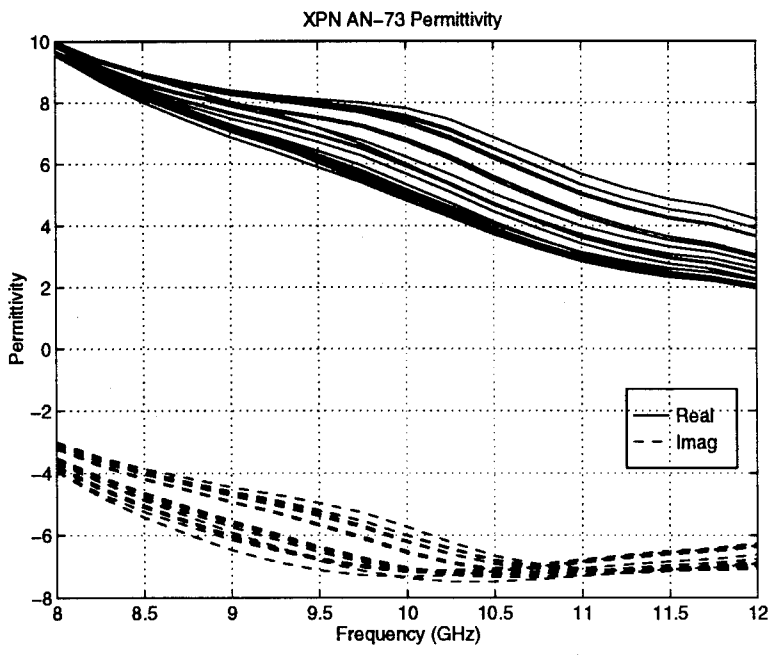

Figure A-8. XPN Waveguide Measurements of Relative AN-73 Permittivity

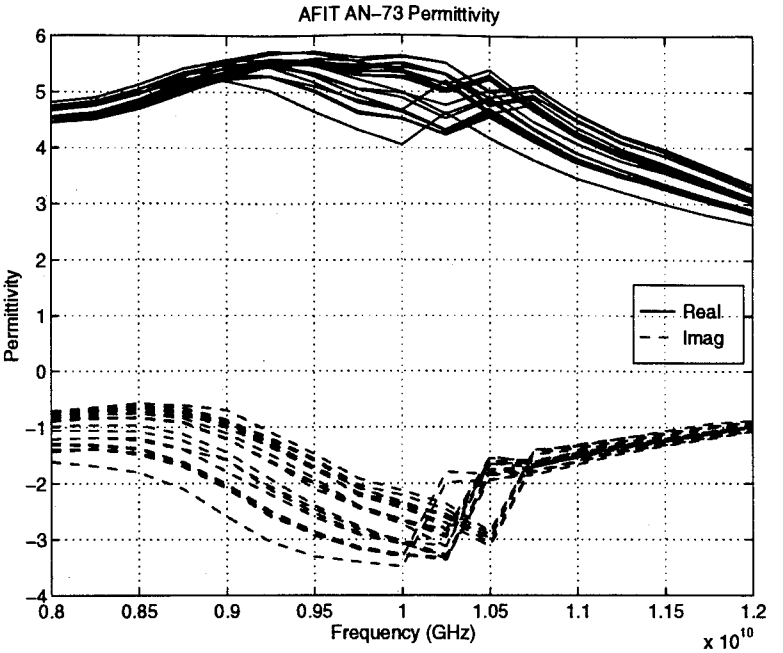

Figure A-9. AFIT Waveguide Measurements of Relative AN-73 Permittivity

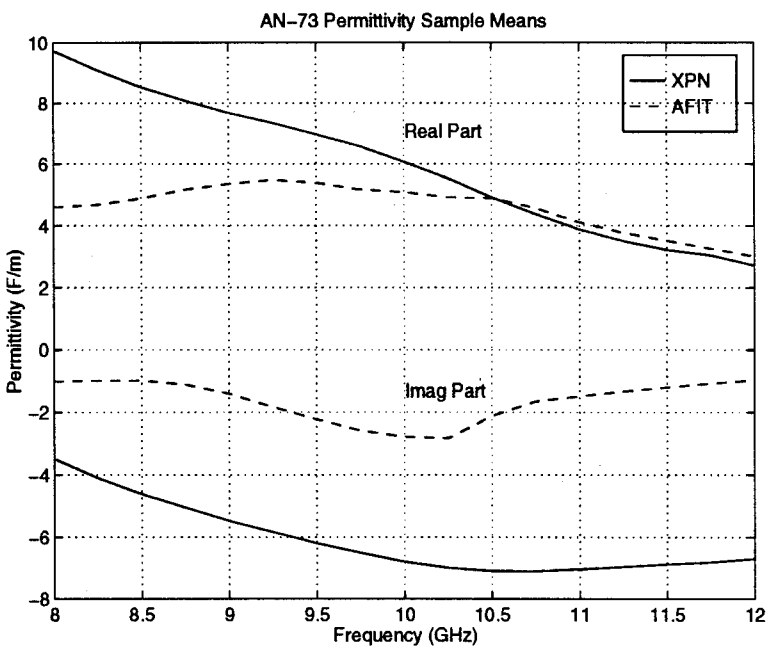

Figure A-10. Relative AN-73 Permittivity Sample Means for XPN and AFIT Waveguide Measurements

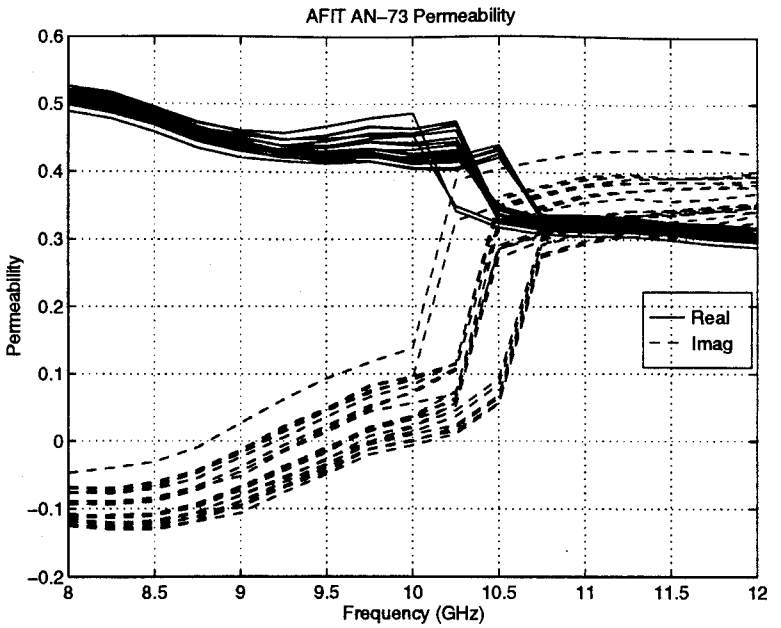

Figure A-11. AFIT Waveguide Measurements of Relative AN-73 Permeability

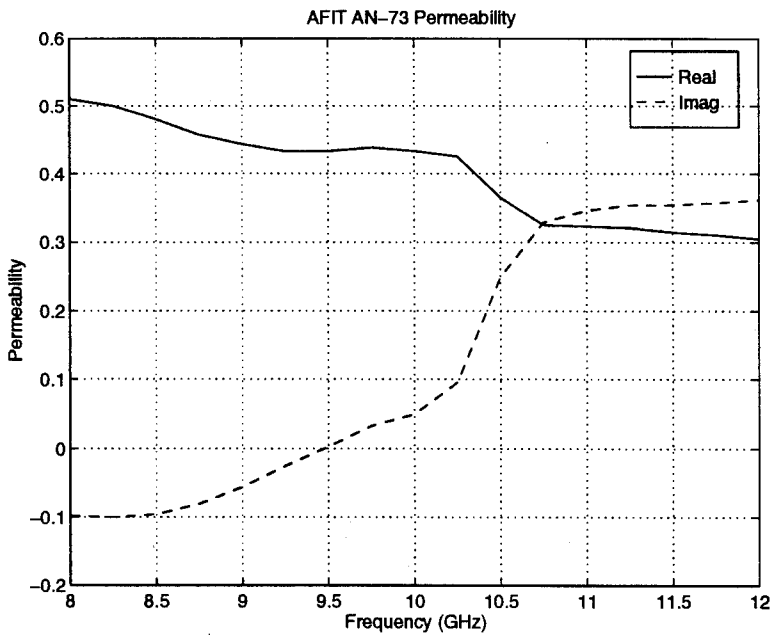

Figure A-12. Relative AN-73 Permeability Sample Means for AFIT Waveguide Measurements

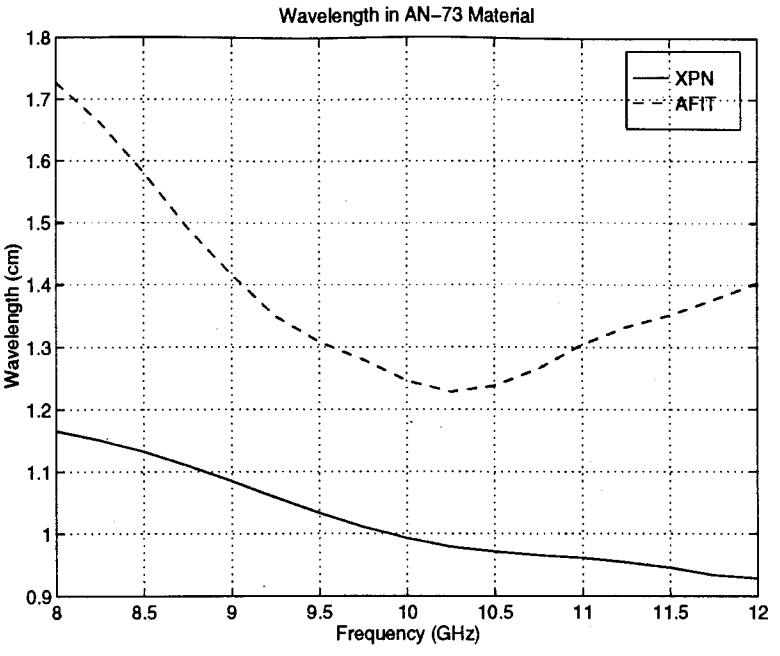

Figure A-13. Average Measured AN-73 Material Wavelength

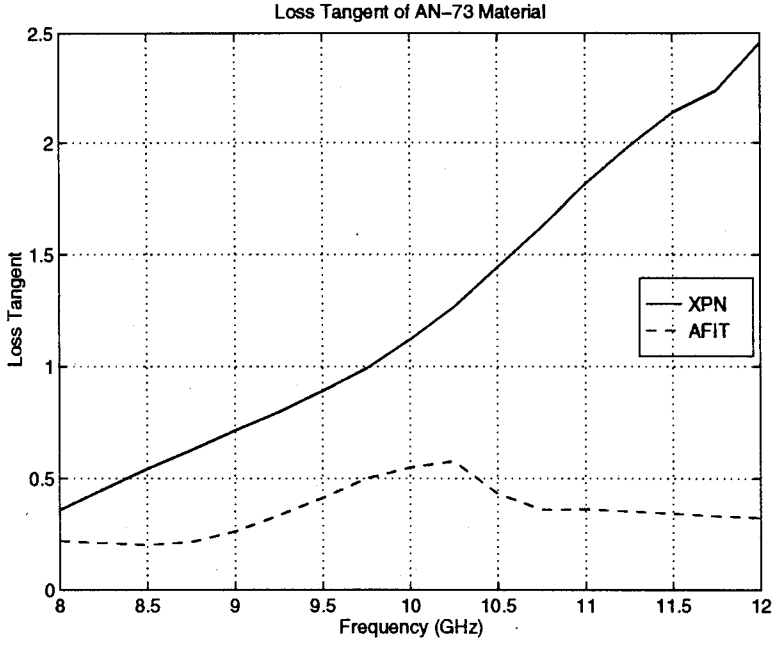

Figure A-14. Average Measured AN-73 Loss Tangent

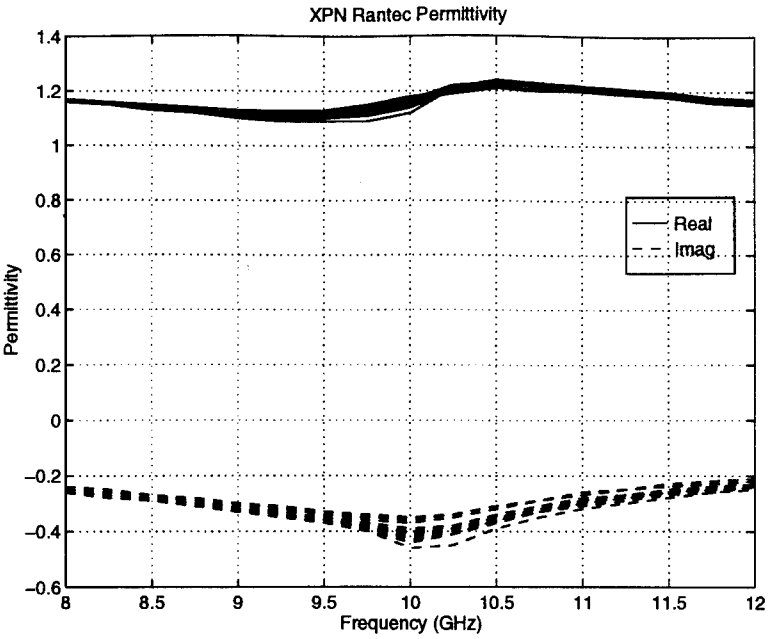

Figure A-15. XPN Waveguide Measurements of Relative RANTEC Permittivity

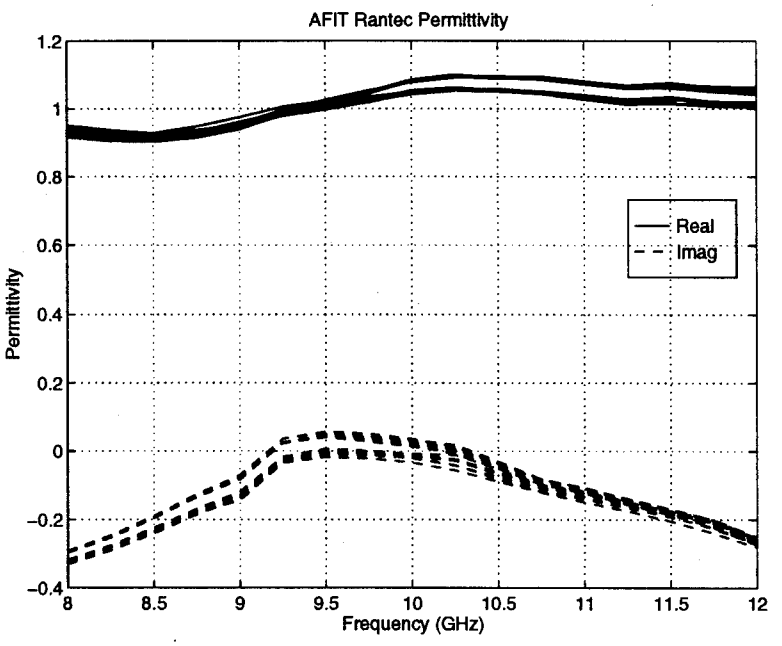

Figure A-16. AFIT Waveguide Measurements of Relative RANTEC Permittivity

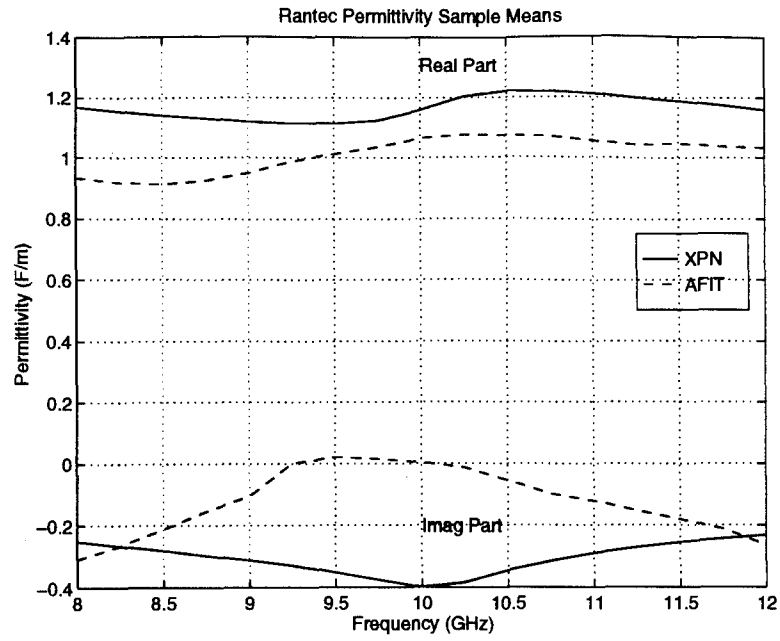

Figure A-17. Relative RANTEC Permittivity Sample Means for XPN and AFIT Waveguide Measurements

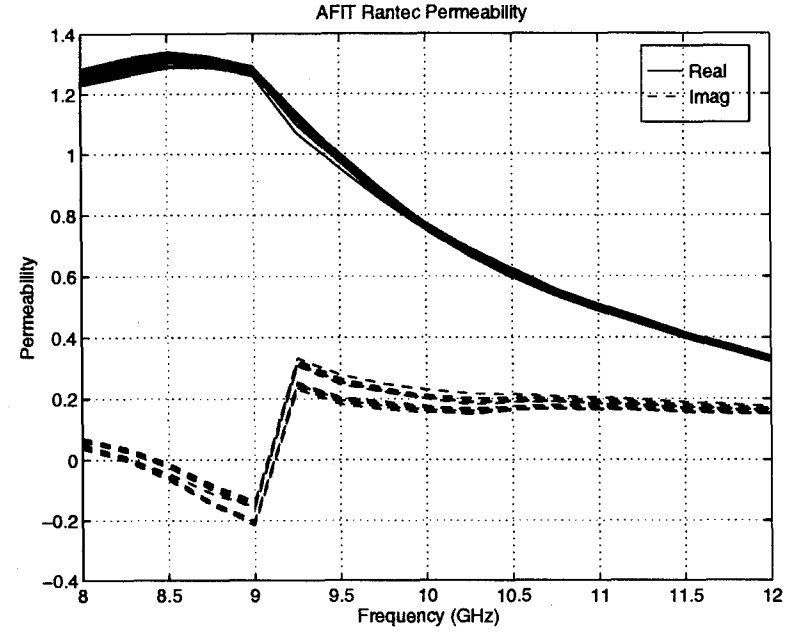

Figure A-18. AFIT Waveguide Measurements of Relative RANTEC Permeability

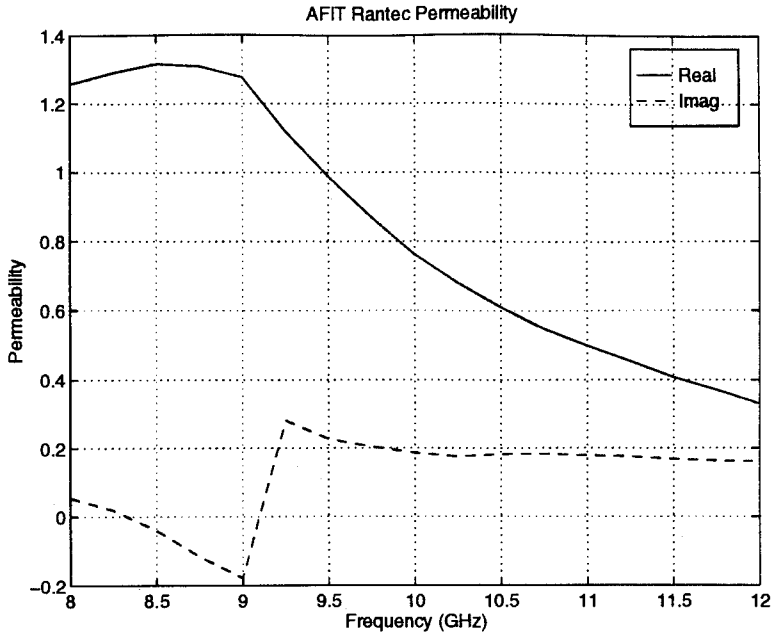

Figure A-19. Relative RANTEC Permeability Sample Mean for AFIT Waveguide Measurements

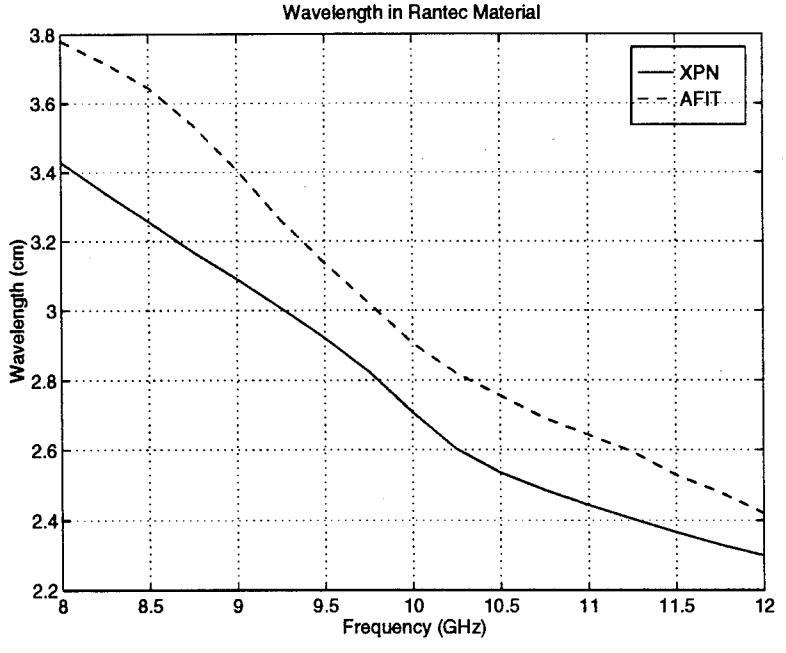

Figure A-20. Average Measured RANTEC Material Wavelength

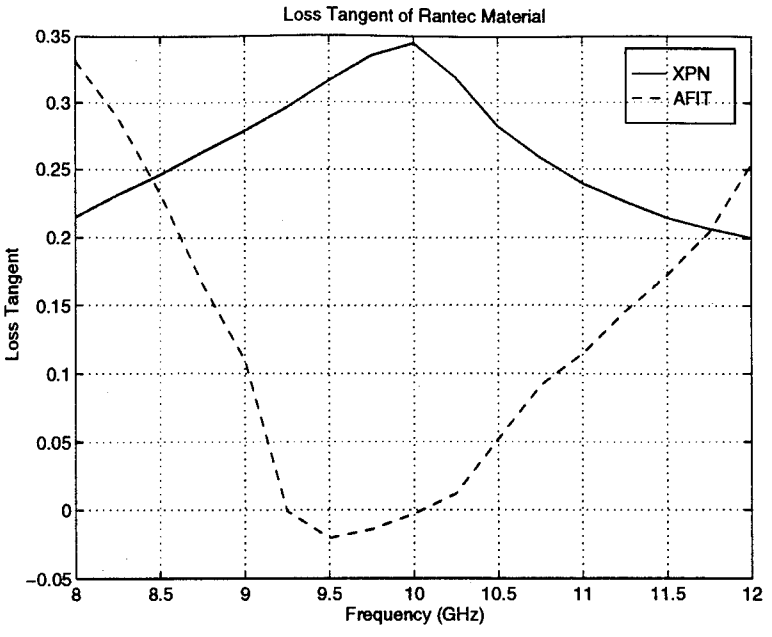

Figure A-21. Average Measured RANTEC Loss Tangent

Appendix B: RCS Measurements and Predictions

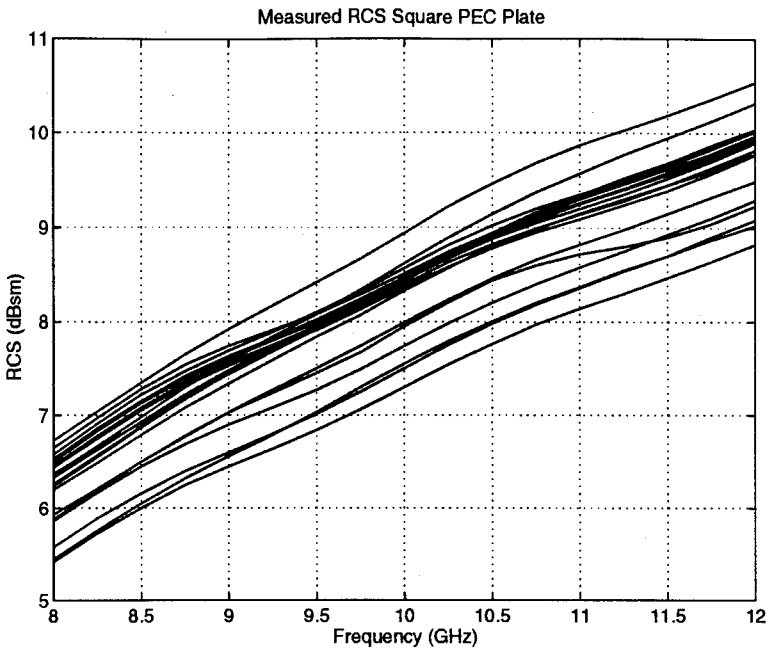

Figure B-1. RCS Measurements for Six Inch Square PEC Plate

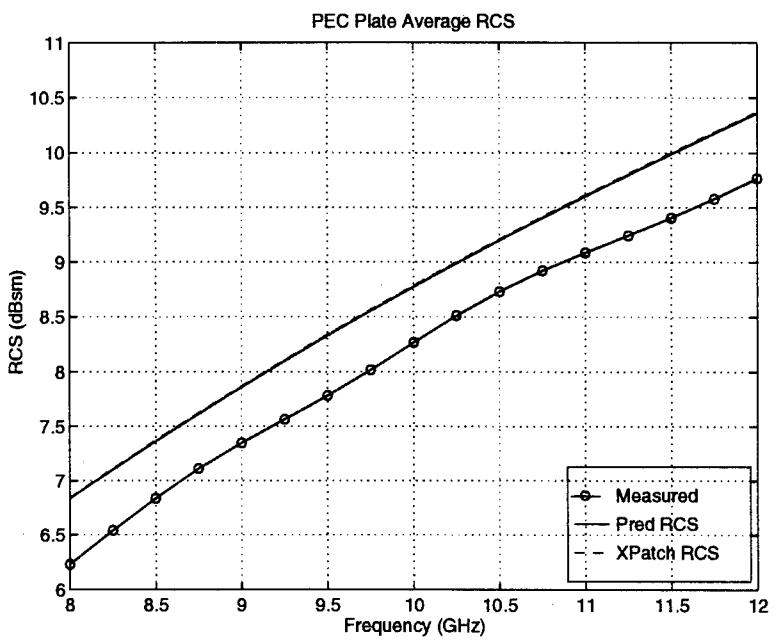

Figure B-2. RCS Prediction and Measured Sample Means for Six Inch Square PEC Plate

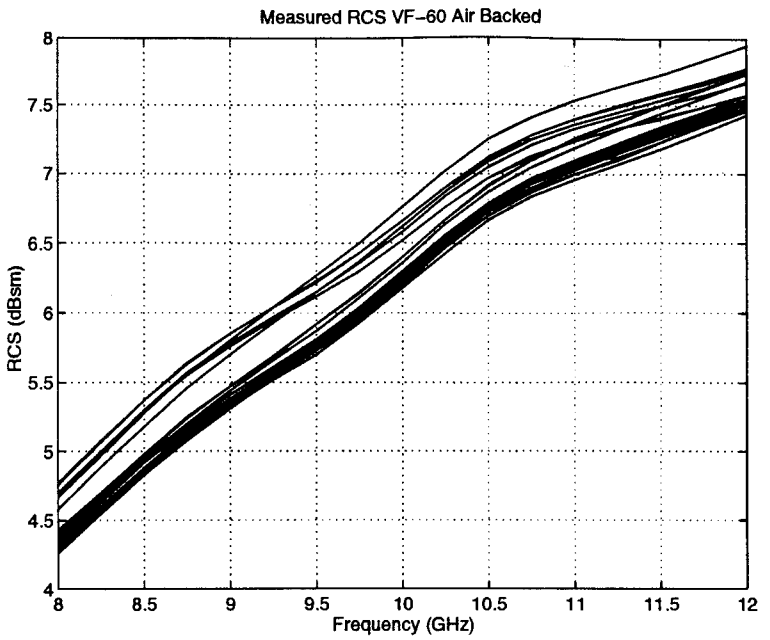

Figure B-3. RCS Measurements for Air Backed VF-60 Material

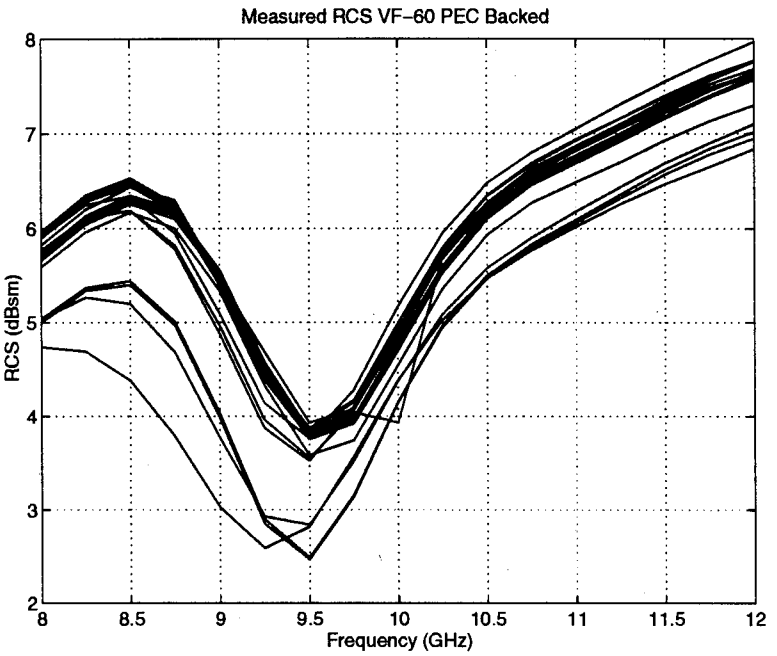

Figure B-4. RCS Measurements for PEC Backed VF-60 Material

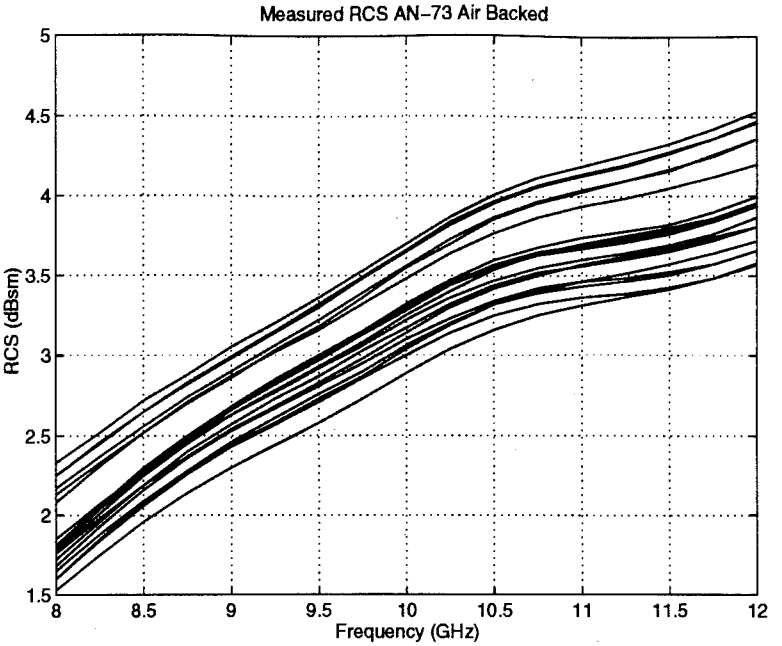

Figure B-5. RCS Measurements for Air Backed AN-73 Material

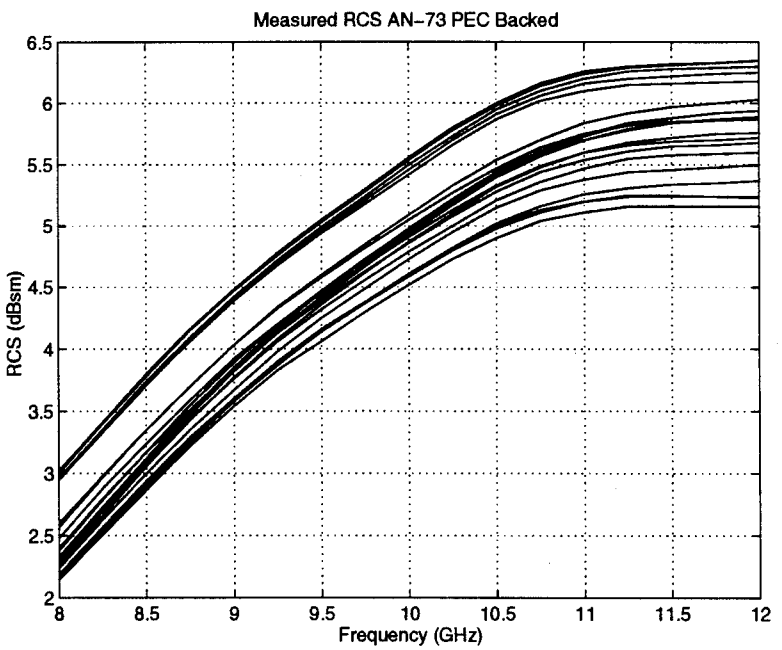

Figure B-6. RCS Measurements for PEC Backed AN-73 Material

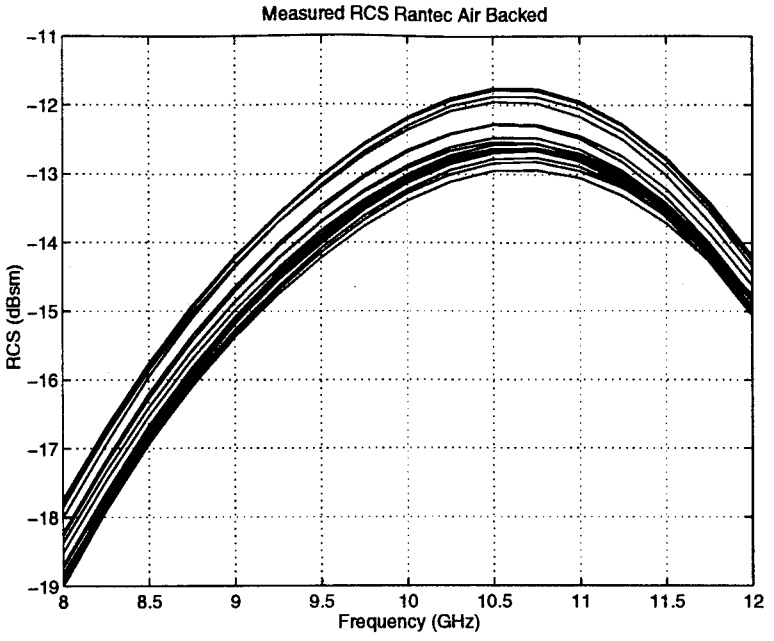

Figure B-7. RCS Measurements for Air Backed RANTEC Material

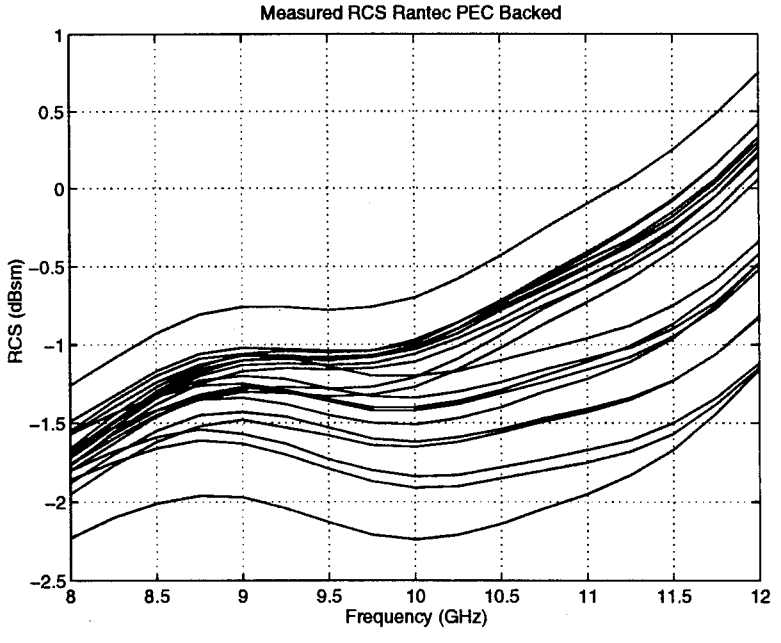

Figure B-8. RCS Measurements for PEC Backed RANTEC Material

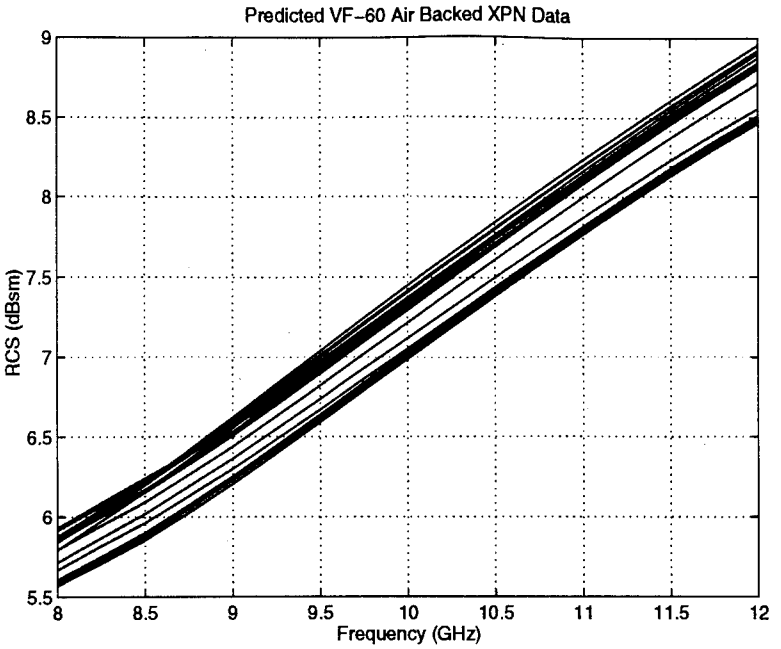

Figure B-9. RCS Predictions for Air Backed VF-60 Material Using XPN Measured Material Characteristics

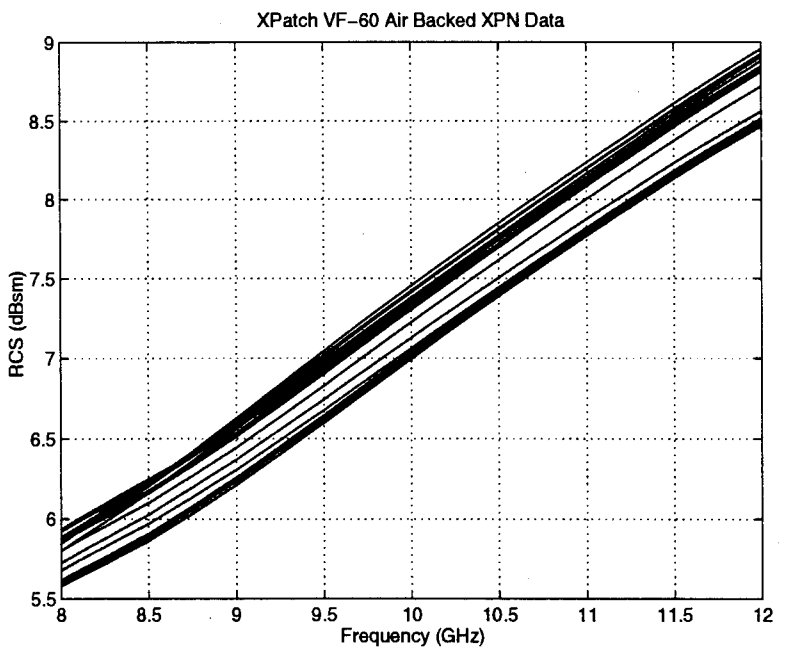

Figure B-10. XPATCH RCS Simulations for Air Backed VF-60 Material Using XPN Measured Material Characteristics

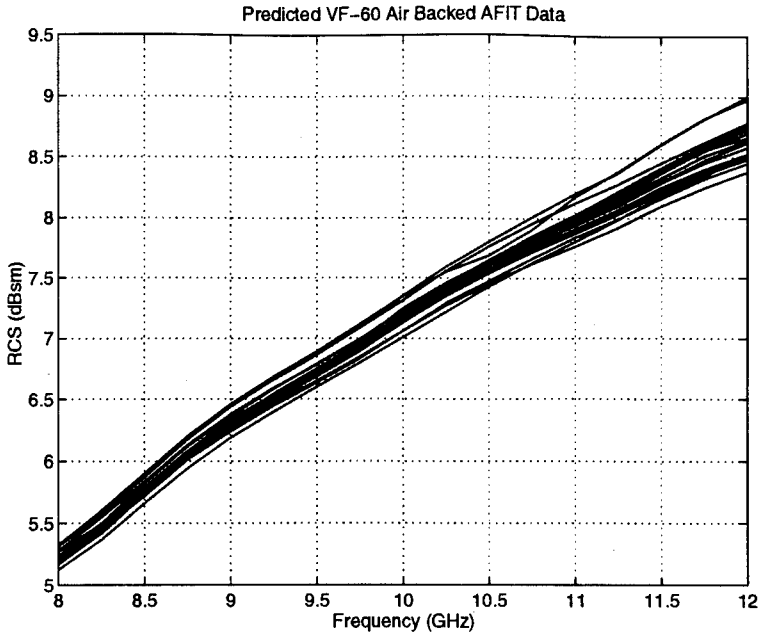

Figure B-11. RCS Predictions for Air Backed VF-60 Material Using AFIT Measured Material Characteristics

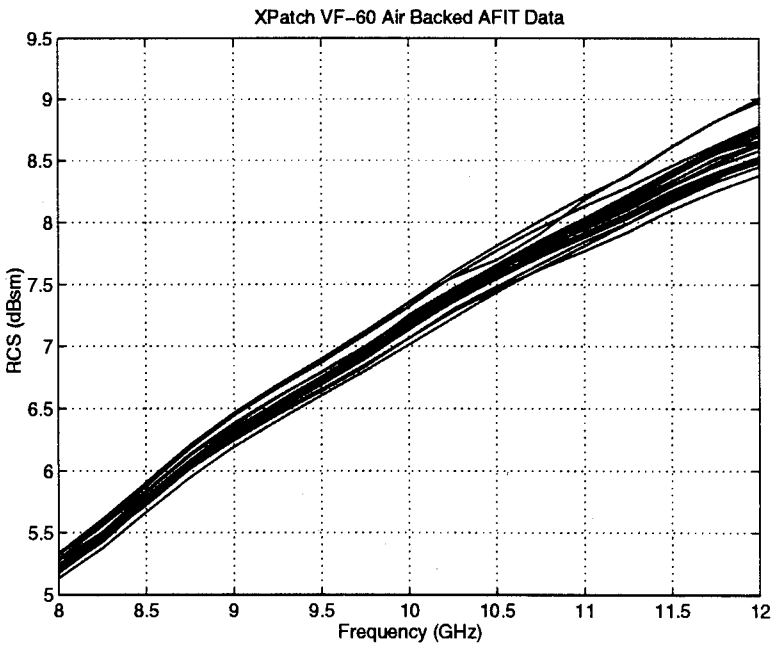

Figure B-12. XPATCH RCS Simulations for Air Backed VF-60 Material Using AFIT Measured Material Characteristics

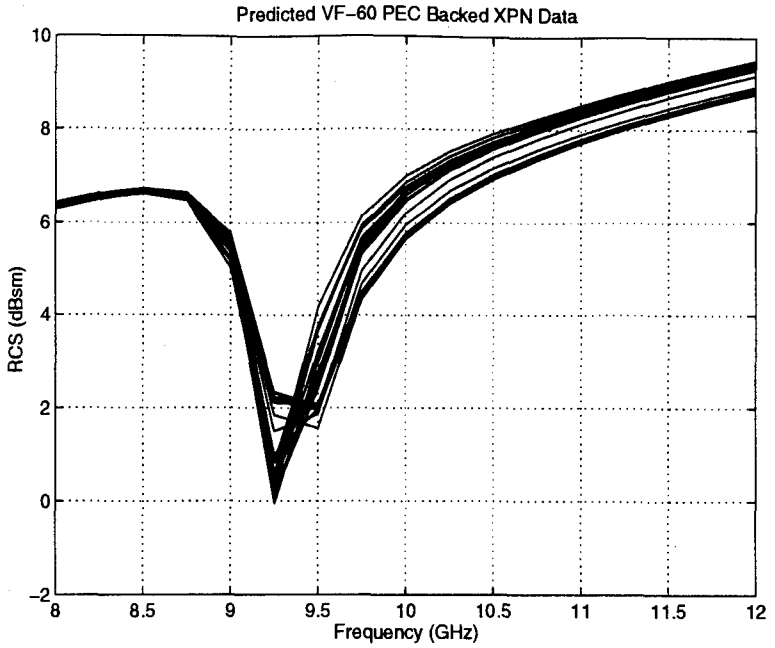

Figure B-13. RCS Predictions for PEC Backed VF-60 Material Using XPN Measured Material Characteristics

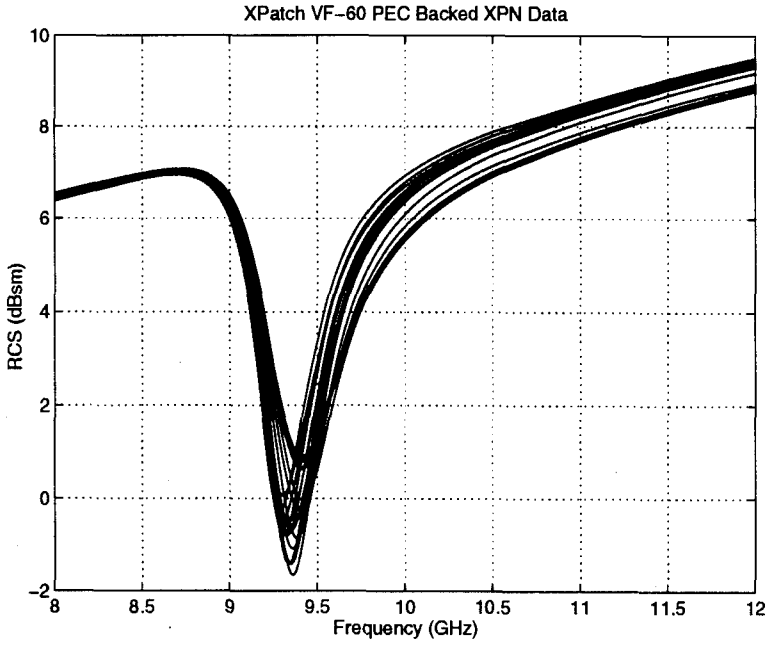

Figure B-14. Xpatch RCS Simulations for PEC Backed VF-60 Material Using XPN Measured Material Characteristics

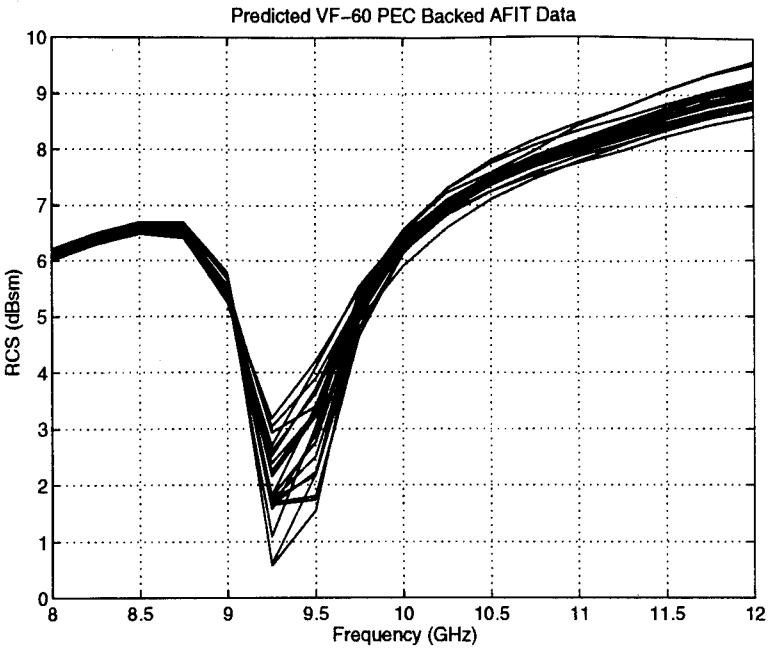

Figure B-15. RCS Predictions for PEC Backed VF-60 Material Using AFIT Measured Material Characteristics

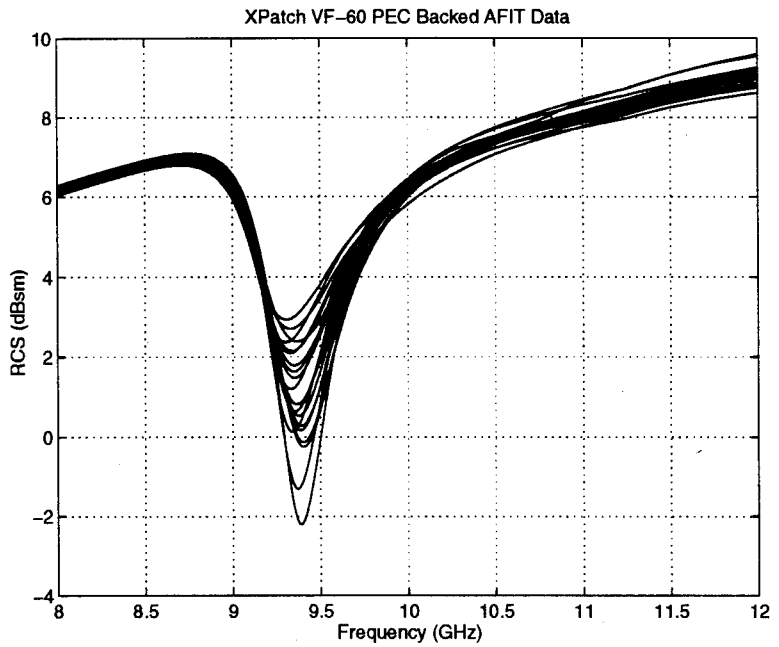

Figure B-16. Xpatch RCS Simulations for PEC Backed VF-60 Material Using AFIT Measured Material Characteristics

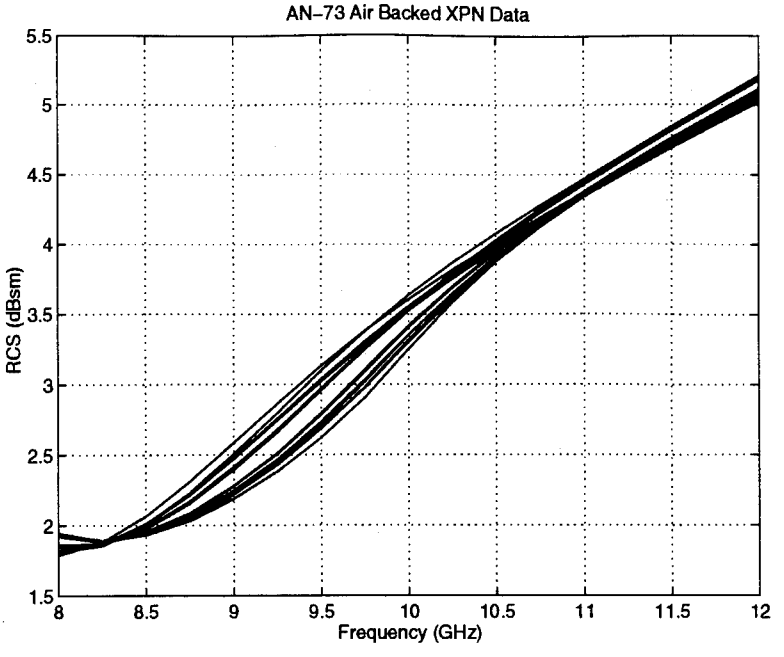

Figure B-17. RCS Predictions for Air Backed AN-73 Material Using XPN Measured Material Characteristics

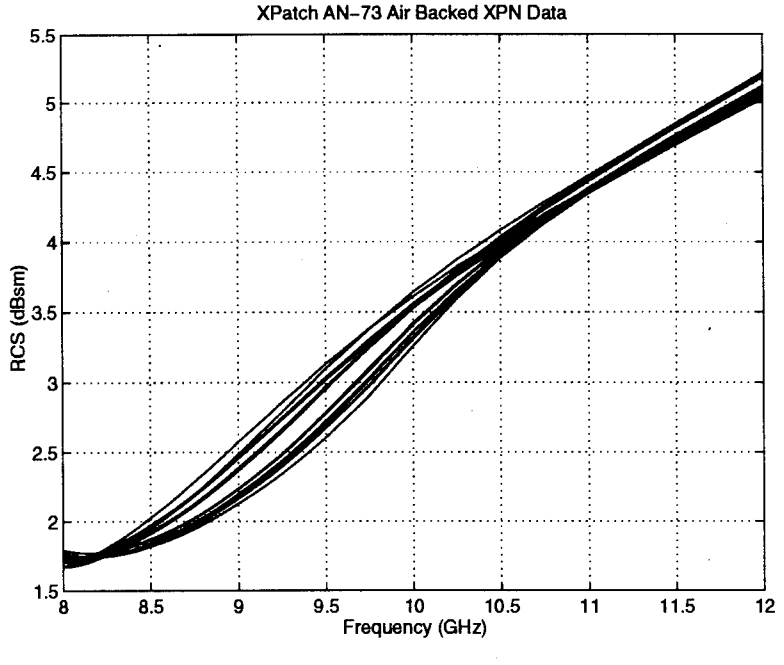

Figure B-18. XPATCH RCS Simulations for Air Backed AN-73 Material Using XPN Measured Material Characteristics

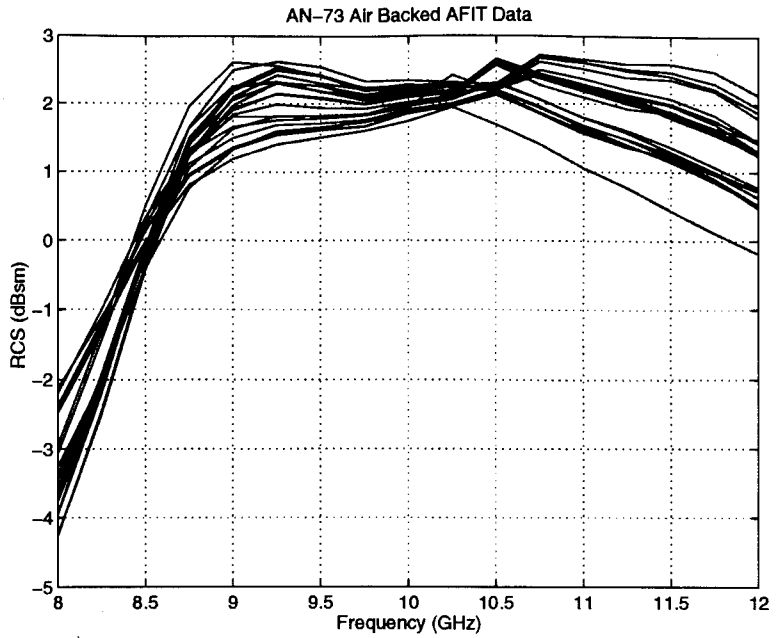

Figure B-19. RCS Predictions for Air Backed AN-73 Material Using AFIT Measured Material Characteristics

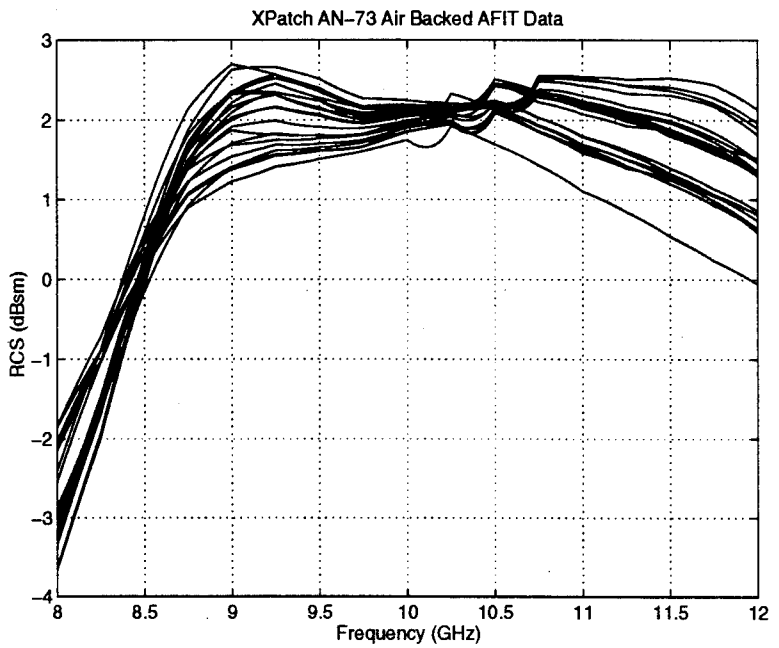

Figure B-20. XPATCH RCS Simulations for Air Backed AN-73 Material Using AFIT Measured Material Characteristics

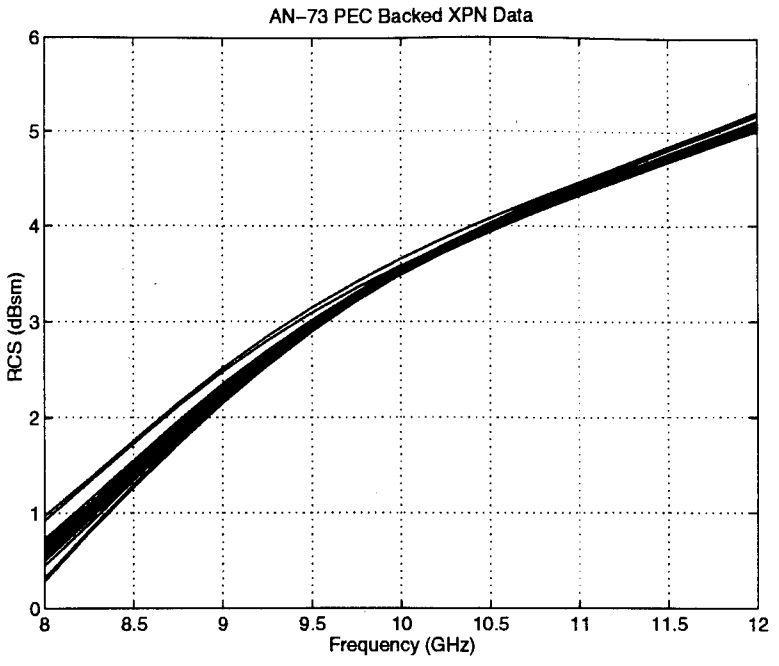

Figure B-21. RCS Predictions for PEC Backed AN-73 Material Using XPN Measured Material Characteristics

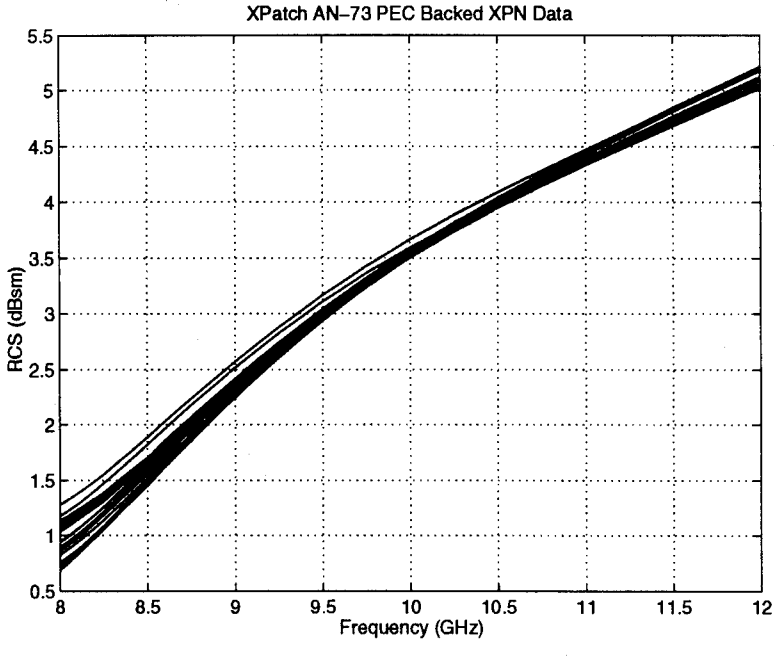

Figure B-22. Xpatch RCS Simulations for PEC Backed AN-73 Material Using XPN Measured Material Characteristics

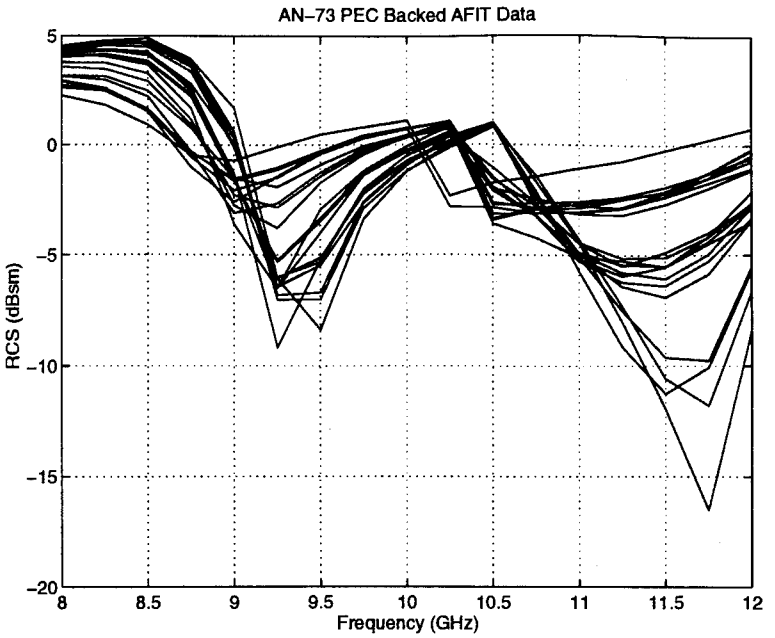

Figure B-23. RCS Predictions for PEC Backed AN-73 Material Using AFIT Measured Material Characteristics

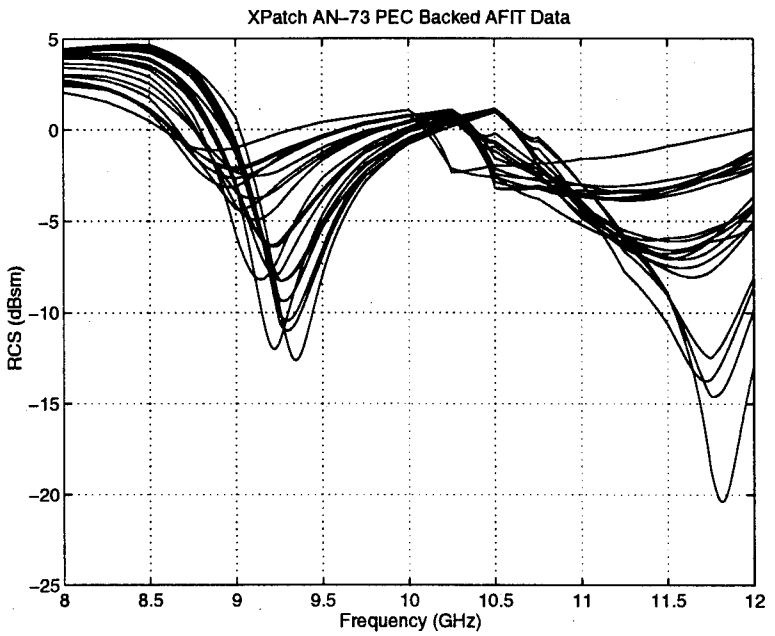

Figure B-24. Xpatch RCS Simulations for PEC Backed AN-73 Material Using AFIT Measured Material Characteristics

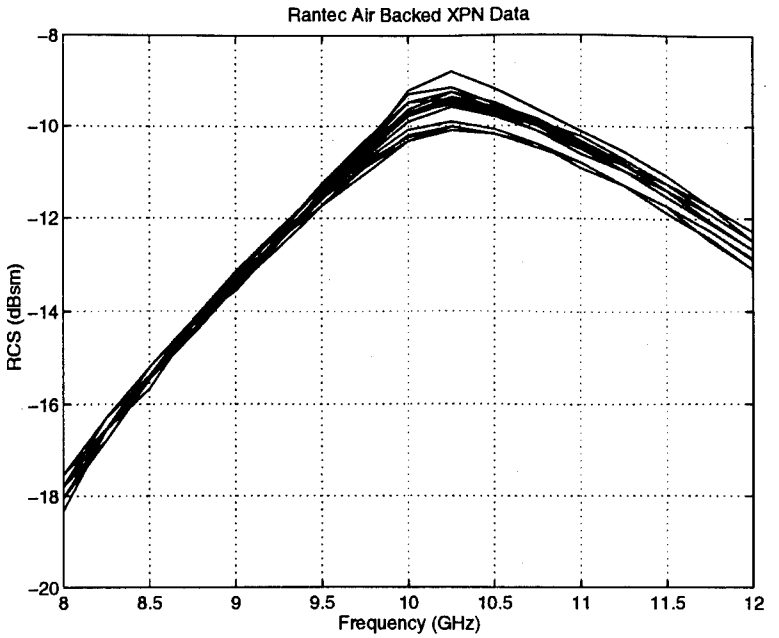

Figure B-25. RCS Predictions for Air Backed RANTEC Material Using XPN Measured Material Characteristics

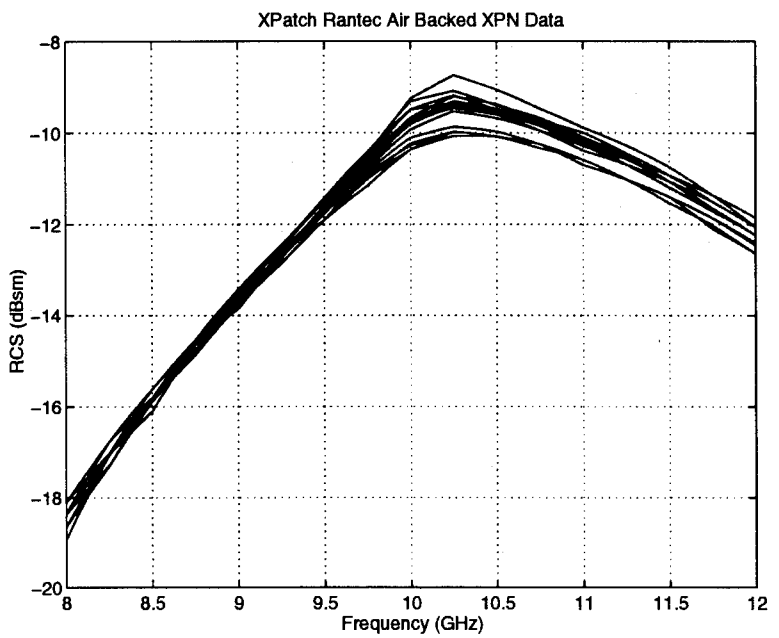

Figure B-26. XPATCH RCS Simulations for Air Backed RANTEC Material Using XPN Measured Material Characteristics

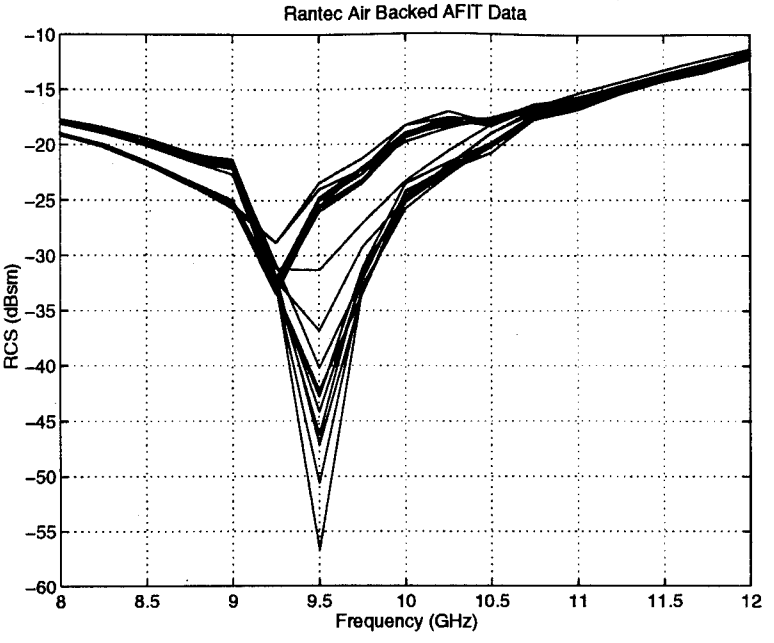

Figure B-27. RCS Predictions for Air Backed RANTEC Material Using AFIT Measured Material Characteristics

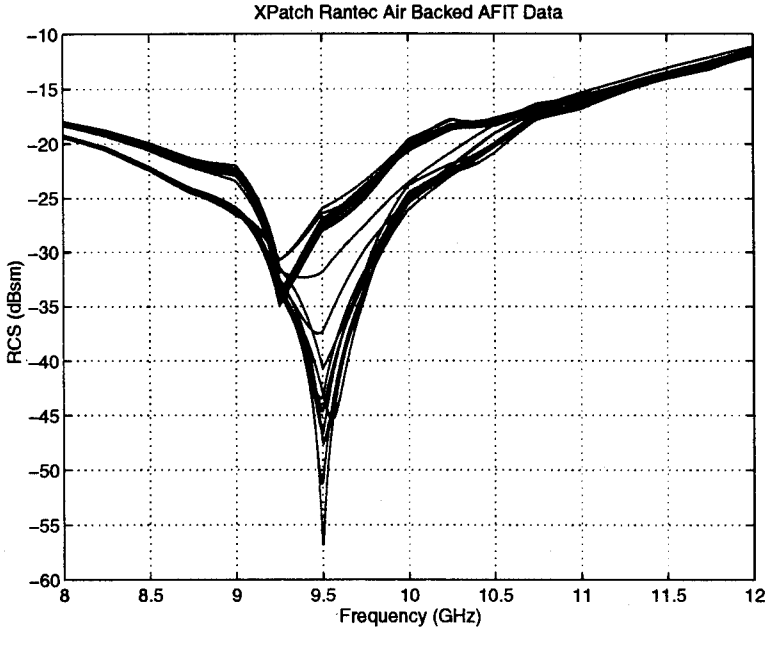

Figure B-28. XPATCH RCS Simulations for Air Backed RANTEC Material Using AFIT Measured Material Characteristics

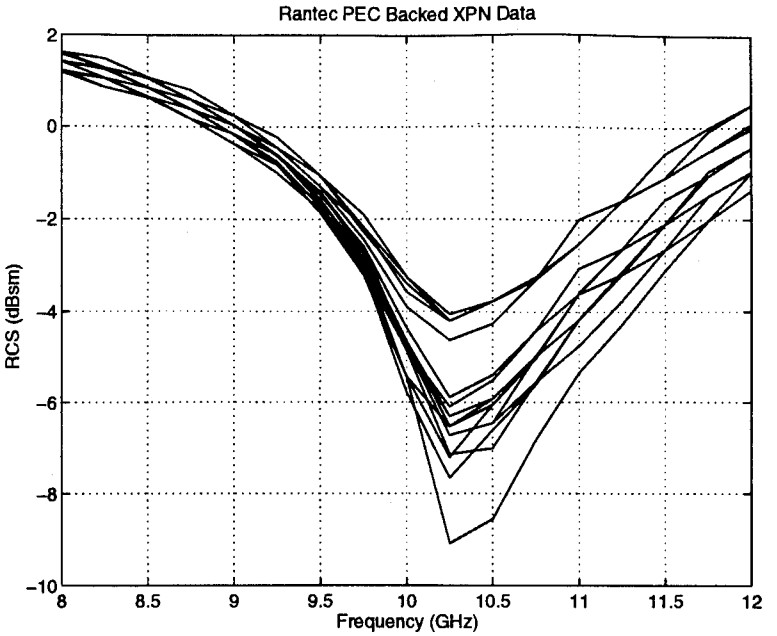

Figure B-29. RCS Predictions for PEC Backed RANTEC Material Using XPN Measured Material Characteristics

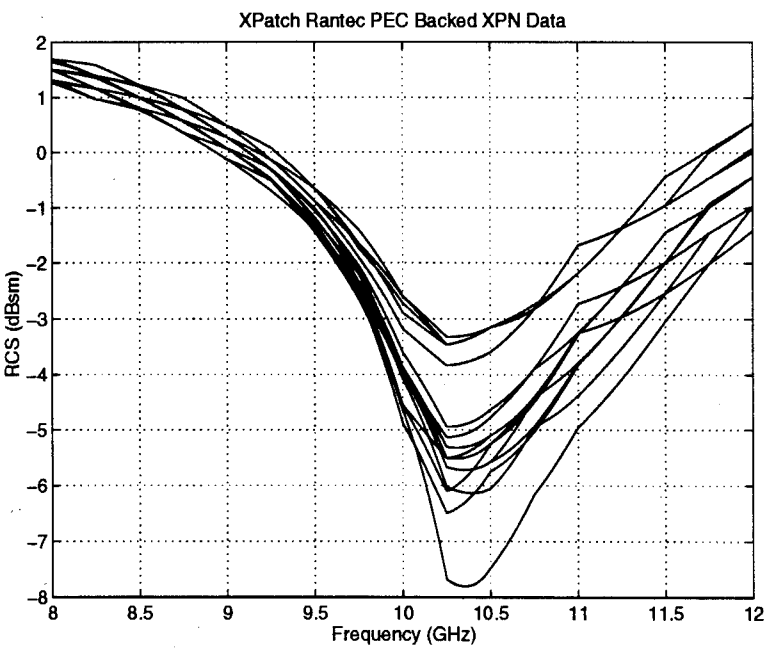

Figure B-30. Xpatch RCS Simulations for PEC Backed RANTEC Material Using XPN Measured Material Characteristics

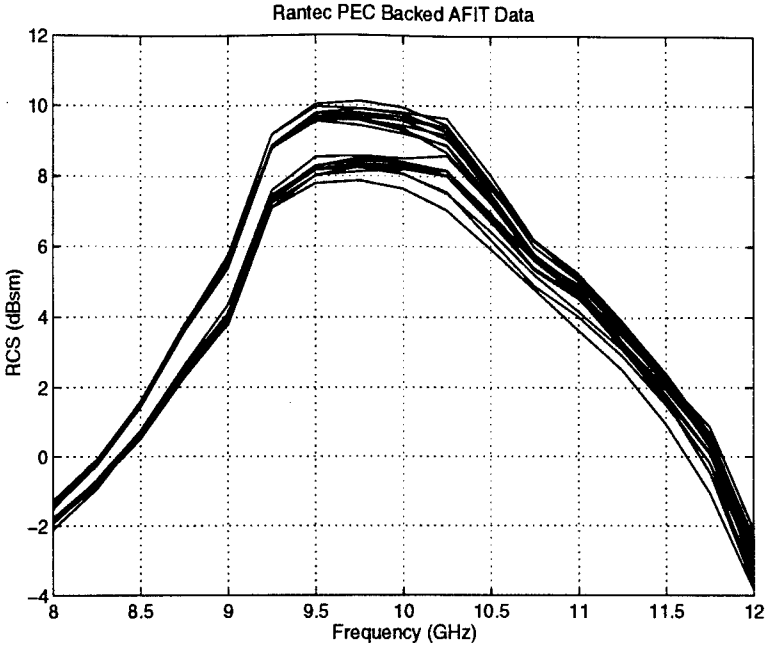

Figure B-31. RCS Predictions for PEC Backed RANTEC Material Using AFIT Measured Material Characteristics

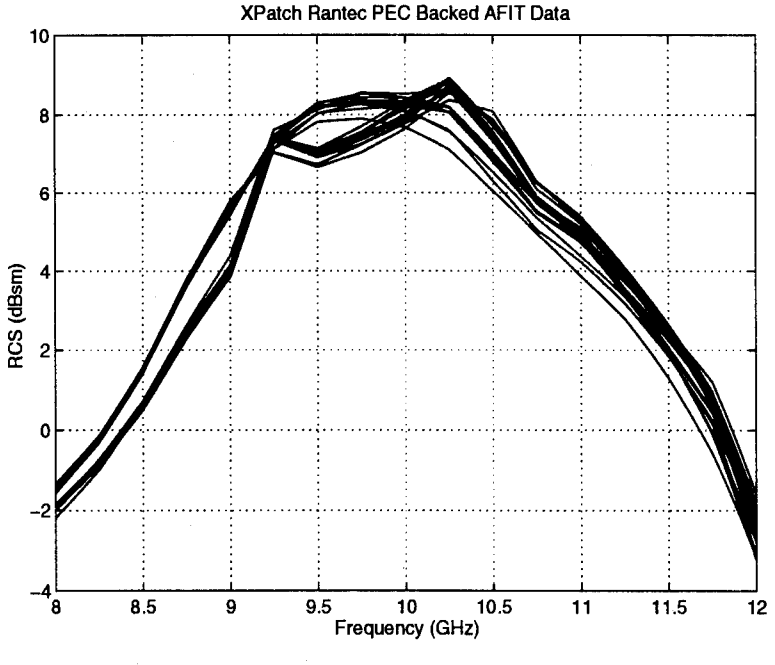

Figure B-32. Xpatch RCS Simulations for PEC Backed RANTEC Material Using AFIT Measured Material Characteristics

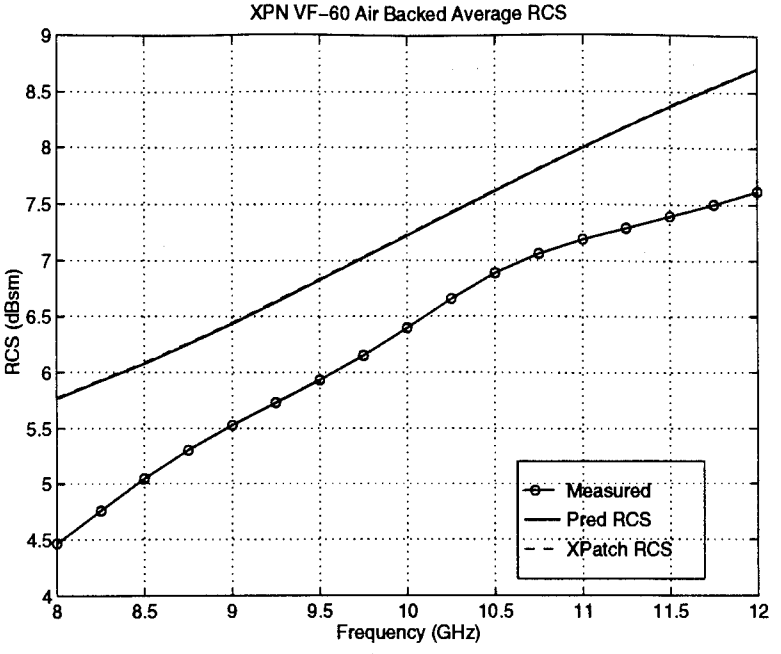

Figure B-33. RCS Prediction and Measured Sample Means for Air Backed VF-60 Material Using XPN Measured Material Characteristics

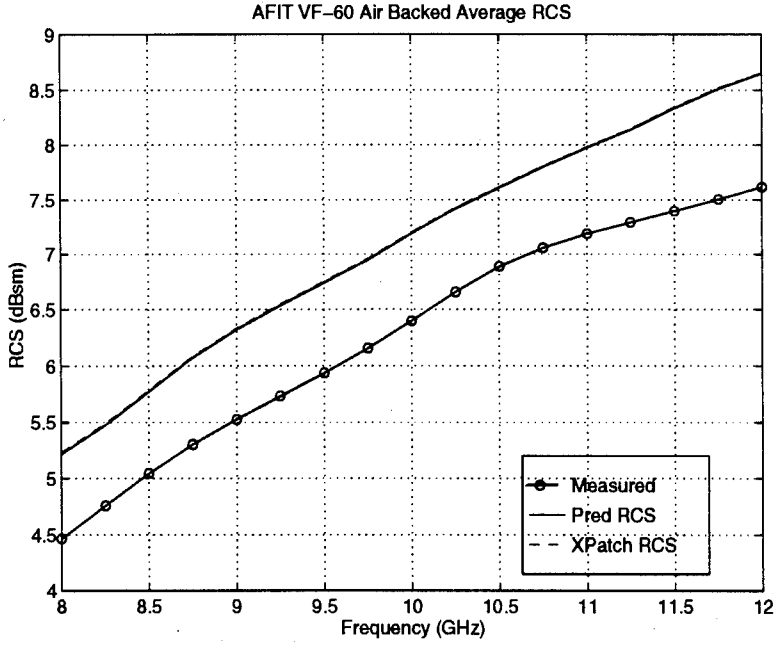

Figure B-34. RCS Prediction and Measured Sample Means for Air Backed VF-60 Material Using AFIT Measured Material Characteristics

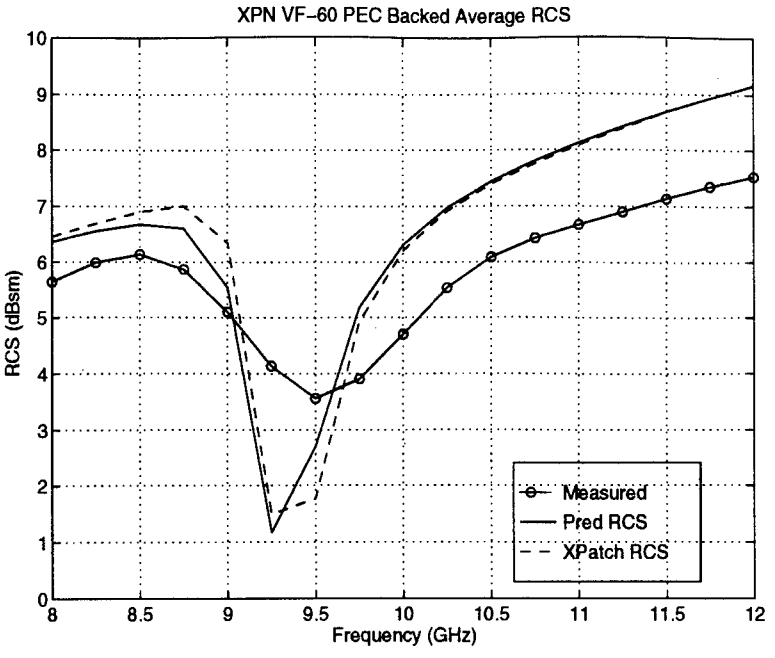

Figure B-35. RCS Prediction and Measured Sample Means for PEC Backed VF-60 Material Using XPN Measured Material Characteristics

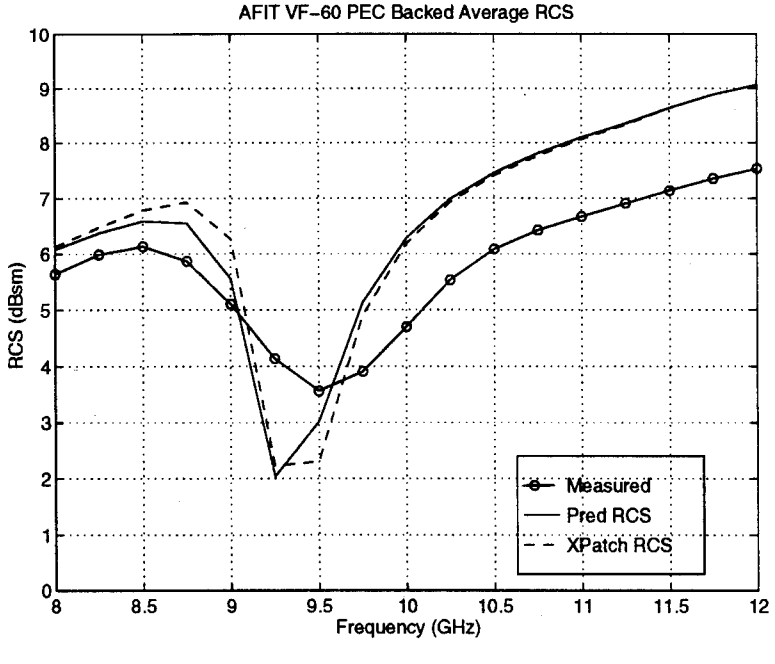

Figure B-36. RCS Prediction and Measured Sample Means for PEC Backed VF-60 Material Using AFIT Measured Material Characteristics

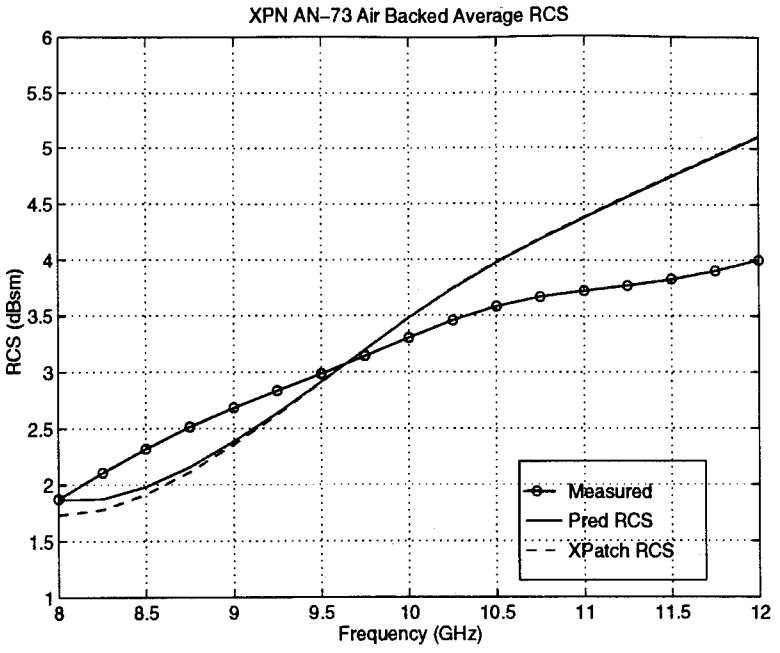

Figure B-37. RCS Prediction and Measured Sample Means for Air Backed AN-73 Material Using XPN Measured Material Characteristics

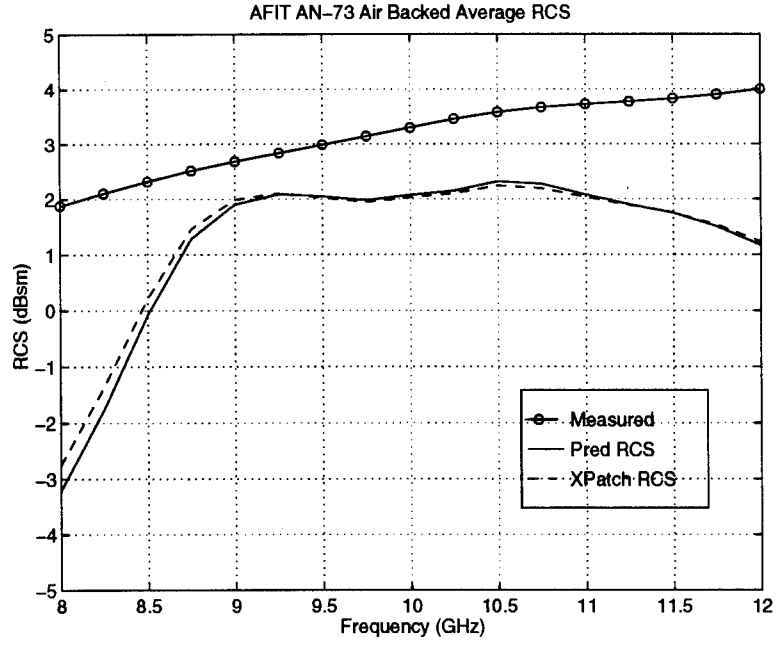

Figure B-38. RCS Prediction and Measured Sample Means for Air Backed AN-73 Material Using AFIT Measured Material Characteristics

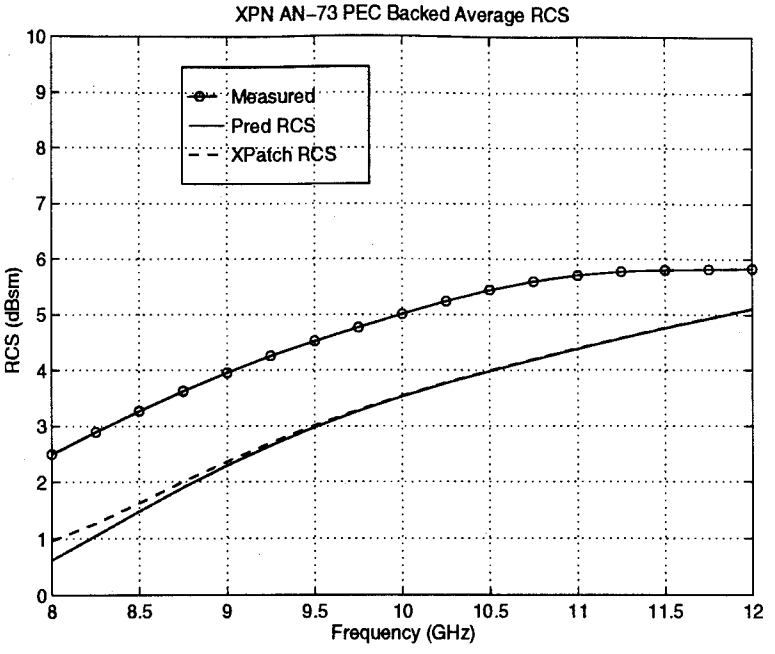

Figure B-39. RCS Prediction and Measured Sample Means for PEC Backed AN-73 Material Using XPN Measured Material Characteristics

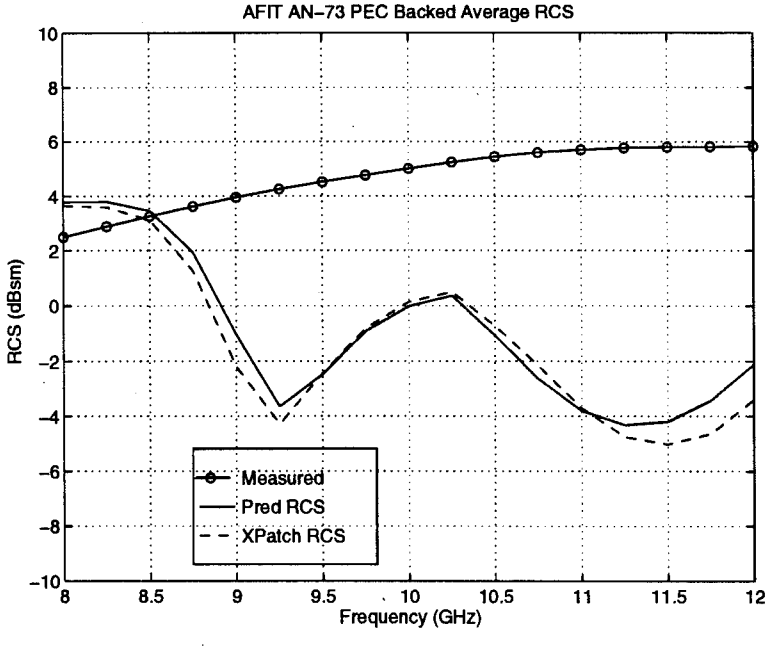

Figure B-40. RCS Prediction and Measured Sample Means for PEC Backed AN-73 Material Using AFIT Measured Material Characteristics

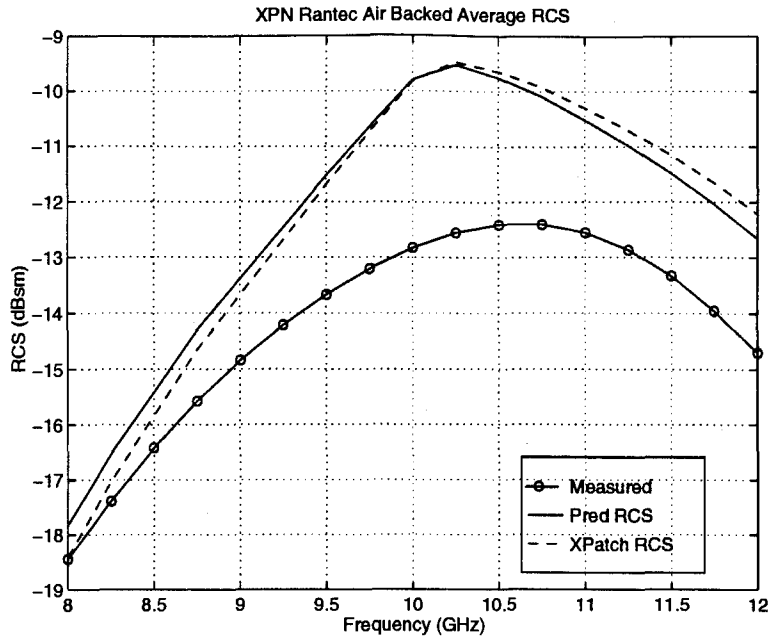

Figure B-41. RCS Prediction and Measured Sample Means for Air Backed RANTEC Material Using XPN Measured Material Characteristics

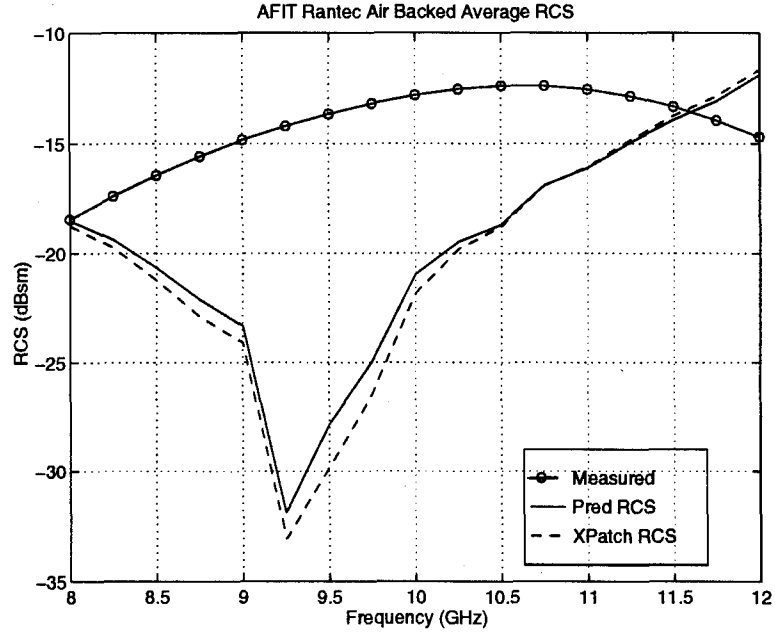

Figure B-42. RCS Prediction and Measured Sample Means for Air Backed RANTEC Material Using AFIT Measured Material Characteristics

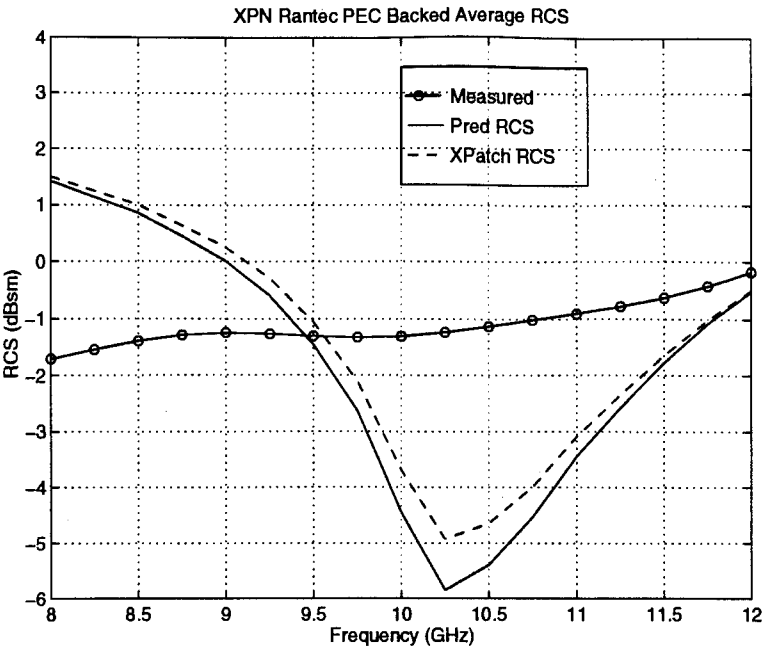

Figure B-43. RCS Prediction and Measured Sample Means for PEC Backed RANTEC Material Using XPN Measured Material Characteristics

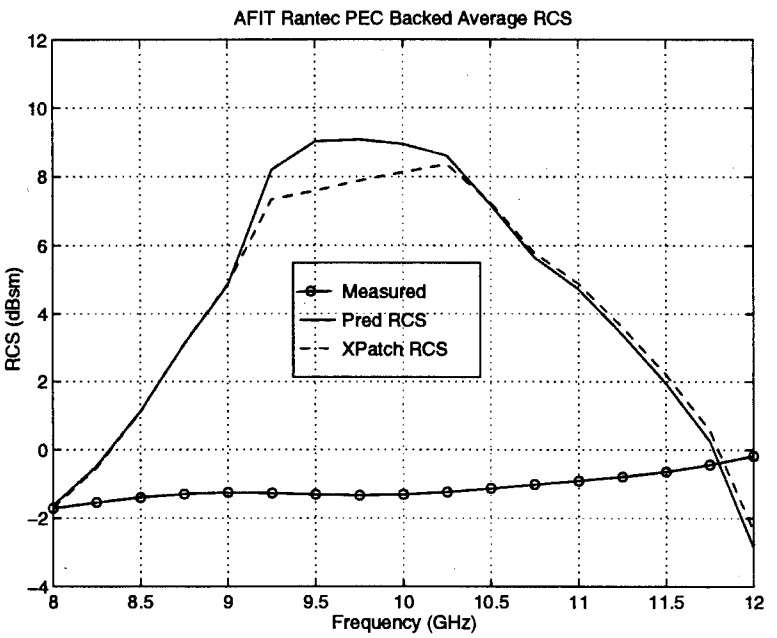

Figure B-44. RCS Prediction and Measured Sample Means for PEC Backed RANTEC Material Using AFIT Measured Material Characteristics

Appendix C: RCS Variations Analysis

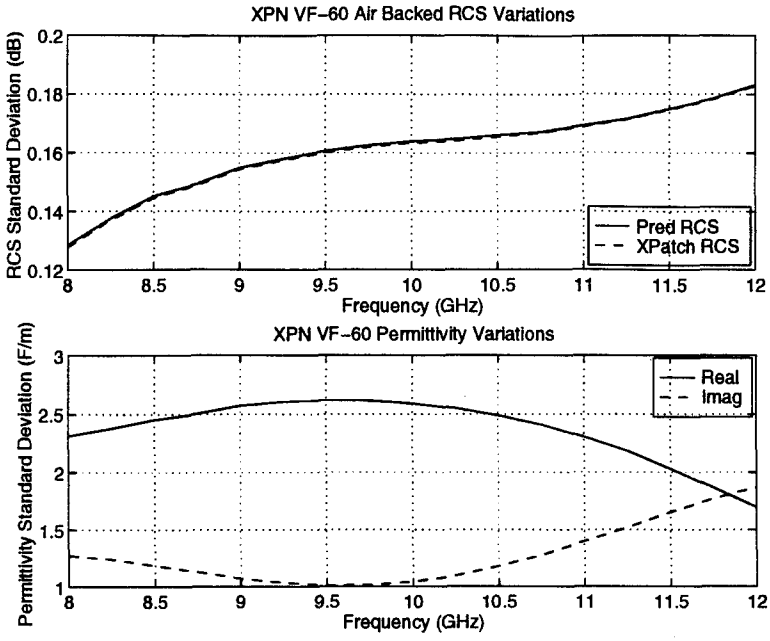

Figure C-1. XPN VF-60 Permittivity Measurement Variations and RCS Prediction Variations for Air Backed VF-60 Material

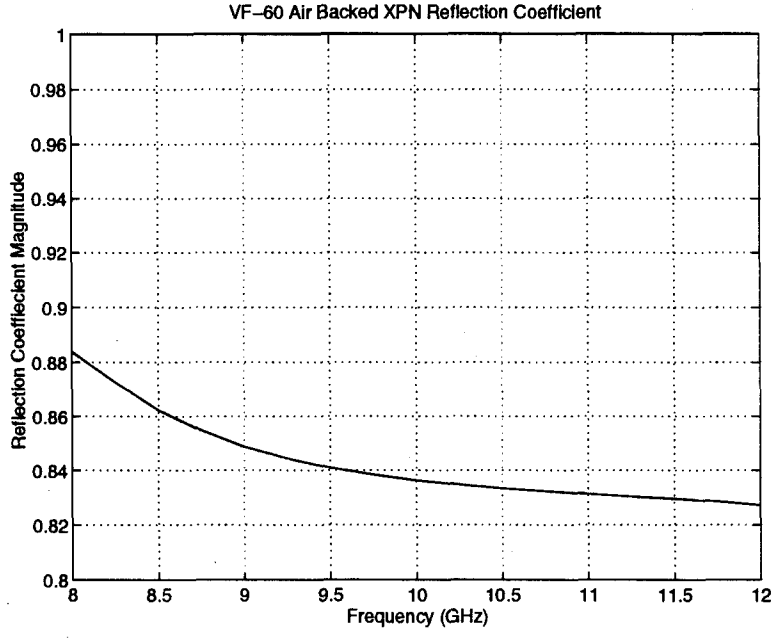

Figure C-2. Average Reflection Coefficient for Air Backed VF-60 Material Using XPN Measured Material Characteristics

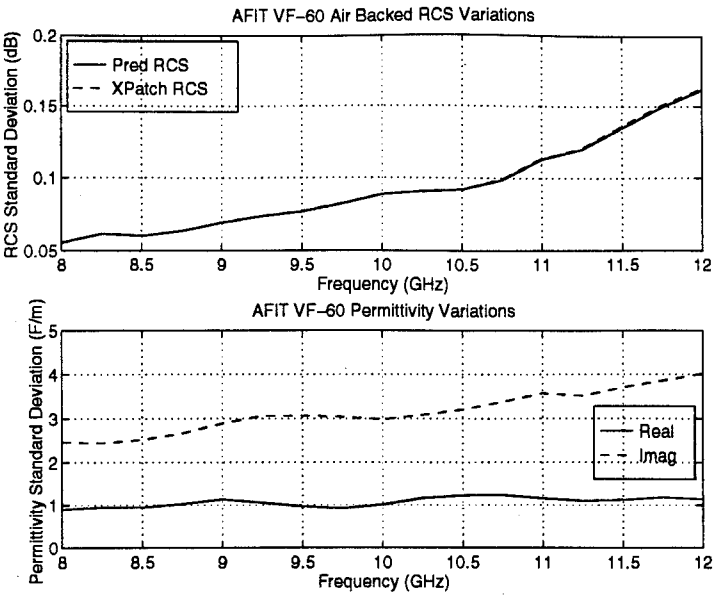

Figure C-3. AFIT VF-60 Permittivity Measurement Variations and RCS Prediction Variations for Air Backed VF-60 Material

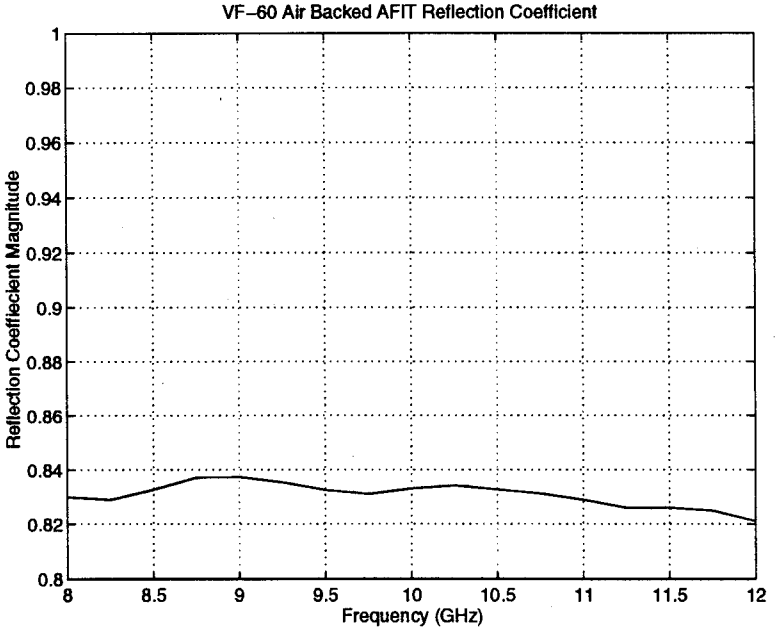

Figure C-4. Average Reflection Coefficient for Air Backed VF-60 Material Using AFIT Measured Material Characteristics

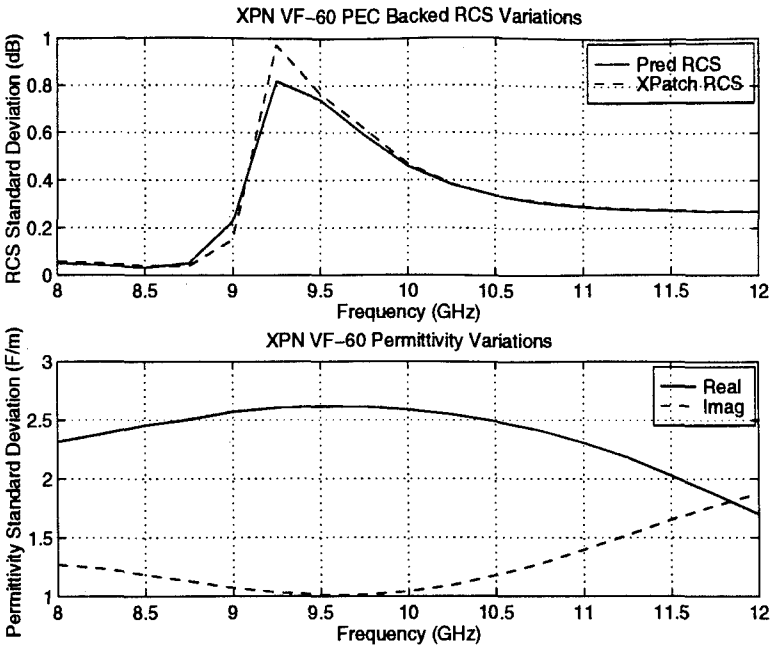

Figure C-5. XPN VF-60 Permittivity Measurement Variations and RCS Prediction Variations for PEC Backed VF-60 Material

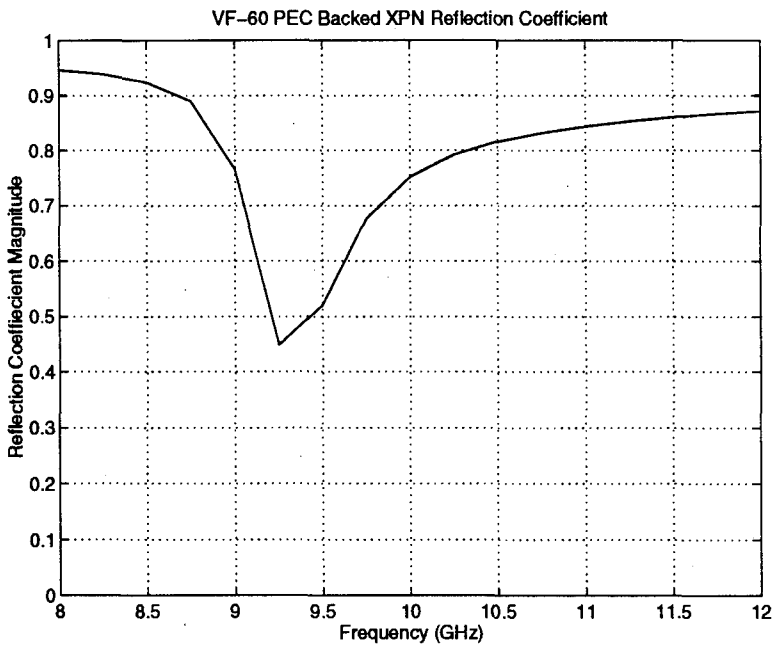

Figure C-6. Average Reflection Coefficient for PEC Backed VF-60 Material Using XPN Measured Material Characteristics

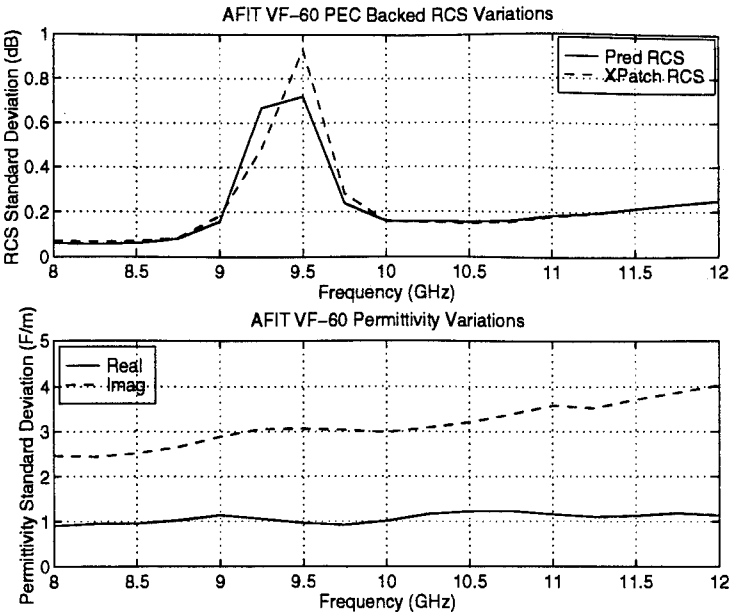

Figure C-7. AFIT VF-60 Permittivity Measurement Variations and RCS Prediction Variations for PEC Backed VF-60 Material

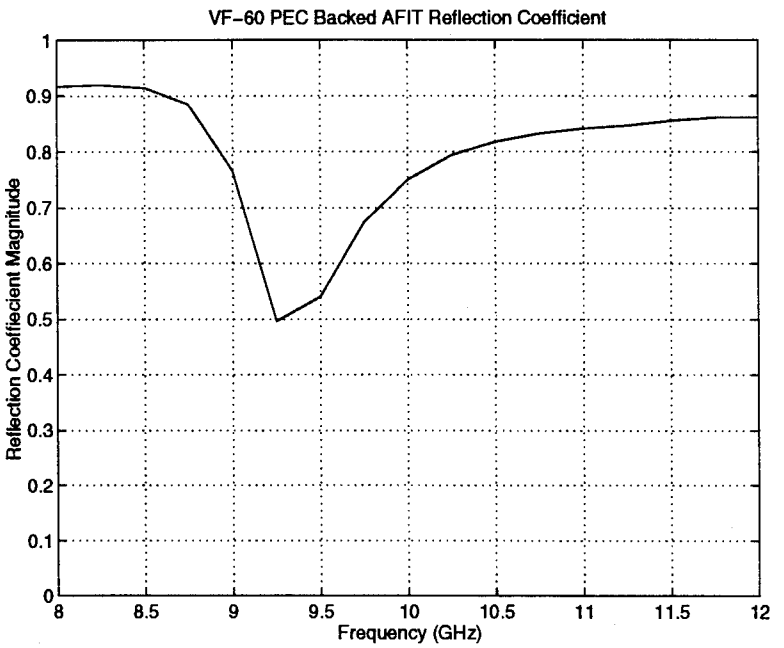

Figure C-8. Average Reflection Coefficient for PEC Backed VF-60 Material Using AFIT Measured Material Characteristics

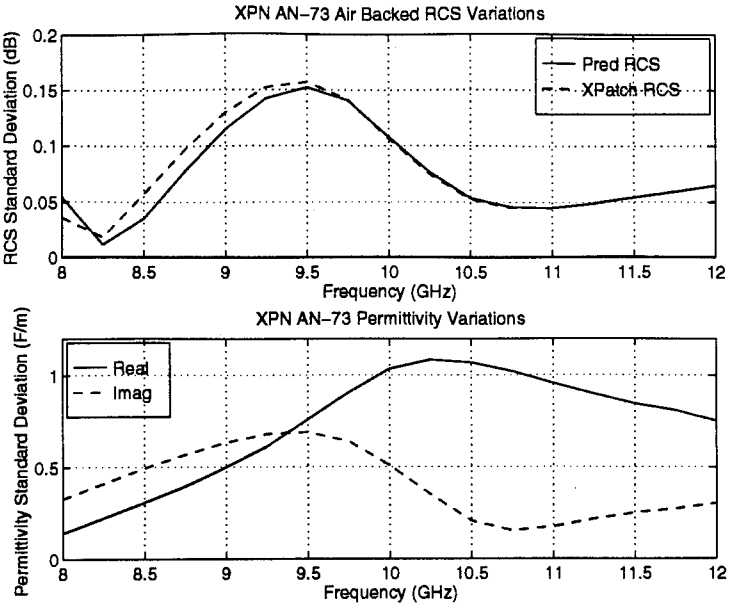

Figure C-9. XPN AN-73 Permittivity Measurement Variations and RCS Prediction Variations for Air Backed AN-73 Material

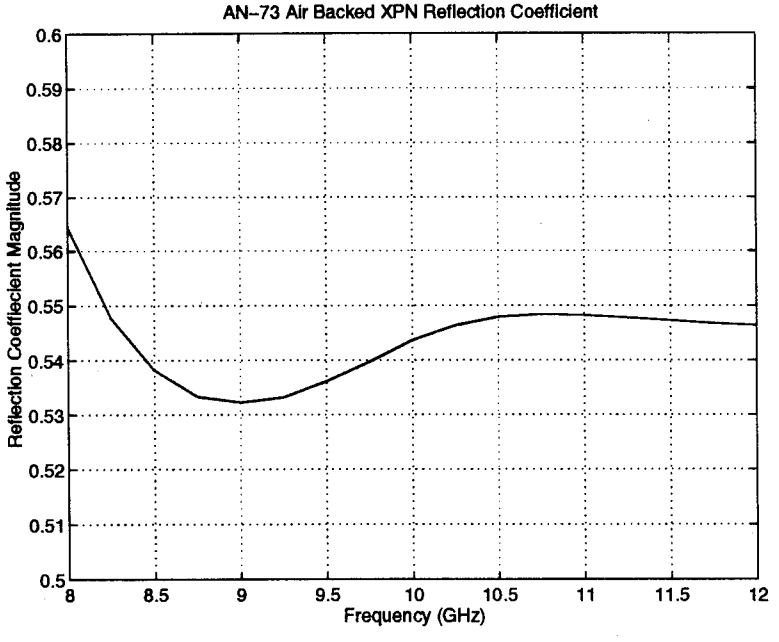

Figure C-10. Average Reflection Coefficient for Air Backed AN-73 Material Using XPN Measured Material Characteristics

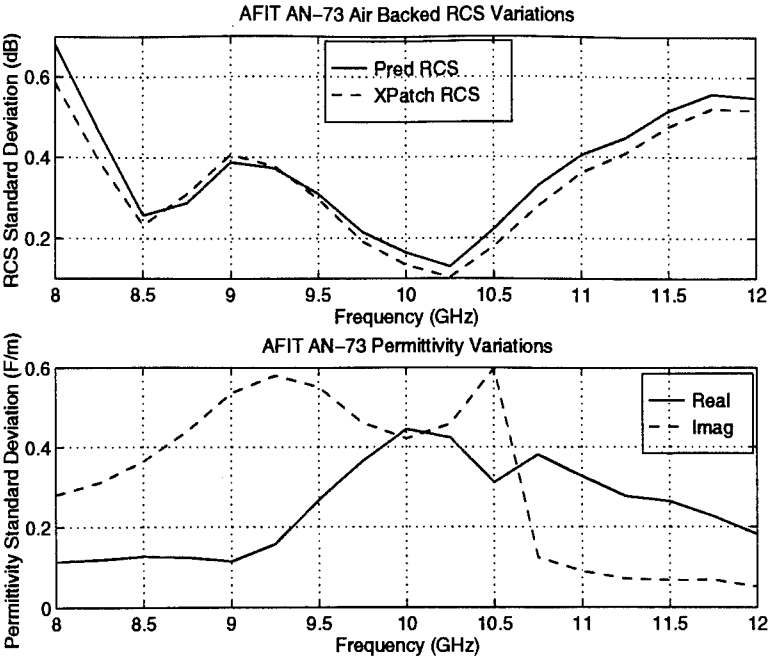

Figure C-11. AFIT AN-73 Permittivity Measurement Variations and RCS Prediction Variations for Air Backed AN-73 Material

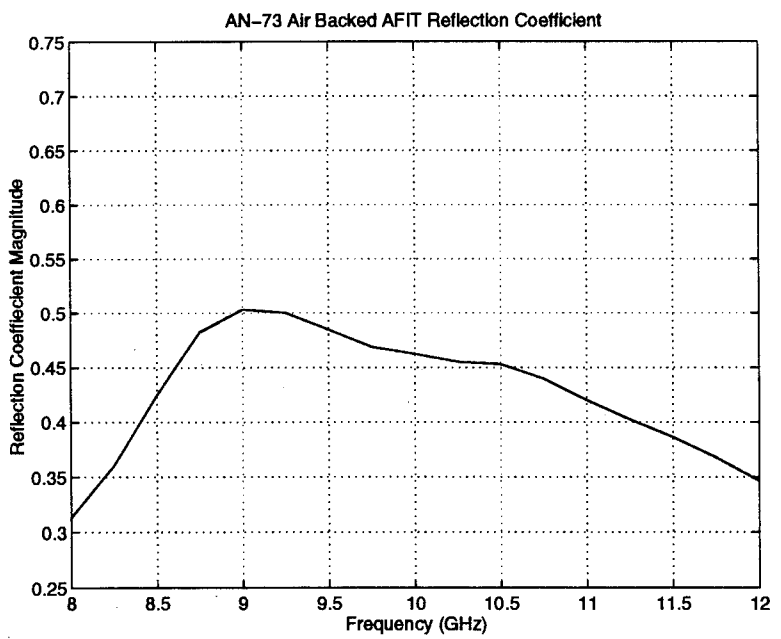

Figure C-12. Average Reflection Coefficient for Air Backed AN-73 Material Using AFIT Measured Material Characteristics

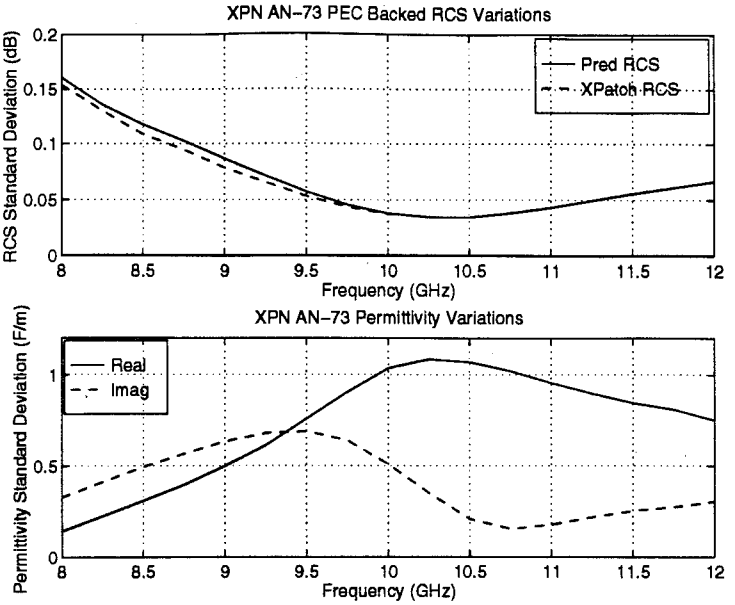

Figure C-13. XPN AN-73 Permittivity Measurement Variations and RCS Prediction Variations for PEC Backed AN-73 Material

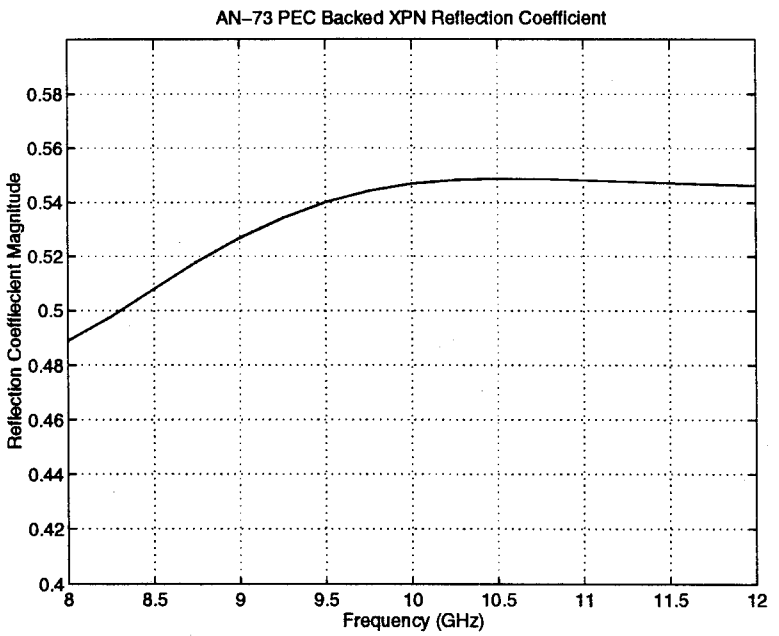

Figure C-14. Average Reflection Coefficient for PEC Backed AN-73 Material Using XPN Measured Material Characteristics

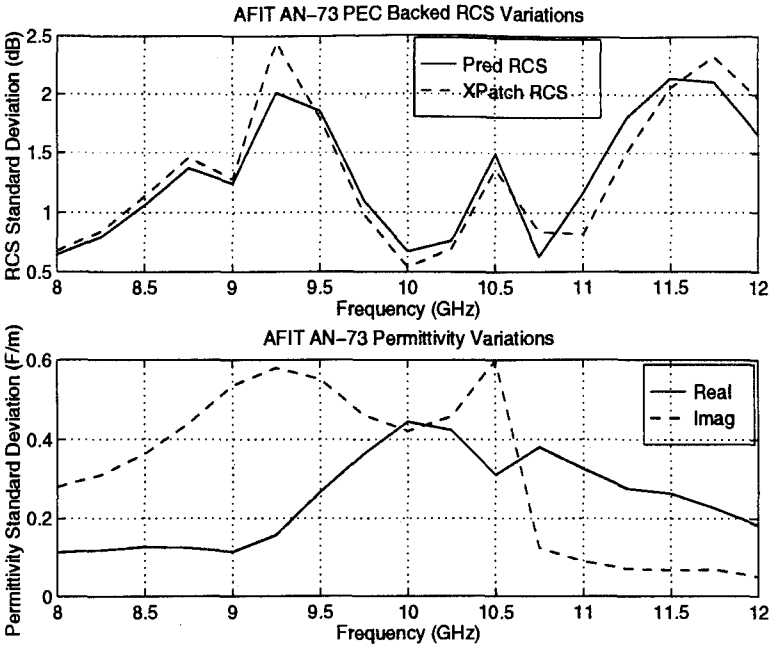

Figure C-15. AFIT AN-73 Permittivity Measurement Variations and RCS Prediction Variations for PEC Backed AN-73 Material

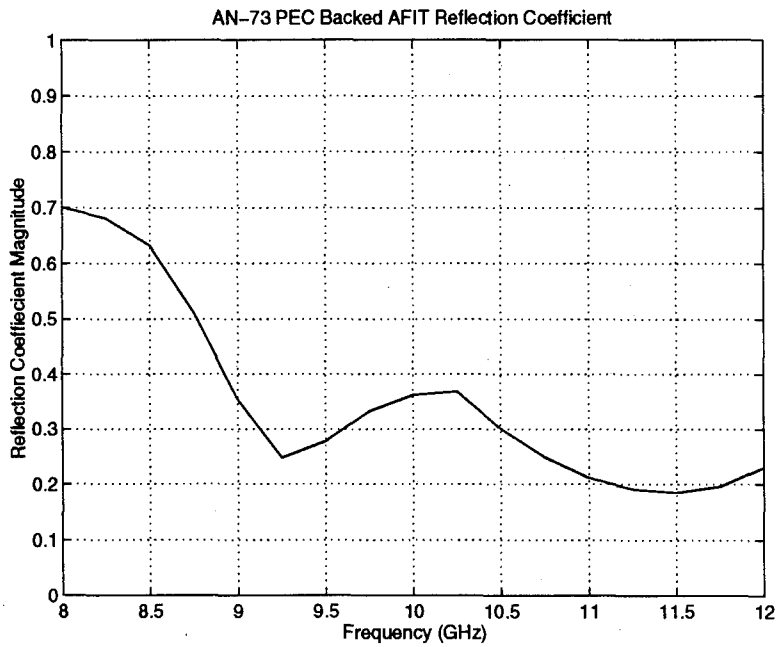

Figure C-16. Average Reflection Coefficient for PEC Backed AN-73 Material Using AFIT Measured Material Characteristics

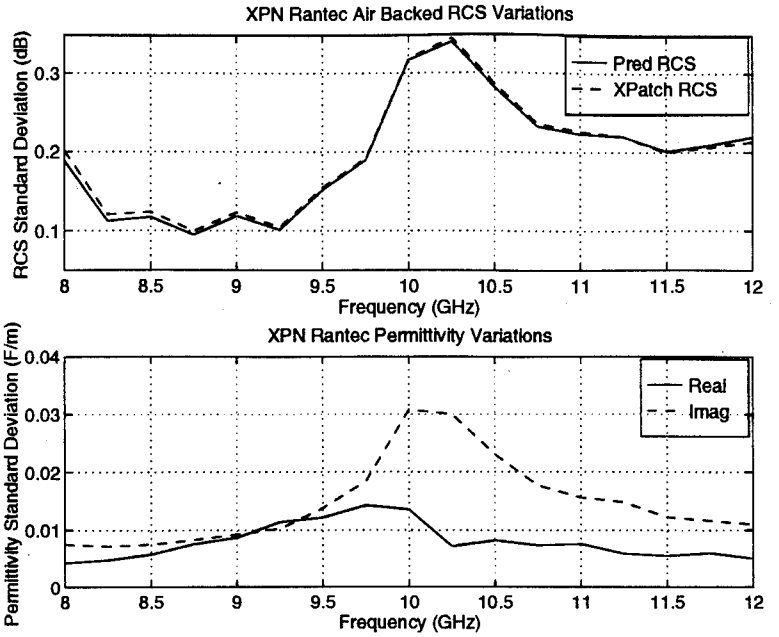

Figure C-17. XPN RANTEC Permittivity Measurement Variations and RCS Prediction Variations for Air Backed RANTEC Material

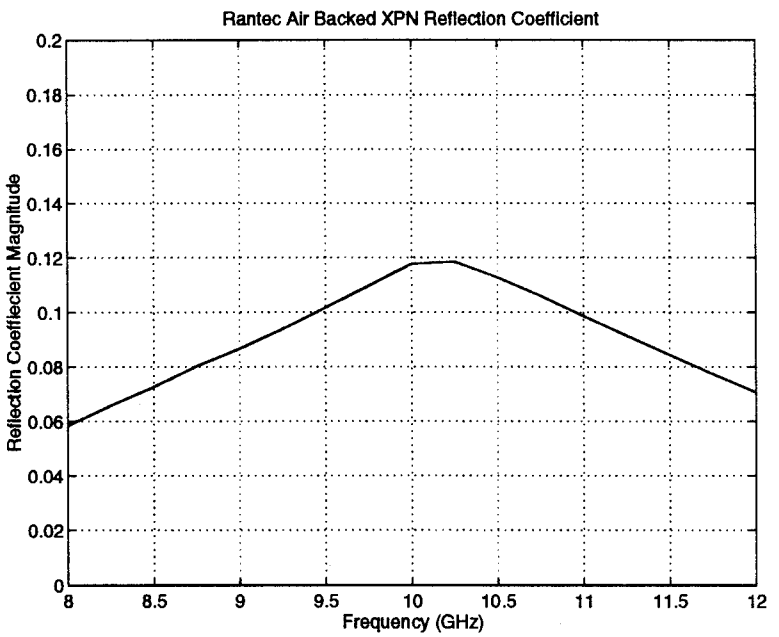

Figure C-18. Average Reflection Coefficient for Air Backed RANTEC Material Using XPN Measured Material Characteristics

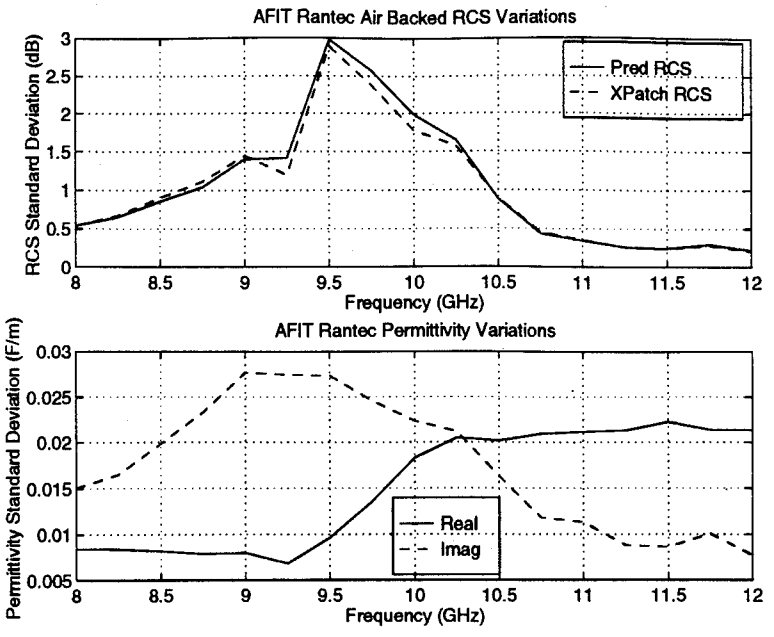

Figure C-19. AFIT RANTEC Permittivity Measurement Variations and RCS Prediction Variations for Air Backed RANTEC Material

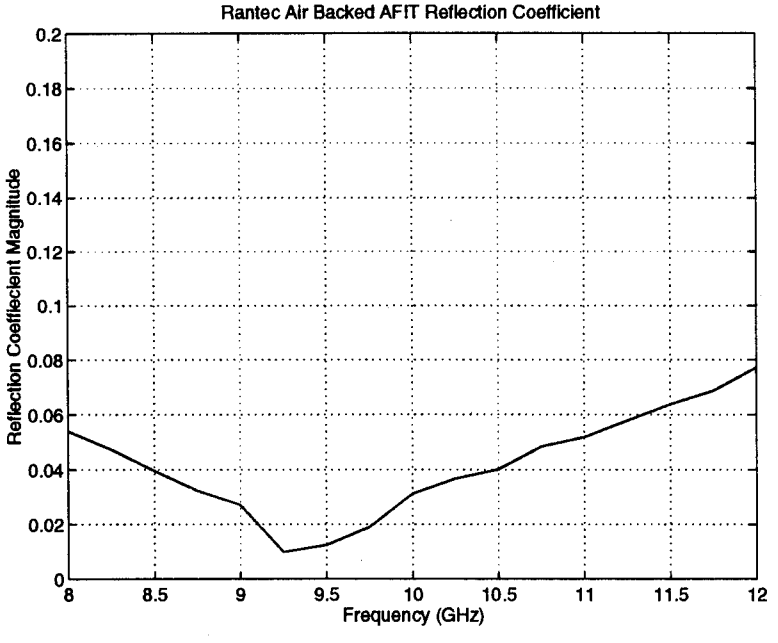

Figure C-20. Average Reflection Coefficient for Air Backed RANTEC Material Using AFIT Measured Material Characteristics

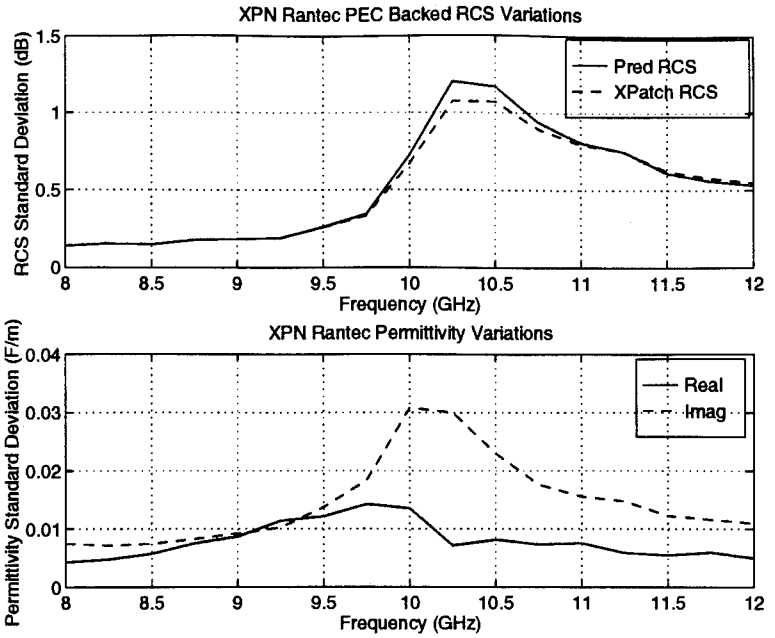

Figure C-21. XPN RANTEC Permittivity Measurement Variations and RCS Prediction Variations for PEC Backed RANTEC Material

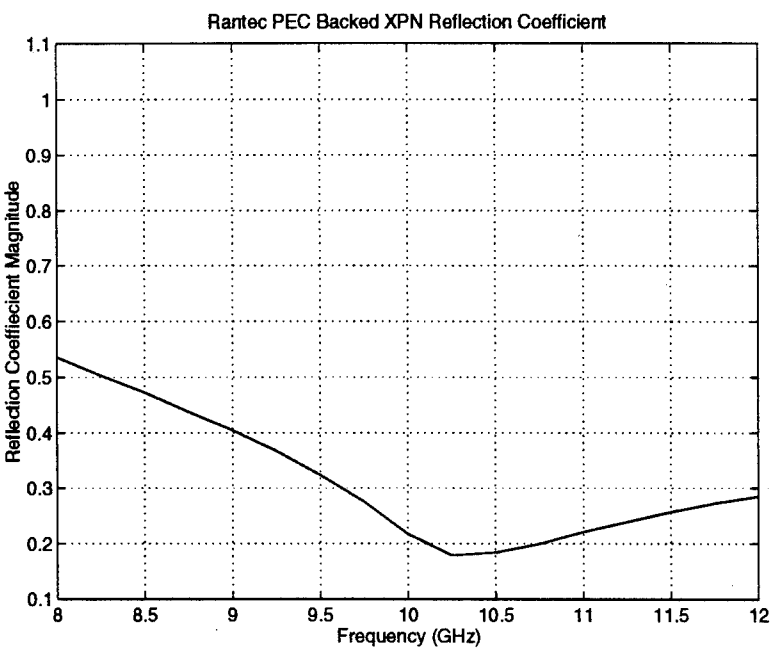

Figure C-22. Average Reflection Coefficient for PEC Backed RANTEC Material Using XPN Measured Material Characteristics

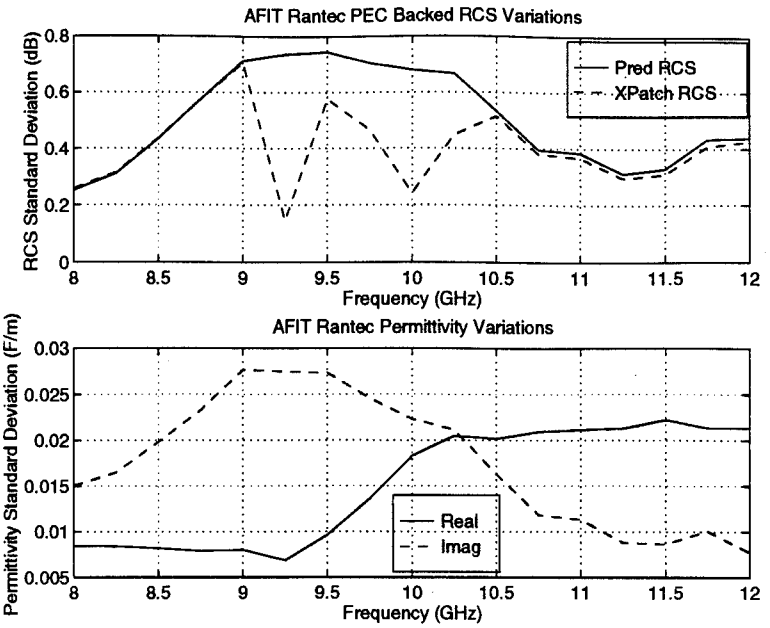

Figure C-23. AFIT RANTEC Permittivity Measurement Variations and RCS Prediction Variations for PEC Backed RANTEC Material

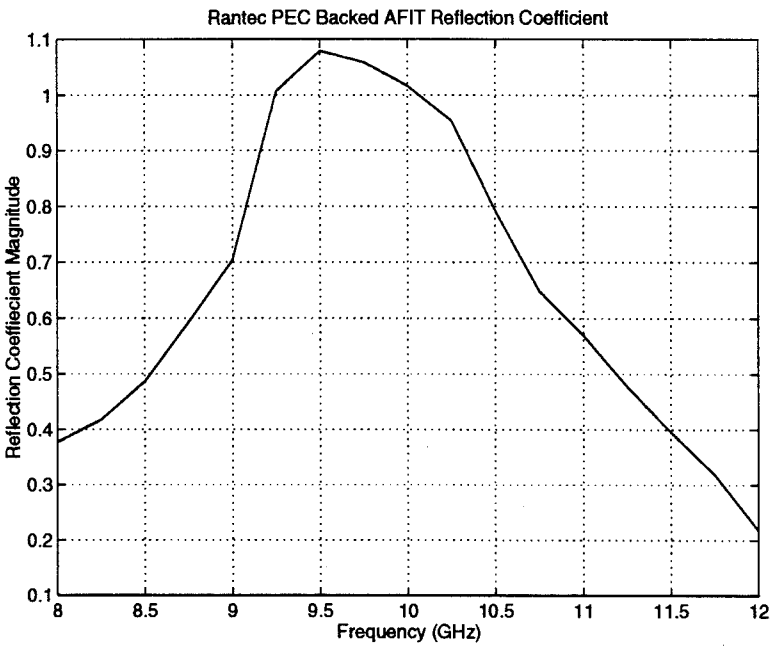

Figure C-24. Average Reflection Coefficient for PEC Backed RANTEC Material Using AFIT Measured Material Characteristics

Appendix D: Xpatch Simulations of MRC Test Body

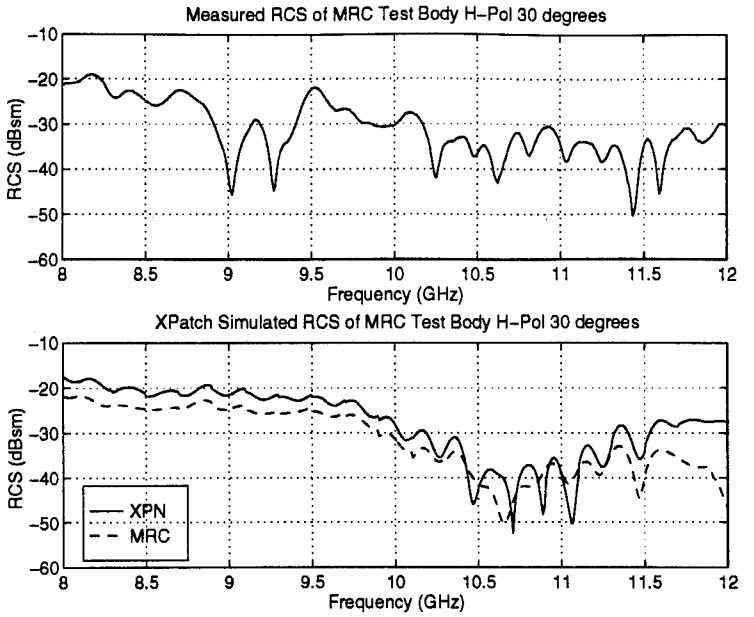

Figure D-1. RCS of MRC Test Body at 30 Degree Incidence at H-pol Measured vs Xpatch Predictions Using MRC and XPN Measured Material Characteristics

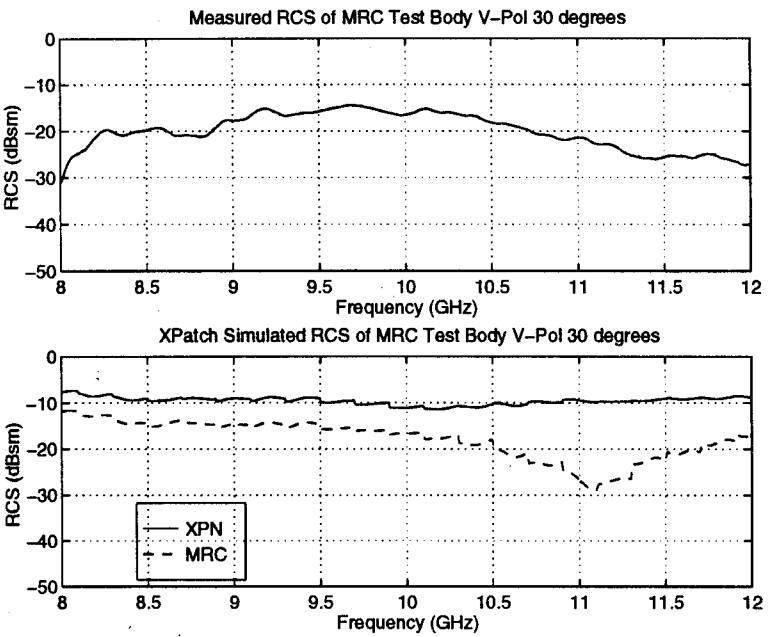

Figure D-2. RCS of MRC Test Body at 30 Degree Incidence at V-pol Measured vs Xpatch Predictions Using MRC and XPN Measured Material Characteristics

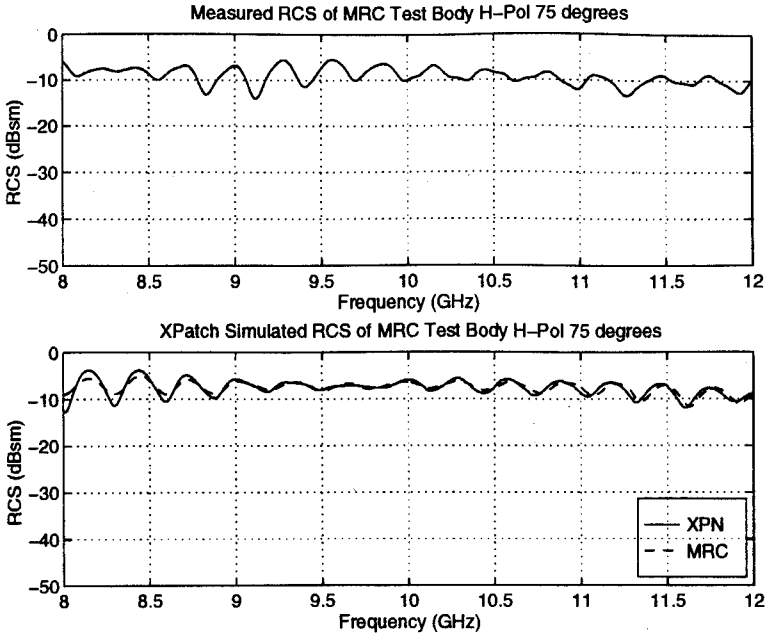

Figure D-3. RCS of MRC Test Body at 75 Degree Incidence at H-pol Measured vs Xpatch Predictions Using MRC and XPN Measured Material Characteristics

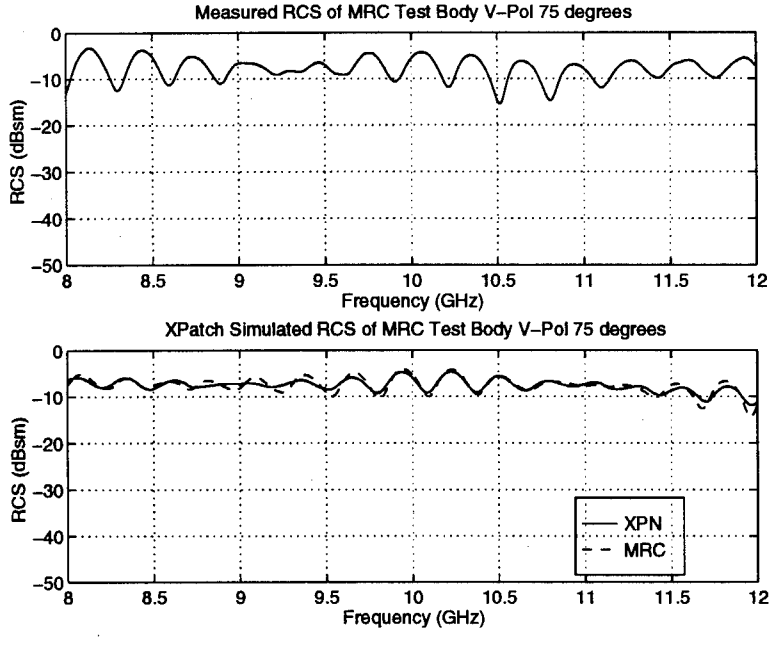

Figure D-4. RCS of MRC Test Body at 75 Degree Incidence at V-pol Measured vs Xpatch Predictions Using MRC and XPN Measured Material Characteristics

Bibliography

[1] M. N. Afsar, J. R. Birch, and R. N. Clarke, "The Measurement of the Properties of Materials," Proc. IEEE, vol. 74, pp. 183-198, Jan. 1986.

[2] C. A. Balanis, Advanced Engineering Electromagnetics. New York: John Wiley & Sons, 1989.

[3] Emerson & Cuming, "Technical Bulletin 2-16 ECCOSORB VF Resistive Plastic Film for Microwaves," Emerson & Cuming, Sept. 1980.

[4] Emerson & Cuming, "Technical Bulletin 8-2-4 ECCOSORB AN Flexible Foam Sheet Microwave Absorber," Emerson & Cuming, Sept. 1980.

[5] Hewlett Packard, "Measuring Dielectric Constant with the HP 8510 Network Analyzer," Hewlett Packard, Santa Rosa, CA, Product Note No. 8510-3, 1987.

[6] R. O. Jernejcic, "Evaluation of Full Radar Signature Predictions Using XPATCH," MS Thesis, Air Force Institute of Technology, 1993.

[7] B. M. Kent, R. Porter, and W. Leeper, "On Improving Broadband Compact Range Technology," Wright Research and Development Center, Wright-Patterson AFB, OH, 1991.

[8] E. F. Knott, J. F. Shaeffer, and M. J. Tuley, Radar Cross Section. Boston: Artech House, 1993.

[9] R. G. Layden, A. B. MacFarland, and W. J. Kent, "A Comparison Between Physical Optics Codes XPATCH and NoseScat Versus Measured Data on the MRC Nose Radome Test Body," Mission Research Corporation, Dayton, OH, Nov. 1994.

[10] S. W. Lee and D. J. Andersh, "User Manual for XPATCH," DEMACO Inc., Champaign, IL, Sept. 1993.

[11] LINTEK Inc., "4000 Series Measurement System Operations Manual," LINTEK Inc., Powell, OH, Dec. 1994.

[12] A. J. Lyon, Dealing With Data. Oxford: Pergamon Press, 1970.

[13] J. P. Meyers, "Quantitative Methods for Comparing and Improving Electromagnetic Scattered Field Prediction Codes," MS Thesis, Air Force Institute of Technology, 1994.

[14] E. M. Miller, "Validation of XPATCH Radar Signature Predictions Using Flat Facet Geometries," MS Thesis, Air Force Institute of Technology, 1992.

[15] R. Moore, T. Targonsky, and C. Thompson, "Program User Instructions for the Network Analyzer System and SCAL-ALL Version 6.0," Georgia Institute of Technology, Atlanta, GA, May 1989.

[16] D. A. Mullinix, "Air Force Institute of Technology (AFIT) Radar Cross-Section Measurement Range User Manual," Air Force Institute of Technology, Wright-Patterson AFB, OH, Aug. 1994.

[17] G. T. Ruck, D. E. Barrick, W. D. Stuart, and C. K. Krichbaum, Radar Cross Section Handbook, New York: Plenum Press, 1970.

[18] W. B. Weir, "Automatic Measurement of Complex Dielectric Constant and Permeability at Microwave Frequencies," Proc. IEEE, vol. 62, pp. 33-36, Jan. 1974.

Vita

Captain Greg A. Barnhart [redacted] to. He graduated from Stebbins High School in Dayton, Ohio in 1986. Captain Barnhart then attended Purdue University, Indiana, where he graduated with a B.S.E.E. and received a commission in the Air Force through the ROTC program in 1990. His first assignment was with the Air Force Material Command, Space and Missile Systems Center, at Los Angeles AFB, California. He worked in the Air Force Satellite Control Network where he was responsible for hardware modifications to Automated Remote Tracking Stations worldwide. Captain Barnhart's second assignment in May, 1994, was with the Air Force Institute of Technology at Wright-Patterson AFB, Ohio, to pursue a Master's Degree in Electrical Engineering. Captain Barnhart is a certified Engineer-In-Training in the state of Indiana. His follow-on assignment will be with the Air Intelligence Agency at Kelly AFB, Texas.

[redacted]

REPORT DOCUMENTATION PAGE

Form Approved
OMB No. 0704-0188

1. AGENCY USE ONLY (Leave blank)	2. REPORT DATE	3. REPORT TYPE AND DATES COVERED
	December 1995	Masters Thesis

4. TITLE AND SUBTITLE
EVALUATION OF THE SENSITIVITY OF RADAR CROSS SECTION PREDICTIONS TO UNCERTAINTIES IN MATERIAL CHARACTERISTICS

5. FUNDING NUMBERS

6. AUTHOR(S)
Greg A. Barnhart, Captain, USAF

7. PERFORMING ORGANIZATION NAME(S) AND ADDRESS(ES)
Air Force Institute of Technology, WPAFB, OH 45433-6583

8. PERFORMING ORGANIZATION REPORT NUMBER
AFIT/GE/ENG/95D-02

9. SPONSORING / MONITORING AGENCY NAME(S) AND ADDRESS(ES)
Major Dennis Andersh, Wright Laboratories (WL/AARA)
2010 Fifth St Bldg 23
WPAFB, OH 45433-7001

10. SPONSORING / MONITORING AGENCY REPORT NUMBER

11. SUPPLEMENTARY NOTES

12a. DISTRIBUTION / AVAILABILITY STATEMENT
Distribution Unlimited

12b. DISTRIBUTION CODE

13. ABSTRACT *(Maximum 200 words)*

Many methods have been developed to predict the Radar Cross Section (RCS), but object material characteristics are key input variables. This research demonstrates the relationship between uncertainties in material characteristics and the accuracies of RCS predictions. The material characteristics of three dielectrics were measured by two separate X-band waveguide set-ups. RCS measurements were made of the materials backed with and without a metal square plate at normal incidence to evaluate the accuracy of RCS predictions using these measured material characteristics. RCS predictions were calculated with: 1) reflection coefficients from transmission line theory and physical optics; and 2) Xpatch, a high frequency RCS prediction code. It was found that variations in RCS predictions were proportional to variations in the imaginary part of the permittivity. Furthermore, the magnitude of the RCS variations corresponded inversely to the relative magnitude of the reflection coefficient.

14. SUBJECT TERMS	15. NUMBER OF PAGES
radar cross section, RCS, material characteristics, Xpatch	118
	16. PRICE CODE

17. SECURITY CLASSIFICATION OF REPORT	18. SECURITY CLASSIFICATION OF THIS PAGE	19. SECURITY CLASSIFICATION OF ABSTRACT	20. LIMITATION OF ABSTRACT
UNCLASSIFIED	UNCLASSIFIED	UNCLASSIFIED	UL